Implications of Percutaneous Delivery of Cardiac Devices on Interatrial Septal Anatomy and Biomechanics

A DISSERTATION
SUBMITTED TO THE FACULTY OF THE GRADUATE SCHOOL
OF THE UNIVERSITY OF MINNESOTA
BY

Stephen Andrew Howard

IN PARTIAL FULFILLMENT OF THE REQUIREMENTS
FOR THE DEGREE OF
DOCTOR OF PHILOSOPHY

Advisor: Paul A. Iaizzo

March 2014

Acknowledgments

A PhD dissertation is not an easy task especially for one person to do alone. Fortunately I had an immense amount of support from individuals of whom I had the privilege to work. They helped to teach, mentor and train me throughout my graduate work. Although it would be difficult to fully extend thanks to all those of whom helped me along the way there are a few that I wish to thank specifically.

In the past 5 years I have been able to work with a number of fellow graduate students. Some for only a couple of months while others almost 4 years. Between the animal studies, late nights in the lab and writing papers there was a lot of camaraderie within our group. So to Eric Richardson, Jason Quill, Mike Eggen, Mike Bateman, Chris Rolfes, Jules Spencer, Ryan Goff, Brian Howard and Stephen Quallich I say thank you for everything. Likewise, to the support staff for the labs, Bill Gallagher, Monica Mahre, Charles Soule, Gary Williams, and Tinen Healy, I thank you for your patients, your teaching and your friendship. All of the help that I received was greatly appreciated.

The academic support, although important, is not the only reason for my success. I would also like to acknowledge my family and my wife for giving me the support and encouragement to continue on even after long, long weeks in the lab. There were many long evenings at the lab where I would either come home late or not at all and without the support and love from my family it would not have been possible to continue through those difficult days. So to them I wish to say thank you dearly for all of the support, encouragement and love that you have given me.

Finally, I cannot fully extend my appreciation for all of the mentoring, support and encouragement from my professor Paul Iaizzo. He is the primary reason that I ended up at the University of Minnesota and even considered pursuing Biomedical Engineering. It was a big turn of events to change over from potentially pursuing Neuroscience to then Biomedical Engineering, especially since the focus is on cardiac engineering. To Paul I must say thank you for helping me and supporting me throughout my graduate school career. I am forever thankfully for everything that you have done for me.

Dedication

This dissertation is dedicated to my loving wife Betsy.

Table of Contents

List of Tables

List of Figures

Thesis Statement

The atrial septum is a seemingly complex anatomical structure when compared to its menial physiological function of separating two cardiac chambers in a healthy adult heart. If studied further, the function and rational for these septal structures and how they ultimately can impact both the patient and delivery of cardiac therapies, become more apparent. For example, to address the concerns of interventional cardiac medical device interactions with the atrial septum, we must first understand the underlying anatomy, structure, physiology and relevant nomenclature of the associated anatomical structures. Subsequently, one can then focus on the impacts that these sorts of clinical procedures have on the atrial septum and any unfavorable clinical consequences of said procedure.

Two common cardiac interventional procedures that are currently performed are transseptal punctures (TSPs) and closures of symptomatic defects within the atrial septum. These procedures rely heavily on the patient's atrial septal anatomy and surrounding cardiac structures to effectively perform and reduce procedural complications. Nevertheless it remains to date, that the specifics and common variations within these anatomical structures and their biomechanical tissue properties have not been fully defined. Likewise, there needs to be an integration of this type of knowledge relative to performing TSPs and the resultant (iatrogenic) defects they can produce as a result of the procedure. In other words, following a TSP, there is commonly an induced hole that can persist within the septum and it has been documented they can be present up to 18 months after the procedure. Importantly, it needs to be recognized that such defects may allow for blood or a potential thrombus to pass from the left to right or right to left atria. There are a number of investigators that are beginning to address these issues, so to determine their

clinical relevance, however more work and further understandings needs to be obtained, especially concerning the biomechanical properties within this cardiac anatomical region [1].

Congenital defects can also produce similar interatrial communications that allow for blood passage from the right to left atrium. One such defect is a patent foramen ovale, which has been reported in adult populations with a prevalence as high as 25% of the populations. The morphologies of this defect have been defined as a channel that allows for blood passage from the right to the left atrium under certain conditions due to the incomplete fusion of the septum primum to the septum secundum. Under what would be defined as typically abnormal physiological circumstances, the pressure within the right atrium can become higher than that of the left atrium and then PFO may act as an atrial communication similar to those found following TSPs. Since the blood effectively bypasses the normal pulmonary capillary filter, there is a chance that there may be blood clots from the venous anatomy that can traverse the PFO and cause an emboli in the arterial vasculature and potentially cause a stroke. To reduce these risks, patients are put on anticoagulative therapies and/or physicians often choose to close such defects. Currently there are no devices specifically marketed for closure of PFOs (that have been FDA approved), so by closing such a defect the physician is utilizing the septal occluder device "off-label." It should be noted that the potential implications of these sorts of septal closures will be explored in this thesis.

In general, the underlying basis for my thesis is to attempt to answer these questions and provide new anatomical and physiological insights of the relative functions of the atrial septum, relating to these aforementioned procedures. To begin appropriate investigations on such requires a solid basis of anatomy and physiology. One way to that this has been performed previously was via gross anatomical descriptions obtained from direct measurements from cadaver hearts and

clinical imaging modalities. Although these are not all encompassing for even the anatomical measurements and certainly not for the study of biomechanical parameters. In such prior work, the investigators either describe the fine anatomy along a 2D plane, or may be biased by imaging artifacts resulting from dynamic nature of the heart. Further, defects in the atrial septum, like a PFO have been studied but only in regards to their 2D anatomies while the 3D structure have only been studied in a very few instances[2,3]. Therefore, in order to address such concerns, here I have employed high resolution MRI scans and 3D modeling to allow for additional measurement capacities that have previously been not available in cadaveric dissections or patient CT or MRI scans.

In summary, my thesis has been compiled in a progressive fashion, so to mimic the progression of clinical knowledge required to bring to market cardiac medical devices aimed at impacting the atrial septum. The thesis begins with an in-depth review of the anatomy and morphologies associated with the atrial septum which is presented in Section I. The knowledge derived from my own research and the reported literature can then show how the anatomy can be presented in a clinically relevant manor and how it typically may change with underlying disease states. Then from this initial knowledge base, my thesis progresses to chapters that describe optimal ways of imaging and visualizing cardiac anatomy (Section II). Imaging of normal or anomalous anatomy can be performed to provide a clearer spatial orientation within the atrial chambers of the heart and achieve a better understanding of human cardiac anatomy as a whole. Subsequently, in Section III, I present how a percutenous cardiac medical device therapy is developed and how physiological data is integrated and utilized with novel knowledge of the anatomy and device tissue interactions. I then go on to describe how the use of pre-clinical bench top and physiologically relevant test methods needs to be utilized to understand not only how a transseptal or atrial septal occluder device would function in a broad range of human cardiac

anatomies, but also how pathophysiological cardiac anatomies will affect the delivery of a given interventional therapy. Finally, Section IV will discuss what sorts of holes, induced defects, or malformations can be elicited within the human atrial septum as a result of septal manipulations with cardiac transseptal devices. This section will begin to address the lack of information surrounding the atrial septal biomechanical properties and specifically how these properties relate to different types of transseptal equipment by testing the puncture, tenting, and tensile forces of the septum when exerted upon by these devices.

Section I: Anatomy and Disease States

Section Preface

This section will cover a review of human cardiac atrial septal anatomy, along with how these structures can change due to disease processes. It provides an essential knowledge base to have for a detailed understanding of cardiac anatomy and how it interplays with cardiac medical devices. For any intravascular cardiac medical device to go to market, there must be 1) a clinical need 2) a device to fit the need, and 3) accepting anatomy, for the device to function safely and correctly. Without these essential requirements, any medical device will likely not be fully developed, may not be accepted by the users, or worst case scenario could cause a fatality. This means it is imperative to critically understand the associated human anatomy, be it normal or abnormal, and understand how these anatomies need to be or might be altered in order to create safe and effective treatments for the patients.

Additionally, it is important to be aware that human cardiac anatomy is not static and that it can change over time. In the pediatric population this is even more important because of the exceptional growth that is occurring. Therefore, it is necessary that the ever changing anatomy and physiology of any cardiac structure you are investigating, needs to be thoroughly understood before a successful device can be created and tested. In the next several chapters of this thesis, the important anatomy regarding the atrial septum will be discussed along with the physiological functions of these structures and how an inherited congenital defect can alter these functions. In the final chapter of this section, I will present a paper that evaluates the relevant changes in human atrial anatomy that commonly occurs in response to a particular disease state.

Chapter 1: A General Review of Atrial Septal Anatomy

Stephen A. Howard
Department of Biomedical Engineering and Surgery

Chapter Preface

Treating cardiac conditions or abnormalities requires a thorough understanding of their underlying anatomies and physiologies. Additionally one needs a keen working knowledge of any existing underlying disease mechanisms to better design devices therapies for a broad spectrum of patients. So to begin such a discussion, a brief review of normal cardiac structures and functions will be presented followed by several examples commonly existing medical conditions where alterations of cardiac anatomy and/or physiology can cause potential clinical symptoms/sequelae. Finally, a discussion of the human cardiovascular anatomies (peripheral and cardiac) that have relevance on the delivery of percutaneous cardiac medical devices will be presented. The large variations within human cardiac anatomies typically drive the design of cardiac devices that need be highly reliable under the rugged, dynamic, conditions of the beating heart. This means that the normal as well as the anomalous anatomy must be fully understood so to deliver the highest quality therapies to all patients requiring cardiac medical therapy that utilizes such devices as a simple delivery sheaths or diagnostic catheters, or even more complex devices used in the placement of implantable cardiac valves.

Cardiac Anatomy

Normal Cardiac Perfusion

In normal functioning adult hearts, the circulatory pattern can be considered as fairly straight forward with blood moving in series between the left and right sides of the heart. The mammalian heart is a four chambered organ responsible for circulating blood throughout the body with two chambers on the left and two on the right side. The basic function of the heart is to pump and circulate blood throughout the body to deliver oxygen and nutrient supplies and also return the blood to the lungs for re-oxygenation. To accomplish this efficiently both at rest and under high work conditions, there are many things that must work flawlessly and in synchrony. Prior to discussing the intricacies of atrial septal anatomies and their implications on device design and delivery, as it relates to this thesis, a detailed discussion of overall cardiac form and function is required.

Starting with the venous system, blood returns to the heart from the systemic circulation via both the superior vena cava (SVC) and the inferior vena cava (IVC), where then enters into the right atrium. The right atrium has another important inlet where blood from the coronary venous system is returning called the coronary sinus ostium (CS Os). The blood from the right atrium both passively flows and it propelled via atrial contraction through the first atrioventricular valve (tricuspid valve). For optimal filling of the right ventricle, the atrial will contract to propel the blood through tricuspid valve and fill the ventricle, this is often known as the “atrial kick.” To move the blood out of the ventricle, this muscular chamber forcibly contracts, thereby increasing the pressure in the ventricle so that it will become higher than the pressure in the pulmonary artery and thus open the pulmonic valve (the first semilunar valve). Once within the trunk of the pulmonary artery the blood will divert into either the left or right lung where it will pass through

an extensive pulmonic capillary beds where carbon dioxide is replaced by oxygen. Following the oxygenation, the blood will flow into the left atrium via one of the four pulmonary veins (PV). It is of interest to note that on average humans have 4 PVS, however 3-5 PVs have been reported in some of the population[4].

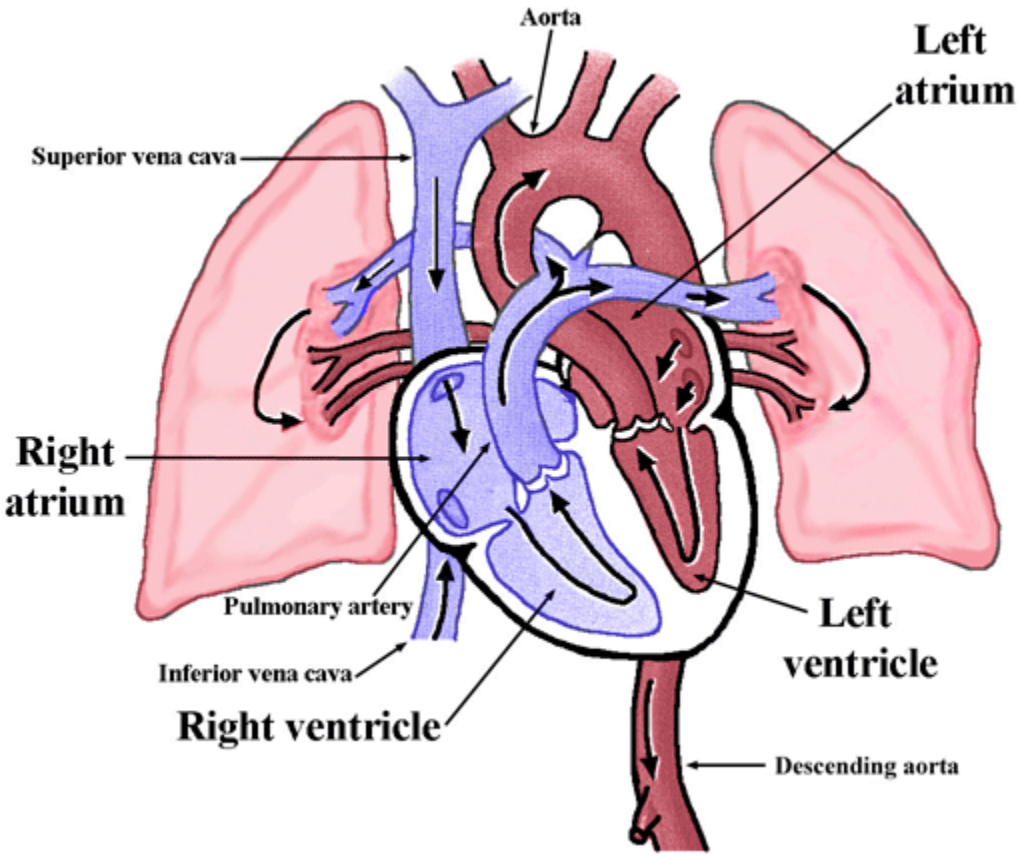

Figure 1.1: A generalized schematic of the blood flow through the human heart. The major chambers of the heart are labeled and the blue and red portions represent de-oxygenated and oxygenated blood respectively. Image from Atlas of Human Cardiac Anatomy [5].

The pulmonary veins form unions with the atrium and the locations where they intersect are called the pulmonary vein ostia. These ostia are defined as the left or right, superior or inferior ostia, and in some instances can conjoin before fully becoming part of the atrium and create what are known as common ostia.

After the blood reaches the left atrium it will flow down its pressure gradient past the second atrioventricular valve, the mitral valve, and into the left ventricle. As with the right side of the heart, atrial contraction aids in ventricular filling. When blood has passed the mitral valve and left ventricle has filled, the thick walled myocardial chamber will contract and the intra-chamber pressure will increase to the point where it will be greater than that in the systemic circulation (i.e. the pressure keeping the aortic valve closed). Once this second semi-lunar valve (aortic valve) opens, blood flows into both the systemic and coronary arterial systems. Once in the aorta the blood can either continue through ascending aorta to the systemic vascular system or during diastole, flow retrograde into the coronary arteries, so to perfuse the heart with blood. Once in the arterial system the blood will travel through smaller and smaller branch vessels, until it reaches the capillary network of a given organ. At this point blood begins its return path back to the right atrium via the venous system which is comprised of smaller vessels coalescing together to form larger ones.

This flow pattern is generated from the differences in pressures that are created during systole and diastole. Each chamber of the heart and the vasculature has different blood pressures. The right side of the heart has lower pressures than the left side and the aorta has the highest mean pressures compared to any other portion of the circulation (Figure 1.2)[6].

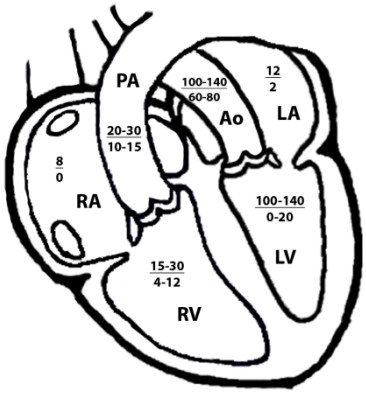

Figure 1.2: Normal blood pressure in various chambers of the heart. The pressures (or range of pressures) shown depict the systolic pressure over the diastolic pressure. RA, right atrium; RV, right ventricle; PA, pulmonary artery; LA, left atrium; LV, left ventricle; Ao, aorta.

Pediatrics Cardiac Perfusion

The normal circulation as described above is only for the post-natal heart. Fetal circulation on the other hand, differs due to the location and return flow of blood oxygenation. Since the fetus does not have functioning lungs, the blood can be only oxygenated via the mother, which returns to the fetal heart through the umbilical cord. The oxygenated blood flows from the umbilical veins into inferior vena cava of the fetus. From there, blood then enters into the right atrium as illustrate previously for the adult heart. The right atrial blood then will flow either antigrade through the tricuspid valve or to the left heart through the septum, via the foramen ovale. The foramen ovale is a flap like structure that incorporates two primary structures, the septum primum and septum secundum. In other words in the fetus, the two septa create a passageway that remains open due to higher pressure in the right atrium than the left (Fig 1.3).

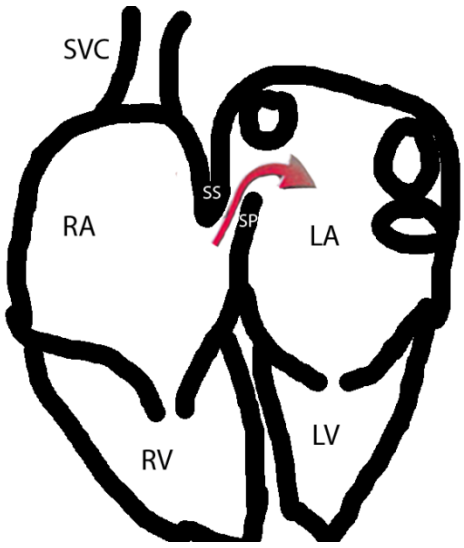

Figure 1.3: Blood flow across the atrial septum during fetal circulation. The blood is able to pass from the right atrium into the left atrium via the foramen ovale, a structure made up of the septum primum (SP) and septum secundum (SS). Due to the higher pressure in the right atrium (RA) as opposed to the left atrium (LA) in the fetus (lungs are non-functional), the flap valve of the SP remains open and allows for the passage of blood.

In post-natal anatomy, the septa are pushed together due to a heightened left atrial pressure with the increase in pulmonary pressure due to the lungs filling with air. For the first year of life this pathway can remain open (resultant anatomy is considered a patent foramen ovale). This may allow some of the blood can effectively bypass the lungs and move to the left heart to be thrust into the arterial supply[7]. However in most cases, the septum primum and the septum secundum will fuse together as one contiguous structure.

Normal Atrial Septal Anatomy

As expected, the function of the atrial septal anatomy is to separate the left and right atria. However, to clinically define the atrial septum, one must first discuss the distinction between what is considered the "true" septum and what is considered as folds or free walls of the atria. A true septum is one which if removed would create communications between the various chambers

of the heart. In contrast, a hole in an area of atrial folding, would create a communication between the chamber and the extracardiac space[8]. This distinction needs to be clear as if one were to perform a transseptal puncture too superiorly or posteriorly on what they consider the atria septum, it may in fact be a portion of the atrial wall and as a result their equipment will traverse into the pericardial space instead of the left atrium.

The true anatomy of the atrial septum includes the structures of the fossa ovalis, which is primarily composed of the flap valve of the oval foramen. This flap valve is a derivative of the fetal structure known as the septum primum. The other portion of the true septum lies anteriorly in a true anatomical sense, and is the anterior muscular ridge of the fossa ovalis which extends into the triangle of Koch. This area is considered to be the true atrial septum since superior to the flap vale is the fetal structure of the septum secundum which is essentially atrial muscular and fat tissue folded in to create this muscular ridge (Fig 1.4). This area directly connects to the insertion point of the superior vena cava into the RA. The posterior portion of the atrial septal wall is bounded by the posterior free wall of the RA, behind which lies the connection point between the right pulmonary veins and the LA. Directly inferior to the fossa ovalis is the inferior caval vein junction with the RA. Inferio-anteriorly to the fossa ovalis is the coronary sinus ostium (cardiac venous inlet) and directly superior to that is the triangle of Koch and the anterior muscular septum[9,10]. Arguably, the most important associated structure related to human atrial septal anatomy is the aorta. As noted above, this vessel carries the highest pressures of all of the parts of the normally functioning heart, and if compromised this could lead to fatal outcomes [11]. The aorta lies directly behind the right atrial wall anterio-superiorly to the fossa ovalis (Fig 1.5). In chapter 7 I will discuss how the aorta may become compromised with percutaneous cardiac interventions.

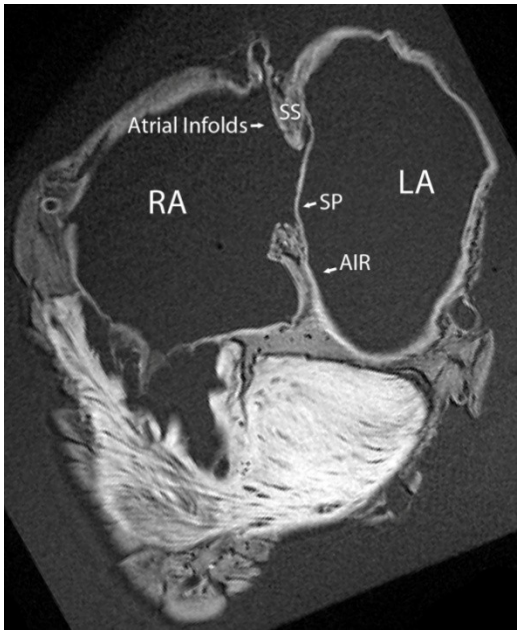

Figure 1.4: Long axis view of the atrial septum. In the figure the atrial septal wall separates the right and left atrium (RA and LA). The structures associated with this divide include the septum primum (SP), anterio-inferior rim (AIR)

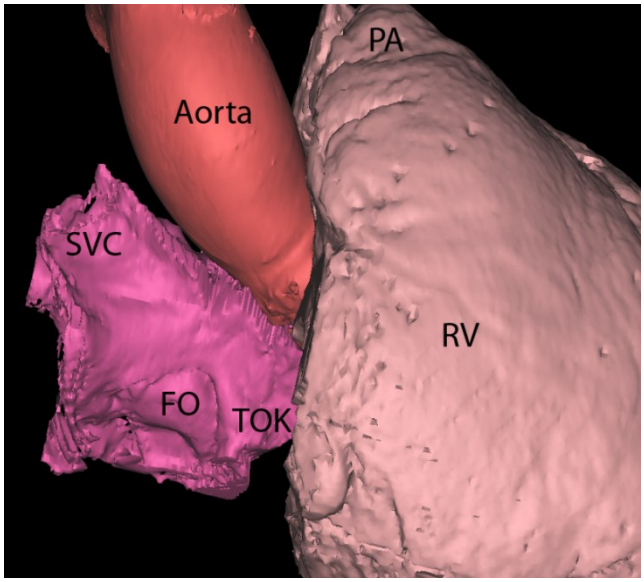

Figure 1.5: Attitudinally correct anatomy within a human heart, specifically indicating the relative location of the atrial septum in relation surrounding structures. This 3D reconstruction of a nromal human heart illustrates the location of the fossa ovalis (FO) to the anterior rim which becomes the triangle of Koch (TOK). Superior to the fossa lies the superior vena cava (SVC) and anterio-superiorly the aorta. Other structures including the right ventricle (RV) and pulmonary artery (PA) are depicted as well.

Anomalous Anatomy of the Interatrial Septum

The atrial septum is prone to congenital abnormalities, namely atrial septal defects (ASDs). These defects have been found to present themselves in a number of different fashions. Ostium primum, septum secundum, sinus venosus or caval defects will result in primary ASDs (Fig 1.6) [13] . Fortunately, the prevalence of these defects within the adult population in relatively low, with only 20% of those living with congenital defects having such a condition. This roughly correlates to about 0.4%-0.05% of the total human population[14–17].

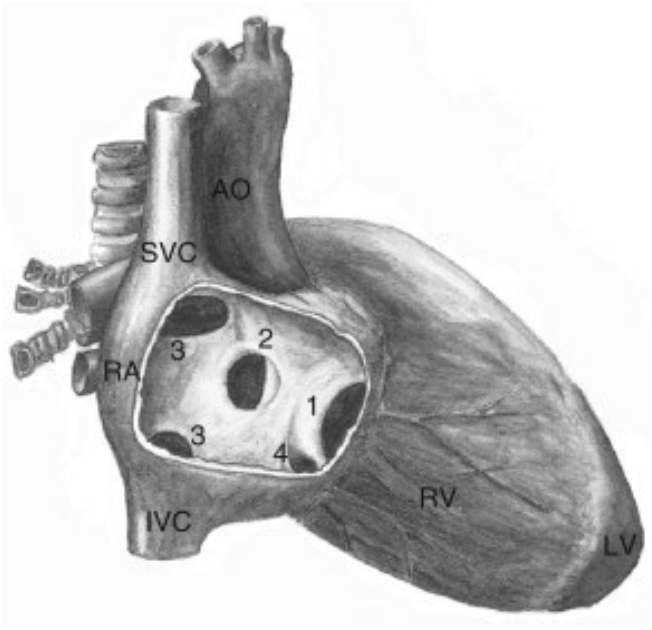

Figure 1.6: Locations of common atrial septal defects. The septum primum/secundum defects (2) are generally found in the area of the fossa ovalis. Caval and sinus venosus defects (3 Upper and lower respectively) will allow drainage of the pulmonary veins into the RA. Figure from [18]. *Reprinted from International Review of Research in Mental Retardation-Volume 39, Vis J. C., Engelen K. Van, Bouma B. J., Bilardo C., Blom N. A., and Mulder B. J. M, "Cardiovascular Disorders among Persons with Down Syndrome," pp. 165–194, ©2010, with permission from Elsevier.*

For the interest of this thesis, I have chosen to focus the following review primarily on defects pertaining directly to the floor of the fossa ovalis which is the structure that arises from the septum primum in the atrial septum. The primary issue with these defects is that the emboli that can form in the venous system like deep vein thrombosis, have the potential to cross the atrial

septum by means of the defect and get into the arterial blood supply[19]. This could potentially cause a fatal infarct in the brain or heart. However, under normal pressures in a healthy heart, the pressure is greater in the left atrium than the right atrium. This creates a shunt between the atria that goes from the left to the right. It is only under abnormal physiology that the pressure would be greater in the right atrium and effectively reverse the shunt direction and go from the right to the left asseen with the Valsalva maneuver (Figure 1.7) [20].

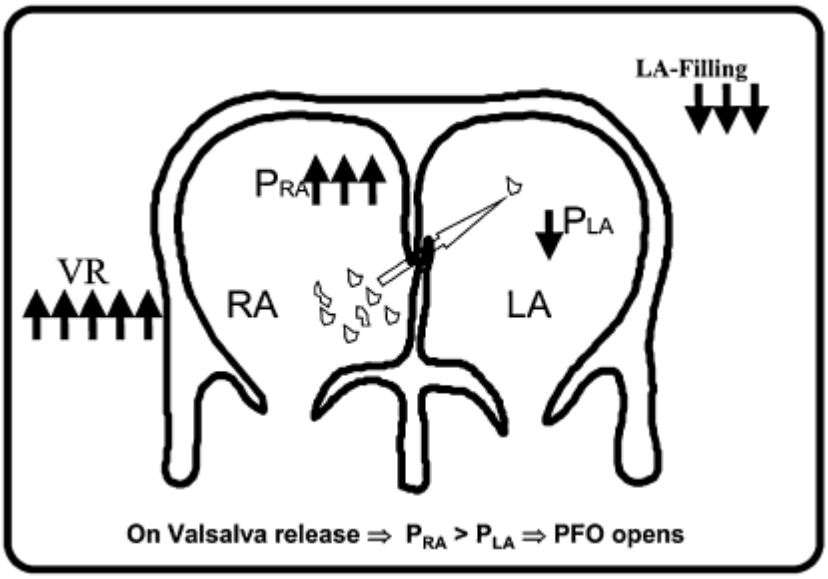

Figure 1.7: Graphical depiction of the pressure changes during the Valsalva maneuver. Normally the PRA < PLA but by performing this procedure, the blood flow can shift to go left[20]. *Reprinted with Permission from Oxford University Press on behalf of European journal of echocardiography © 2007*.

The most dominant form of atrial malformations is the presence of a patent foramen ovale. About 25% of the population have what would be considered a probe patency of the atrial septum[7,16,21]. This is when the septum primum does not fully fuse with the septum secundum. In common terms it is referred to as a 'secundum defect', however this is not aptly named since the defect is generally not due to any deficiency within the septum secundum but rather a non-adherence of the septum primum to it. The reason for the terminology comes from the fact that it is found on the superior side of the flap valve of the fossa ovalis which is where the septum

secundum lies[10]. The full description of a probe patent foramen ovale, including size and shape, will be presented in chapter 5.

Importance to Medical Treatment

The atrial septum is a common landmark when considering percutaneous cardiac therapy. Due to its location and ease of access, it is often used as a delivery route for medical therapy[22,23] or even the site of device treatments[24–27]. The fascination of the fossa ovalis as an access route has been around since the early 1960s [22,28] since it allows for access to the left atrium via the venous system. Some of the issues with passing catheters through the arterial system are maintaining hemostasis under higher blood pressure, potential for worse complications associated with thrombus formation and a more tortuous access route to obtain access to the left atrium (LA).

When utilizing the atrial septum as an access route to the LA, the catheters have to cross the atrial septum and perform a procedure called a transseptal puncture (TSP). In this procedure a sheath is advanced via the venous system, generally through a femoral access point [28], though in recent years subclavian access has been utilized in special cases [29]. The fossa ovalis is visualized and the sheath will begin to tent the thin membranous structure whereupon the needle will be advanced and puncture the septum, creating a hole through which the delivery sheath system can pass into the LA [23]. A thorough description of the TSP method and indications will be described further in chapter 7.

Once access to the LA is obtained then the medical treatment can begin; initially this procedure was primarily use for pressure monitoring of the left atrium [22]. This procedure

became outdated when more advanced methods for pressure detection were created, but the technique has in recent years become more popular for medical therapies. Currently a transseptal puncture can be utilized in procedures for cardiac ablation procedures (both atrial and ventricular)[30], mitral valve repair or replacement[31], closure of the left atrial appendage[32], fixing perivalvular leaks in the mitral valve, endocardial pacing[33,34], and ventricular assist device placement [35].

Another medical treatment that involves the atrial septum is an atrial septostomy. The goal of the procedure is to perform a TSP and inflate a balloon within the LA. The balloon is retracted through the atrial septum, thus ripping and creating an atrial septal defect (ASD) [36,37]. This procedure is primarily for patients with severe pulmonary hypertension [37,38]. This allows for blood flow to go from the right atrium to the left atrium and decompress or reduce the pressure on the right side of the heart. Obviously there is the issue of creating a hole in the septum and having potential issues of emboli crossing into the arterial stream, but in these patients, the hypertension outweighs the risk of the potential emboli.

Repair of Atrial Septal Defects

Most of the time, an ASD is not a favorable consequence of a TSP procedure. One of the downfalls of all of these treatments is that the mere act of performing the TSP creates holes in the atrial septum. This defect that has been created is not anything new for physicians, they have been dealing with incompetent septa since the 1950s [39,40]. Due to the advances in catheter technologies the congenital defects that were presented above along with these iatrogenic atrial septal defects (IASDs), which are holes in the septum as a result of procedures involving TSP, are able to be repaired by a number of atrial septal occluder devices (Fig 1.8). The placement of such

devices is a simple procedure in which the catheter is passed through the septal defect, then by some mechanism sandwiches the ASD with a disk or sheet on both sides of the defect.

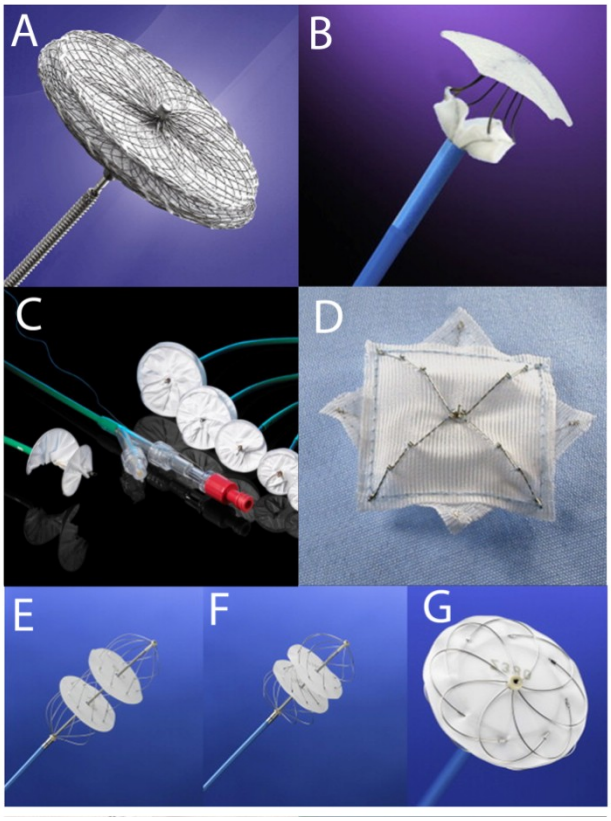

Figure 1.8: Current devices for ASD closures. (A) Amplatzer septal occluder (B) Atriassept ASD Device (C) Gore HELEX septal occluder (D) CardioSEAL device (E-G) Solysafe Septal Occluder open to fully closed. Images obtained from [41]. *Reprinted from Progress in Pediatric Cardiology, Vol. 33, Albers E, Janssen D, Ammons D, and Doyle T, Percutaneous closure of secundum atrial septal defects, 115-123, ©2012, with permission from Elsevier.*

Chapter 2: Anatomical Variations in Diseased Hearts

Preface

Cardiac anatomy can be highly variable from patient to patient. The differences can be due to patient phenotypic differences, lifestyle conditions or medical history. Understanding the differences that are created when someone has a cardiac condition will help in treating this population.

Multiple studies have worked to determine anatomical and physiological differences between normal and diseased hearts [42]. Some of the primary causes of cardiac morphology changes related to disease states include hypertension[42], myocardial changes (eg. Ischemia or dilation), valvular stenosis or incompetence, and cardiac rhythm disorders [42–45].

From the standpoint of a biomedical engineer, the generalized anatomy of the heart is in many cases insufficient for creating percutaneous cardiac medical therapies. Engineers are challenged to design devices for diverse hears that may be sick, many times are enlarged, have had previous surgeries, or even hearts presenting with congenital anatomy. Thus, the devices that they are creating must be able to accommodate and take into consideration all of the anomalous anatomy their device may encounter.

For instance, a percutaneous heart valve replacement may be placed in a valve that is insufficient due to excessive calcification. This greatly decreases the orifice area in which the new valve can get across or even the amount of space that is available after it has been delivered. A surgeon performing a similar procedure, however, has the ability to remove the leaflets

completely and therefore get rid of any interactions of the new valve with the calcifications (ie. causing blockage of the coronary arteries or creating emboli from fragmentation of calcium nodules). Between these two surgeries, the end result is to replace the faulty valve with a new fully functional one. However, there are limitations placed on the device in either case and the percutaneous valve implantation will be very different from the surgical replacement valve. These slight variations in anatomy and procedural approaches have to be accounted for when designing such devices.

With this motivation we studied a population of anatomies from patients with a particular cardiac disease which has been shown to elicit remodeling in the anatomy. These specimens were diagnosed with atrial fibrillation (AF) [46]. For the purpose of this dissertation, it is important to note that this population often undergoes atrial septal manipulations including transseptal punctures (TSP) or atrial septal ablations. This brings relevance to the issue of cardiac remodeling in AF patients as it pertains to the atrial septum.

Cardiac Remodeling as a Consequence of Atrial Fibrillation: An Anatomical Study of Perfusion-Fixed Human Heart Specimens

Christopher D. Rolfes, BA[1,2]
Stephen A. Howard, BA[1,2]
Ryan Goff, BS[1,2]
Paul A. Iaizzo, PhD[1,2,3]

Department of Biomedical Engineering[1]
Department of Surgery[2]
Department of Integrative Biology and Physiology[3]
University of Minnesota
Minneapolis, MN

This paper has been published in the Journal of Geriatric Cardiology
2011, Volume 8, Issue 3, Pages141-146

Background Atrial fibrillation (AF) causes a continuum of atrial anatomical remodeling.

Methods Using a library of perfusion fixed human hearts, specimens with atrial fibrillation were compared to controls. During this preliminary assessment study, direct measurements were taken of atrial volume, pulmonary vein (PV) circumference, and left atrial wall thicknesses.

Results Hearts with AF typically had larger atrial volumes, as well as a much larger variation in volume compared to controls (range of 59.6-227.1mL in the AF hearts compared to 65.1-115.9mL in control). For all hearts, right PVs were larger than left (mean 171.4 ± 84.6 for right and 118.2 ± 50.1 for left, $p < 0.005$). Left atrial wall thicknesses ranged 0.7-3.1mm thick for both AF and control hearts.

Conclusions Hearts with AF had a large range of sizes which is consistent with the progression of atrial remodeling during AF. The large range of thicknesses will influence the amount of energy needed to create transmural lesions during ablation procedures.

Keywords: Left atrial dimensions, volumes, pulmonary vein ostia, atrial fibrillation

Introduction

Atrial fibrillation (AF) is the most prevalent tachyarrhythmia, with a prevalence of 1% in the general population [47]. One of the particular clinical features of this arrhythmia is its self-perpetuating nature. Paroxysmal AF (self-terminating episodes) may eventually turns into persistent (> 7 days) and then even permanent AF [48–50]. This progression is considered in part, due to both structural and electrophysiological remodeling of the tissue that provide substrates for maintenance of such arrhythmias. Structural remodeling associated with AF refers to physical changes, such as dilation of the atria and interstitial fibrosis. The electrophysiologic remodeling

results the shortening of the atrial effective refractory periods, thus aiding the perpetuation of an arrhythmia and/or limiting the ability to terminate fibrillations. More specifically, the self-perpetuation is especially disturbing symptom when patient long-term prognosis is taken into account: mortality rate doubles and stroke occurrence averages up to 5% per year in patients with AF, which is 2 to 7 times the rate of individuals of similar ages whom are uninflected with AF [50].

The prevalence of atrial fibrillation in relation to age and associated risks

The clinical treatment of AF is an especially relevant topic in geriatric cardiology due to the well documented increasing prevalence with age. When considering an overall general population, the relative prevalence of AF is 1%, yet in persons over 40 years of age the prevalence reaches 2.3% and then climbs to 5.9% for individuals over 65 [51]. The geriatric population, defined by the WHO as persons with age greater than 65, contains over 75% of people suffering from AF [47]. It should also be noted that AF has also been found to be more common in men than women (1.1% versus .8%) [47].

Atrial fibrillation is well known to be associated with decreases in quality of life: as reported by as many as 68% of patients with paroxysmal AF [52]. Interestingly the psychological, not physical, quality of life may be impacted more [53]. In addition to stroke [50], AF has also been associated with many other health problems that would cause decreases in quality of life such as depression, professional and sex life complications [54], etc. However, it is debated whether or not AF is or is not associated with cognitive decline [55–57]. It is highly probable that because AF causes an increased risk of stroke and emboli, that cognitive decline in part be linked

to the potential for multiple small and transient cerebral infarcts, yet this will also be dependent on the given patient and their anticoagulation management [58].

In addition to the above detrimental effects of AF, anatomical remodeling of the atria can occur within the heart. Patients who have AF tend to have larger left atria and larger pulmonary veins which could potentially lead to the further propagation of AF [4]. Alternatively, the reverse has also been shown: upon return to sinus rhythm after radiofrequency ablation, there is a measureable reduction in left atrial size [46,59]. Depending on the length of AF and the stage of remodeling, patients with the arrhythmia may have large variation in their anatomy.

Left Atrial volume measurements

Heart left atrial (LA) volumes have been selected here to be measured in this sample of perfusion fixed human hearts, due to reported AF related atrial remodeling (dilations). For example, the work by Leung et al. found that increases in LA volumes could be used to independently predict the increased risks of cardiovascular death, heart failure, AF, stroke, or MI [60]. Further, subsequent reductions in LA volumes (reverse remodeling) has been found to be a strong predictor of the successful treatment of AF using either catheter based [61] or surgical [62] ablations. Relative LA volumes for a given patient have also been found to predict the potential for recurrence of AF after cardioversion [63] and conversion of atrial flutter to AF after successful ablation [64]. More specifically, the probability of relapse after catheter ablation was found to be significantly higher for LA volumes greater than 145 ml [61]. LA volume index greater than 135 ml/m2 was found to have 100% specificity and LA diameter greater than 60mm was found to have 100% sensitivity for prediction of surgical Maze failure [62]. Not surprisingly, normal LA volumes have been found to be associated with absence of thrombus [65] and relative

LAA dimensions have been found to be a positive predictor for stroke/TIAs in patients with AF [66].

Pulmonary vein sizes

Since the clinical discovery that the pulmonary veins (PVs) can be substantial site-sources of ectopic beats [67], PV anatomy has attracted increasing attention. A patient's pulmonary vein sizes are useful measurements when planning for an ablation since some procedures, such as cryoballoon ablation, offer multiple sized devices to optimize PV isolation. The PV circumference was chosen because even though the PVs (especially the left PVs) are typically oval in shape [68], they are also considered as compliant and a balloon pushed against the ostium will slightly change its shape. In other words, using simply the long or short axis for planning may lead to the decision to use a balloon that is too big or small, respectively.

Left Atrial Wall Thicknesses

Left atrial wall thicknesses are also commonly assessed and were done so here as well. The area on the posterior wall near each of the PVs was measured as well as the center of the posterior wall. These locations were selected not only because they are smooth in comparison to the left atrial appendage, but they are often areas of therapeutic focus during AF ablation procedures. Variation in LA wall thicknesses is also important to consider during radiofrequency ablation procedures, since it should influence the amount of energy to be applied [69].
One of the primary goals of this preliminary assessment study is to present our ongoing investigations as to human cardiac anatomy. Our Visible Heart® Laboratory has a current library of over 200 human heart perfusion fixed specimens that we can uniquely employ for such investigations. In addition, many of our obtained images are and videos of functional cardiac

anatomies are available to the general public, via our free-access web site, “The Atlas of Human Cardiac Anatomy” (http://www.vhlab.umn.edu/atlas).

Methods

Human hearts deemed not viable for transplantation were donated for educational and research purposes. Following similar guidelines for transplantation, the hearts were stopped, cooled and transported to our lab. Within 24 hours of being excised, these specimens were weighed and the aorta, superior vena cava, pulmonary artery, pulmonary veins and the inferior vena cava (when possible on a given specimen) were cannulated and attached to a perfusion fixation chamber as described previously [70]. This approach will preserve the hearts in a modified end-diastolic state (fully expanded atria and ventricles). These hearts were fixed with 10% formalin in PBS solution for at least 24 hours under normal physiologic pressure and then stored in formalin.

Heart specimens have been collected and added to our library since 1997 and to date the library has grown to over 200 in the collection. Anatomical studies can be performed on this large collection so to better understand the variation in anatomy between different hearts. For most of such specimens, pertinent clinical histories are also available, thus allowing us to assess the variation in anatomy with respect to the relative disease state of the heart. In the present study, we identified and used hearts that had a clinical diagnosis of AF and compared them to hearts with no indication of AF or mitral/tricuspid regurgitation (normal anatomies). The AF hearts were sex, age, weight, and height matched to control hearts. For all but 2 of this sample of 10 AF hearts, acceptable control hearts were found and/or were measureable (Table 2.1).

Table 2.1: Patient information from atrial fibrillation and their corresponding control hearts. For all but two AF hearts suitable matches were found as controls based on subject genders, ages, weights and heights for these collected specimens.

	AF	Control
n	10	8
age (sd)	69.9 ± 11.6	63.9 ± 12.5
male (%)	6 (60)	4 (50)
weight (kg)	80.8 ± 21.8	93.5 ± 31.5
CAD (%)	2 (20)	0 (0)
HTN (%)	4 (40)	5 (62.5)
Valve insufficiencies	0	0

To measure the volumes of the atria, the hearts were oriented such that the annulus of the atrioventricular valves would be parallel to the ground while measuring their respective side. To measure the volume of the left atrium (LA), the aorta and all but one PV were clamped off and the LA and left ventricle were filled with deionized water. After the LA was completely filled the water was drawn out and collected until the water level reached the level of the annulus of the mitral valve, which was determined by visualization using a fiberscope. The weight of the water was taken and this process was repeated a minimum of three times. The right atrium (RA) was measured the same way; however the pulmonary artery, inferior vena cava, coronary sinus and posterior interventricular vein were closed up and the water was drawn out to the level of the tricuspid valve. The siphoned water was weighed and repeated three times. Note, that since deionized water was used, the weight of the fluid is equivalent to the volume of the chamber.

All of the other anatomical measurements that were recorded were obtained using standard calipers or a C-clamp micrometer. The thicknesses of the LA were determined using the C-clamp at five distinct locations: the center of the posterior LA wall and the junction of the right superior, right inferior, left inferior and left superior PVs. The junction of a PV was defined as the

location in which the vein transitioned into the wall of the left atrium. To determine the relative areas of the PVs, the opening of each vessel was pinched together to measure half of the circumference (Figure 2.1) and obtain an area assuming the vessel is circular. Although it has been found in the literature that the PVs are generally oval in shape, it was decided that comparing the vessels as circular would alleviate the problem of re-approximating the oval shape of the pulmonary veins. Furthermore, in some of these cases, the PV can be slightly distorted due to the nature of the fixation process.

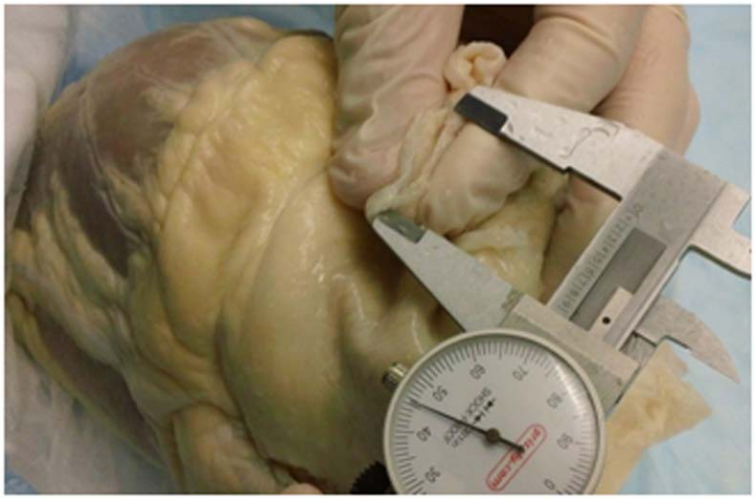

Figure 2.1: Illustration of the half circumference measurements taken to obtain diameters and area measurements of the various PVs.

The size of the fossa ovalis (FO) in each specimen was also measured; it should be noted that since the FOs were not collapsed during the fixation process, we were able to obtain accurate assessment of these structures. These areas were determined by measuring the diameters along the superior/inferior and the anterior/posterior direction of each FO.

Values presented are mean with standard error unless otherwise noted. For comparisons of continuous variables between two groups a Student's t test was used.

Results

Within these investigated hearts, as expected the AF hearts had larger LA, RA and total atrial volumes compared to the controls hearts (Figure 2.2). However when we compared individual AF heart to their specific sex, age, weight and height matched control, there was no clear correlation as to which types of heart had larger atrial chamber sizes. Yet, the data did suggest that there was a higher variability within the hearts from the AF patients compared to the controls: with a range of 59.6ml to 227.1ml in the AF hearts compared to 65.1ml to 115.9 ml in the control hearts. Note that the differences in ranges for both atria are over 3 times larger in the AF group than in the control group.

Table 2.2: The mean and median values of the pulmonary vein ostia between AF and control heart specimens.

	All PVs		Right PVs		Left PVs	
	Mean (mm^2)	Median (mm^2)	Mean (mm^2)	Median (mm^2)	Mean (mm^2)	Median (mm^2)
AF	152	139	193	170	116	109
Control	138	120	156	126	121	100

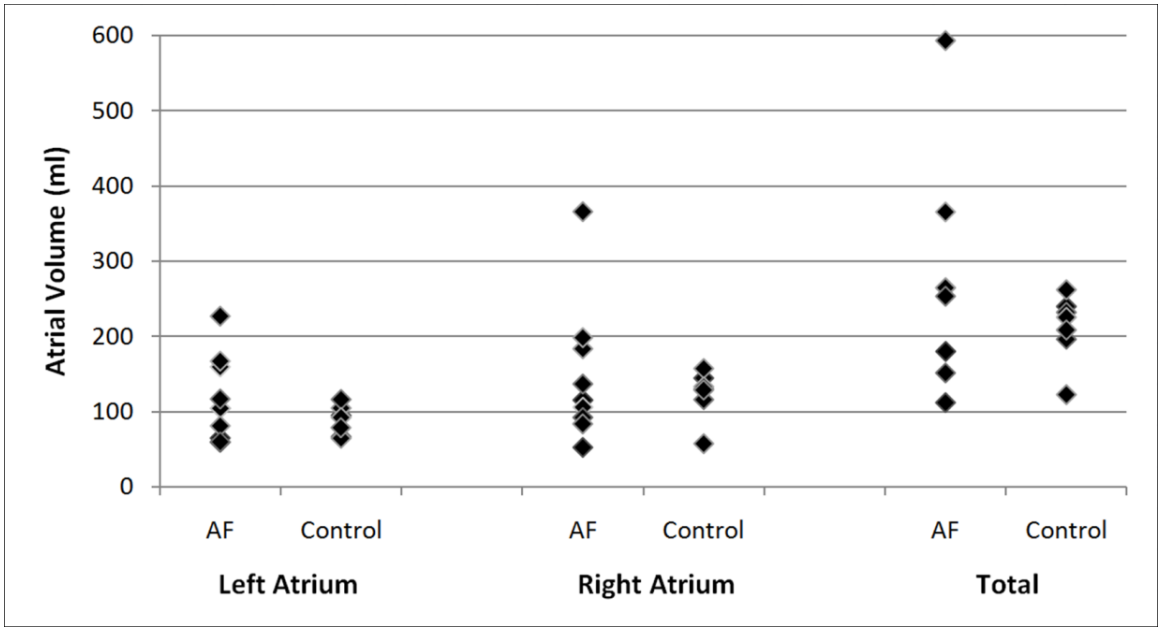

Figure 2.2: Comparisons of the paired left, right and total atrial volumes between the matched AF and control hearts. Note that the AF hearts had greater variability of volumes compared to the controls.

As noted above, the sizes of the pulmonary veins were assessed by assuming all as circular openings (Figure 2.3). Between the two groups, the control hearts had smaller PV ostia for both the left and right veins. One can observe two different peaks on these histograms; with the higher peak associated with the data from the AF hearts. This finding was consistent also when the right and left PVs were compared separately (Figure 2.3). Interestingly, there was also the observed trend that the left PVs were smaller than the right PVs in both the control and AF specimens (Table 2.2). Further, when trying to determine that the right PVs were larger than the left, while looking at the whole population of hearts, there was a significant difference seen between the two (mean 171.4 ± 84.6 for right and 118.2 ± 50.1 for left, $p < 0.005$).

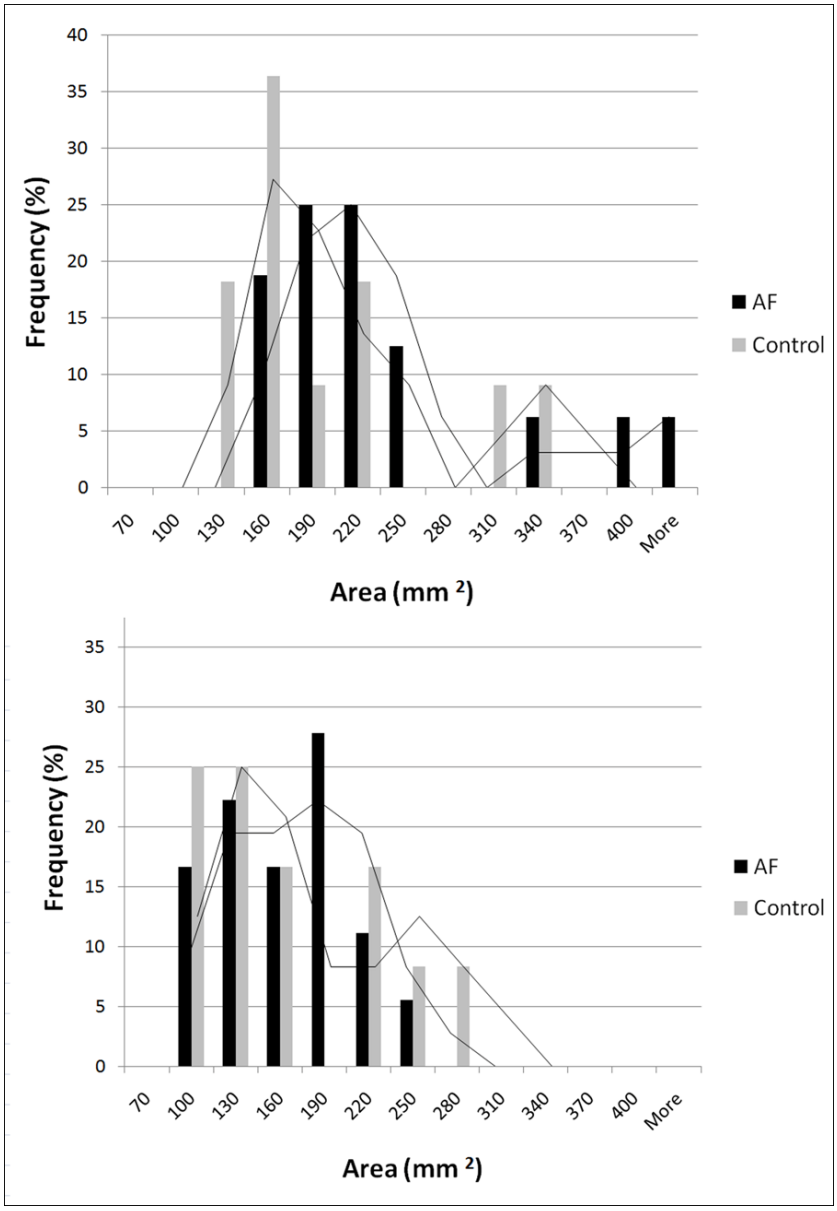

Figure 2.3: The relative variation in pulmonary vein ostia sizes between the two groups of heart specimens. The histograms provide the corresponding areas of these ostia. Top: the relative distributions of pulmonary vein sizes of the right pulmonary veins; with means of 24.2mm^2 and 21.6 mm^2 and medians of 23.1 mm^2 and 19.9 mm^2 respectively. Bottom: the left pulmonary vein areas, means of 18.7 mm2 and 19.0 mm2 and medians of 18.4 mm^2 and 17.7 mm^2 respectively. The trend lines depict the two point moving averages of the distributions and illustrate the relative differences between these two heart populations.

Although there were observed trends between the relative areas of the PV ostia of these two groups, in contrast there were minimal differences in the thicknesses of the LA walls within

our samples: the means and medians were 1.19mm and 1.24mm for the AF population and 1.26mm and 1.21mm for the control population, respectively. The histograms and population spreads between the AF and control groups appear to elicit a fair amount of overlap; in other words, they appeared similar between the groups and were not dependent upon the diagnoses of AF (Figure 2.4). Similar findings were also observed when examining the relative sizes of the FO in these hearts. The FO dimensions only had slightly larger sizes in the anterior-posterior (AP) vectors, whereas they elicited minimal or no differences in the superior-inferior vectors (SI) (Figure 2.5).

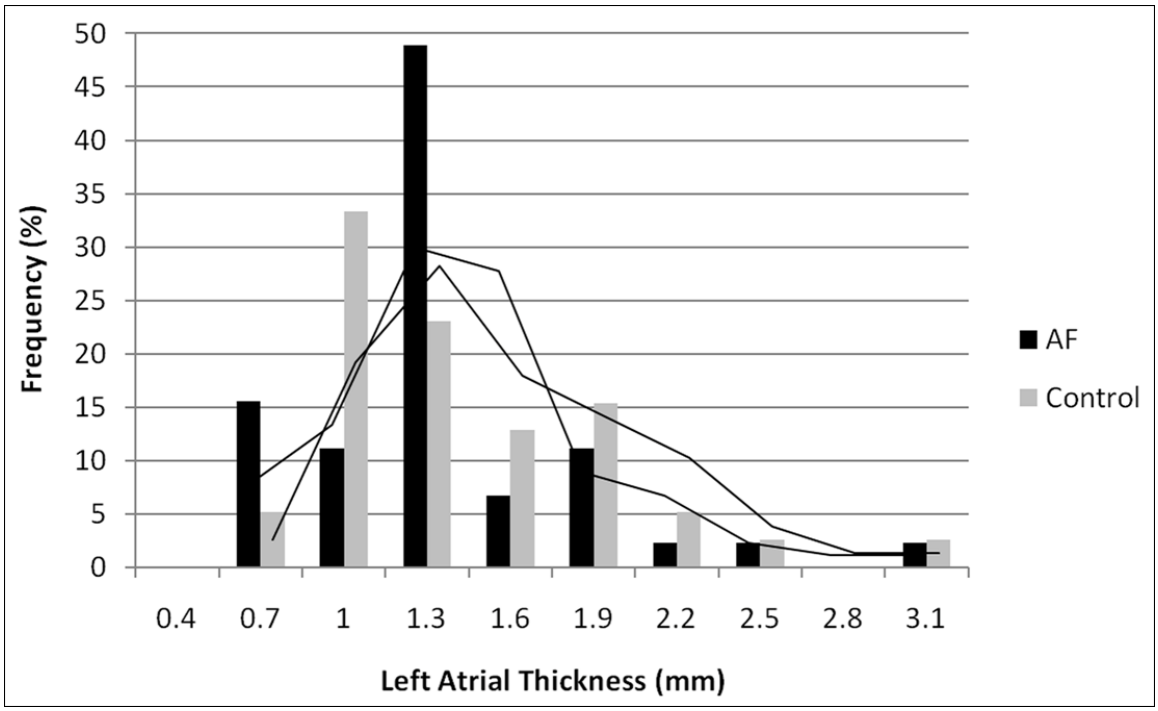

Figure 2.4: Relative distribution of thicknesses of the left atrium between the AF and control hearts. These thicknesses values were determined by taking measurements from each of the four pulmonary vein junctions in each heart, as well as the center of the posterior walls of the left atria. The trend lines depict the two point moving averages of the population distributions.

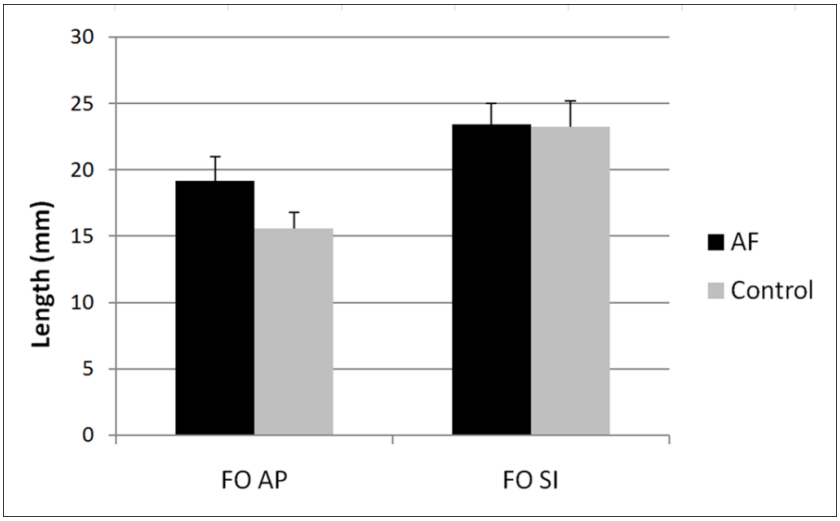

Figure 2.5: Average widths and heights of the fossa ovalis sizes between the two populations of hearts. The relative widths of the fossa ovalis were designated as the fossa ovalis anterior-posterior (FOAP) measurements and the heights were designated as the fossa ovalis superior-inferior (FOSI) measurements (error bars represent the SEs). It was observed that there were no significant differences between the calculated averages of the measurements taken of and the distributions of the sizes showed similar trends between the AF and control hearts (data not shown).

Discussion

In the present study we describe novel measurements of relevant cardiac anatomies obtained from our unique library of perfusion fixed human hearts. In this preliminary assessment study, we describe approaches to allow for the detailed quantifications of specific atrial anatomies. The presented information provides useful insight as to the changes in structure that may occur when the human heart remodels following the development of AF, and we plan to continue these studies as our relevant library of specimens grows.

Current imaging modalities, including MRI, ultrasound, and CT scans, allow for relative approximations of the volumes and sizes of the LA and RA using algorithms available in various software packages or by simply estimating diameters. Yet, it is considered that measurements of LA volumes are more accurate than diameter data, especially as a given heart dilates, i.e., small

increases in diameter will provide for larger increases in derived LA volumes [71,72]. Our volume measurements take into account the variability of chamber anatomies from heart to heart, and thus resulted in a more accurate representation of the total chamber sizes. Therefore, these chamber volumes, along with thickness measurements of the LA, were considered to better point to variations in anatomies due to a given pathological state. However based on our data on this somewhat small sample size, we could not make correlations as to the clinical state based solely on these measurements. Yet, it should be noted that even in the absence of AF, large atria are often indicative of other cardiovascular issues [73], thus in these hearts we studied from this elderly population of subjects it was likely that the non-AF hearts, or so-called controls, may have been not truly normal.

Our initial characterization of these AF hearts confirmed various trends that have been reported within current literature, such as the increased sizes of right PVs compared to the left PVs [4]. However, as with most anatomical studies a large sample set is required so to potentially produce statistically significant results. With our growing library of these perfusion-fixed human hearts, we will be able to perform ongoing anatomical studies so to better assess the differences within various populations of heart disease states or demographics. Our collection of specimens to date has allowed us to obtain useful insights as to the common anatomical features of the atria from patients with AF with a high degree of accuracy. The variety of physical specimens also allows for physician education and therapeutic device feedback as any number of devices can be placed within the hearts. The continued study of the details of human cardiac anatomy will provide further insights as to the changes in structure that may occur when the human heart remodels or reverse remodels due the presence of disease or following treatment, respectively. Though above study shows that PV measurements are not sufficient to diagnose AF, it illuminates the variety of anatomies that accompany the arrhythmia within the population. This

large variation observed in the diseased patients is important for the physicians who treat AF, the educators, and engineers who must design medical devices to fit the whole range of anatomies. Using the fixed hearts we plan to continue to employ the study methods described here to further build an anatomical database, which we hope to compare to MRI, CT and 3-D models derived from each.

Conclusion

Atrial fibrillation comes with a great deal of anatomical and physiological changes. Anatomically, the size of the atria can vary greatly, but the pulmonary veins and vena cavae do not remodel significantly. The variation in anatomy has great importance and should be considered when treating and designing devices for AF.

Section II: Optimal Visualization of Anatomy

Section Preface

As noted above, the knowledge of cardiac anatomy and general structure is pertinent information for both the clinician and cardiac device designer to posses. However, to obtain a more comprehensive working knowledge of the dynamics of cardiac movements, visualization of functional anatomy must be employed. This section of my thesis will focus on the methods and anatomical findings from the utilization of both direct visualization of functional anatomy and subsequent 3D reconstructions of these anatomical features. As presented in the previous section, anatomical differences can be seen and must be appreciated associated with different patient disease populations such as atrial fibrillation. In the following text I will present several observed cases employing these unique visualization methods so to characterize various cardiac malformations, be they congenital or procedural in nature.

Chapter 3: Visualization of Anomalous Human Cardiac Anatomy

Preface

When studying and attempting to better understand cardiac anatomy, the first sources people typically turn to are anatomical reference books, like Netter's Atlas of Human Anatomy[12]. These contain exquisite drawings of generalized human anatomy, often portrayed in various anatomical slices and views. Their study can provide one with a strong knowledge base of static cardiac anatomy. Yet, a full appreciation of the dynamics of the functioning heart is hard to obtain from these static 2D images alone and the generalized structure presented in these anatomical text books, the models fail to depict the full spectrum of ways in which the defect may present itself due to patient to patient variability.

Furthermore, to understand how specific cardiac structures can vary between individuals, the best method currently remains to utilize cadaveric dissections. Through these studies, anatomists can identify and begin to understand the anatomical differences in population of individuals with known medical histories. Typically such cadavers will be embalmed in a fixative and the heart can be found in a hyper contracted state due to the standard methods of preservation. In other words, such cardiac specimens will often be in slightly altered anatomical states: some may contain blood clots, others will be dried out which often makes them difficult to use in some instances. Likewise, this means to study anatomic specimens can be quite costly and as such are used primarily for teaching medical students or anatomists. Therefore, my colleagues and I have considered that alternative methods to visualize cardiac anatomy would be highly desirable for the further education and assessment of the cardiac structures.

The heart is arguably one of the most functionally dynamic organs within the human body due to the flow of blood, its rhythmic contractions and relaxations, the dynamic open and closing of 4 valves and self-excitation via the conduction system. It must work efficiently and effectively constantly without failure so to avoid catastrophic consequences. With the interconnectedness of the anatomy to the proper function of a given heart, a working knowledge of how this anatomy changes throughout the cardiac cycle is necessary so to understand how a particular heart performs. Likewise, cardiac defects need be understood in the same dynamic way. More specifically, when an anomalous anatomy is present in a specimen, viewing the functioning anatomy will provide greater insight into the defect, compared to simply studying a static images or specimens if one hopes to best correct the associated complications. To that end, our laboratory has been able to utilize the Visible Heart® approach to uniquely identify particular anatomies and/or anomalous morphologies. This has allowed us and others to gain a greater appreciation for the resultant functional anatomies and how it can impact and interact with the surrounding structures and/or employed devices within [74,75].

Description of Visible Heart Methodologies

The Visible Heart methodologies and apparatus were created in 1997 by our lab. The premise behind this technology is that it can reanimate large mammalian hearts (primarily porcine, human, canine and ovine) with a clear perfusate and keep them alive and functioning for a number of hours outside of the body. The term reanimation is used to describe the state in which the heart is fully functional without the reliance on external stimulation or cardiac assist devices. Only fluid, nutrients, ions (via a modified Krebs-Henseleit buffer [Krebs]), oxygen and consistent temperature are required by these hearts to function efficiently. Essentially each isolated heart becomes active and fully functional *ex vivo* and in one sense the procedure simulates a cardiac transplantation.

Methods

Specimen Collection

The hearts are collected fresh (up to 8hrs post excision) and flushed with cooled St. Thomas cardioplegia or another heart preservation solution so that the myocytes become depolarized and unable to contract. This along with further cooling the heart to ~10 °C, minimizes the metabolic demands of the heart and helps to retain the function of the heart while it is being prepped to be placed on the apparatus. Next, the heart is cannulated with tubing connectors so that it can be hooked up to a series of fluid reservoirs that provide pre-load and after-load pressures similar to those found in the heart. The perfused fluid is maintained at approximately 37.5°C to account for heat loss from the system and thus ultimately allows the myocardial tissue to be maintained at 37°C for the experiment.

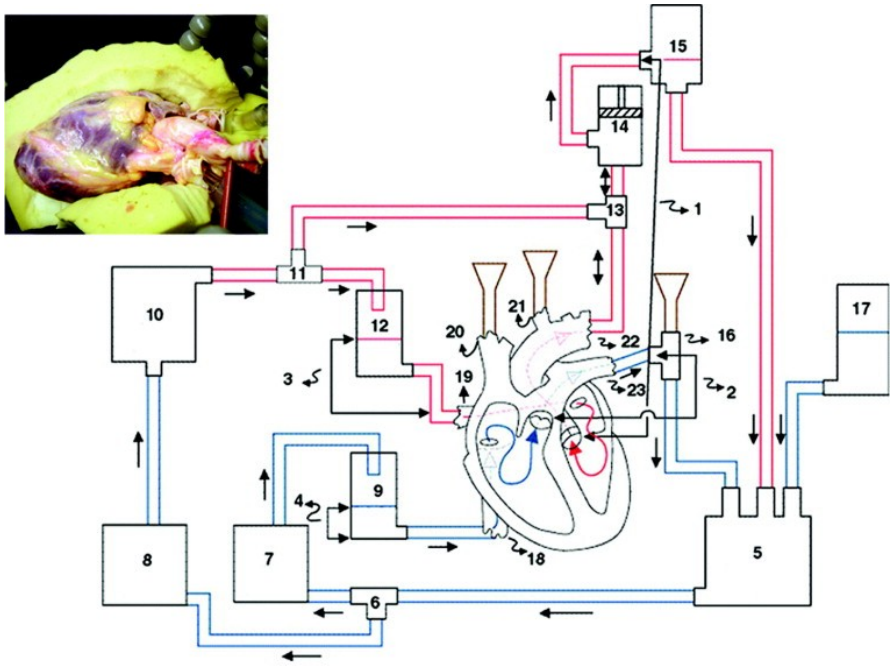

Figure 3.1: Visible Heart Setup [74]. *Reprinted from The Annals of thoracic surgery, Vol 79, Hill A. J., Laske T. G., Coles J. A., Sigg D. C., Skadsberg N. D., Vincent S. A., Soule C. L., Gallagher W. J., and Iaizzo P. A., In vitro studies of human hearts, pp 168-77, ©2005, with permission from Elsevier.*

Visible Heart Functionality

The unique functionality designed into the Visible Heart apparatus allows a given heart to function either in a standard Langendorff mode, a right sided working mode or in a full 4-chamber working mode. It should be noted that the Langendorff perfusion model has been around since 1895 [76] and is basically a method to perfuse the coronary arteries by retrograde perfusion via an aortic cannula. In other words, this method of perfusion does not allow fluid to pass through the left side of the heart as it would during normal heart function and only that going through the coronary system passes through the right side (via return flow through the coronary sinus). Yet, this means of perfusion provides a constant supply of oxygen and nutrients to the heart, which is unphysiologic, but in turn this allows for the heart to last longer on the apparatus. The "right-sided working mode" can be considered as a slightly modified Langendorff perfusion, in which supplemental buffer is allowed to pass through the right chambers while perfusing the

aorta retrograde. Hence 3-5 liters a minute of buffer can be passing through the right-side of the heart while in this partial Langendorff perfusion. The “full-working mode” allows flow pattern of buffer to pass normally through both sides of the heart simultaneously. Thus the heart relies on itself to produce a high enough aortic after-load pressure to fill the coronary arteries during diastole. It is important to note that full-working mode places a much higher metabolic demand on the heart in relation to the amount of oxygen and nutrients that it receives. This is due to the greater work placed on each chamber during active filling and systolic contractions compared to minimal flow through the heart during continuous aortic perfusion in Langendorff mode.

It should be emphasized that perhaps the most important aspect of this model is the fact that we utilize a clear buffer solution in the heart. This allows for endoscopes to be placed into the various chambers and we then can clearly see what is happening within the heart. While this is of great benefit, the issue with the prep is that the solution is water based and water cannot carry as much dissolved oxygen as blood due to the lack of hemoglobin within the red blood cells contained within. If red cells or hemoglobin were to be incorporated into this methodology, a visualization problem would occur and the cells and proteins would increase the opacity of the fluid to a point where the visualization portion of the method would become severely impaired.

Since its inception, our laboratory has reanimated over 55 human hearts. These hearts were received as donations for research from the organ donors whose hearts were deemed not viable for transplantation and with permission granted by their families. In each of those reanimations, the functional cardiac anatomy was inspected with endoscopes, which allowed for internal assessment of their unique anatomies and their pathophysiological states (Fig. 3.2). We have been fortunate to not only have studied normal anatomies, but throughout the years hearts, we have observed hearts with valve replacements or congenital defects. One such reanimation

involved a heart from a 45 yr old male that had a double orifice mitral valve. The endoscopic videos we recorded, allowed us to assess the anatomy and determine how it functioned with a connection between the anterior and posterior leaflet of the mitral valve (published study discussed later in this chapter). We also performed histopathologic studies on this heart as another means to assess the relative nature of the valve and the particular anatomy of the double orifice mitral valve (Appendix A). It should be noted, that there are surgeries and devices currently available to create this sort of cross bridge across the mitral valve to help fix mitral insufficiency, and by discovering this congenital defect we showed that there are anatomies that currently exist and may not result in clinical complications due to the leaflet fusion.

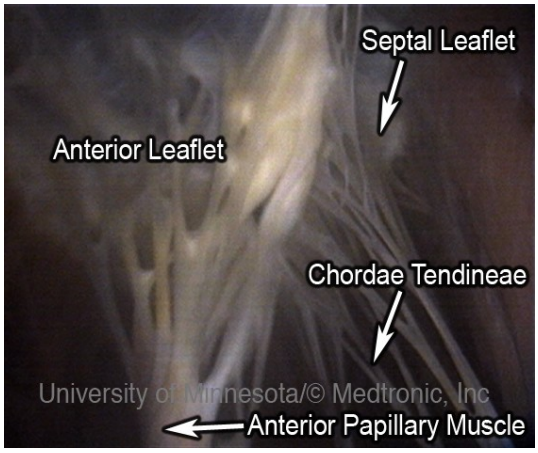

Figure 3.2: An example picture of internal anatomy seen by endoscopic imaging. The tricuspid valve is seen here with the two distinct leaflets and chordae tendineae. As the heart functions the movement of the valve is captured and can be further analyzed following the study.

Specimen Fixation and Post-Imaging

Additonally, the human hearts deemed not viable for transplantation were donated to our laboratory through LifeSource (St. Paul, MN) a local organ procurement agency or via the Bequest organ donation program at the University of Minnesota. When we recieved the specimens, we determined whether or not we would reanimate them utilizing the techniques described above. In most instances, the specimen or other factors disallowed the reanimation of

the heart. However for every heart we perfusion fixed them to preserve the anatomy for future studies.

These specimens were obtained fresh (typically within 24 hours post-mortem) and then perfusion fixed with 10% formalin in phosphate buffered saline (PBS). To do so, each heart was cannulated with standard tubing connectors. The aorta, SVC, IVC, pulmonary artery, and pulmonary veins (if present and long enough to be cannulated) were fastened to tubing connectors. Each heart was then placed in a chamber of formalin and attached to an upper chamber that fed the 10% formalin PBS solution directly into the heart at approximately 50mmHg of pressure [70]**Error! Reference source not found.**. This in turn dilated the heart's hambers to a pseudo end-diastolic shape wherein the atrial and ventricular chambers are fully expanded in a more true to form anatomical shape as compared to specimens fixed within a cadaver (Fig 3.3 & 3.4).

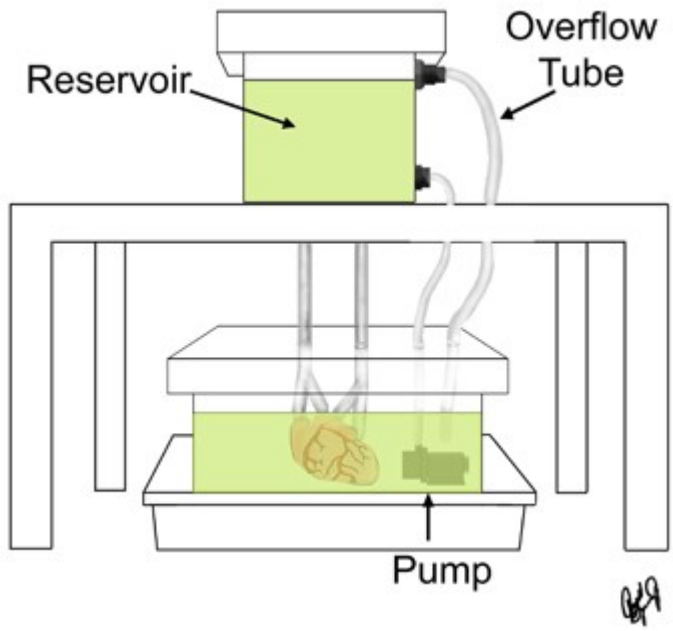

Figure 3.3: Perfusion Fixation System. Fixation apparatus use to perfusion fix fresh heart specimens in order to help maintain correct anatomy. Phosphate buffered saline with 10% formalin is circulated throughout this system to perfusion fix the hearts. The height of the reservoir is maintained via an overflow tube in order to

keep a constant pressure of 40-50mmHg that is fed to the internal chambers of the heart, effectively keeping it in a pseudo end-diastolic shape[5]**.**

The reason that it is considered to be a pseudo end-diastolic shape is primarily because the fact that technically at the end of diastole there is an "atrial kick" that will decrease the atrial volume and increase the ventricular volume. This kick is caused by the contraction of the atria which is the opposite of what is happening to the chamber in these specimens. Likewise the pressure in the atria generally is not at the level of 40-50mmHg. This pressure range is a compromise between the aortic and ventricular pressures which is generally between 60-80mmHg and 0-20mmHg respectively. This allows for sufficient perfusion of the arteries via the coronary artery ostia as well as dilation of the chambers.

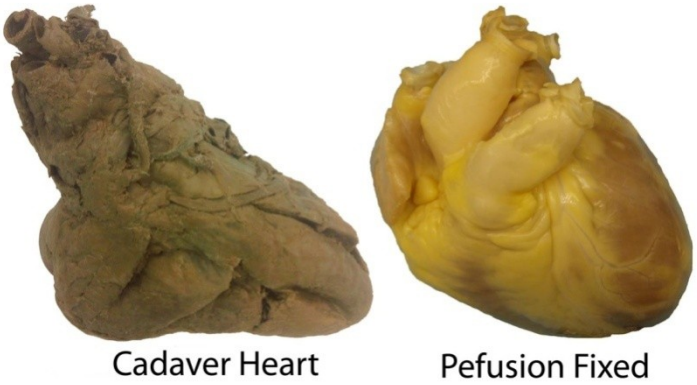

Figure 3.4: Comparison of Fixation Methods.

All fixed specimen can then be more or less be stored in formalim indefinitely. Our laboratory's library currently contains over 270 human hearts. Of these, 110 have been MRI scanned in a 3T scanner and the generated dicom files from these scans can subsequently be imported in a 3D reconstruction software, MIMICs (Materialize, Leuven, Belgium) to reconstruct the anatomy of the hearts (Discussed further in Ch. 4). These 3D generated models allow us to perform unique assessments or measurements in 3D space which can be very difficult to do with calipers or other tools placed within a given specimen itself.

Conclusion

Ultimately, both the Visible Heart methodologies, and the other 3D assessment approaches on perfusion-fixed human hearts are novel means for either viewing what goes on inside of the heart as it functions or precisely studying static anatomical feature in 3D orientations. The aforementioned anatomical approaches have been utilized in a number of studies that I will be presented in this dissertation, including: 1) visualizing a mitral valve defect (following section), 2) an ASD visualization (Ch. 4), and 3) the tenting force study (Ch. 6).

In Vitro Images of a Double Orifice Mitral Valve in a Reanimated Human Heart

Stephen A. Howard[1], BA,
Michael G. Bateman[2], PhD,
Alexander J. Hill[2], PhD,
Robert H. Anderson[3], MD, FCRPath
Paul A. Iaizzo[1], PhD

This paper has been published in *Annuls of Cardiothoracic Surgery* 2013; Volume 95 Page: 1456.

Departments of Biomedical Engineering and Surgery, University of Minnesota[1]
Medtronic, Inc., Minnesota[2]
Institute of Genetic Medicine, Newcastle University, Newcastle Upon Tyne, United Kingdom[3]

Manuscript body

By use of Visible Heart methods [74], the heart from a 45-year-old man (body mass index 30.4, preoperative blood pressure 145/70 mm Hg, heart rate 107 beats/min, regular rhythm, and normal heart tones), which was deemed not viable for transplantation to a recipient patient, was explanted to an isolated heart apparatus. Briefly, this method uses a clear Krebs-Henseleit buffer to provide nutrients and oxygen to the heart and allow for native ex vivo functionality while providing the opportunity to visualize the internal anatomy with endoscopes. Upon reanimation, the left ventricular and left atrial pressures were 95/12 mm Hg and 13/15 mm Hg, respectively, during sinus rhythm. The patient's heart had no signs of any other congenital pathologic features, and preoperative ultrasonography indicated a 65% left ventricular ejection fraction, normal chamber dimensions, and trivial mitral regurgitation. The double orifice mitral valve can best be defined as an incomplete bridge, situated toward the superior commissure of the valve and supported by the superolateral (anterolateral) papillary muscle. Shown here is a series of four screenshots of the valve in both systole (**Error! Reference source not found.** A, B) and iastole (**Error! Reference source not found.** C,D) from the left atrium (**Error! Reference source not found.** A, C) and the left ventricle (**Error! Reference source not found.** B, D). These images clearly show the fibrous connection between the mural (posteroinferior) and aortic (anterosuperior) leaflets in the central region. Interestingly, the chronic presence of the fibrous bridge in this patient had a seemingly negligible effect on overall cardiac performance. The video demonstrates functional footage of the valve.

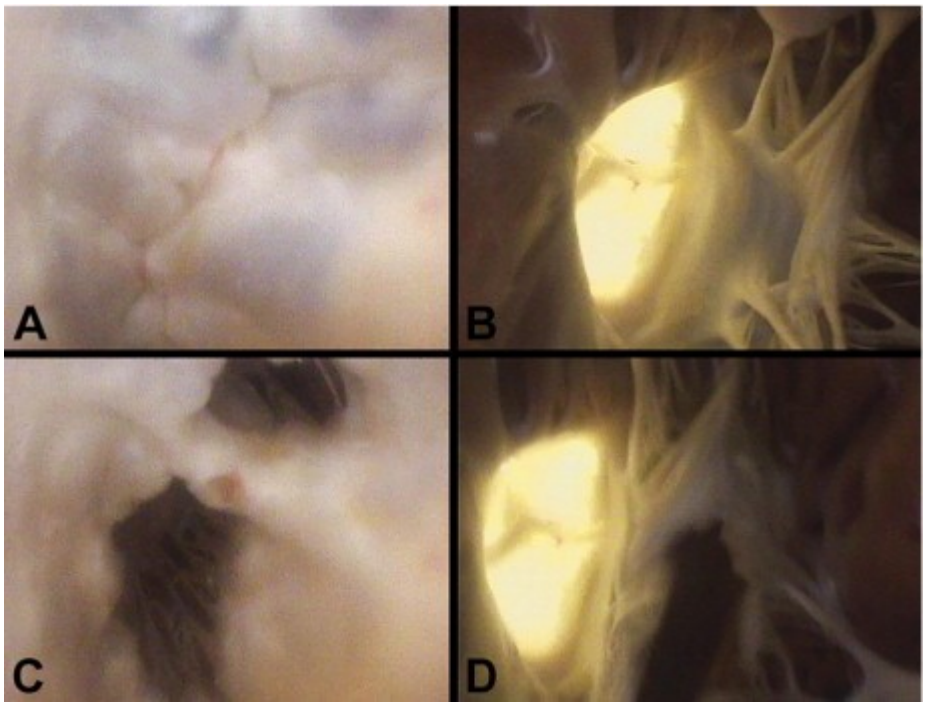

Figure 3.5: Atrial and Ventricular views of the mitral valve in systole (A and B) and diastole (C and D). The mitral valve connection can be seen clearly in C and slightly discernible as the upper portion of the MV opening in D.

Additional Images for Dual Orifice Mitral Valve

The paper presented above distinctly shows that usefulness of the Visible Heart apparatus for imaging congenital defects. Furthermore, additional imaging can and has been done on this particular anatomy along with a more complete write-up of this particular specimen (Appendix A). Three dimensional modeling was performed on the mitral valve and its subvalvular complex. In brief (and more extensively described in Ch. 4), MR imaging was performed on this heart and the images were imported into a modeling software, MIMICs (Materialize, Leuven, Belgium). With the software, the region of interest (ie. the valve, chordae and papillary muscles were segmented out and rendered in 3D (**Error! Reference source not found.**).

This produced a highly accurate rendering of the anatomy segmented out into its individual components. With the 3D image, the connection point and subvalvular apparatus anatomy shows the exact location of the defect and how the chordae connect to the leaflets within this anatomy.

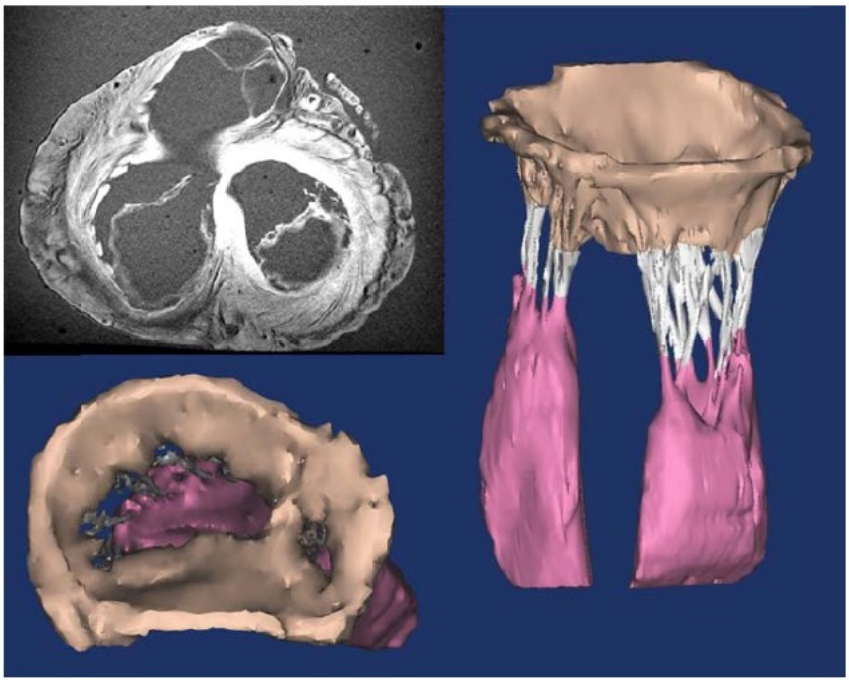

Figure 3.6: 3D representation of the DOMV. Valve (tan), chordae (white), and papillary muscles are represented in this depiction The Mitral valve connection is seen in the lower left portion of the image, clearly separating the valve into two distinct sections.

Chapter 4: Modeling Cardiac Anatomy

Preface

To understand the anatomical features of the human interatrial septa and deficiencies they may possess, novel 3D models and videoscopic imaging has be employed. In this section of my thesis, I will discuss the importance of creating these models and illustrate multiple ways in which they can be utilized, not only for education, but also for obtaining accurate measurements or clinically relevant bench top testing methods. With the increased prevalence of computer modeling both in the research and clinical settings, a large database of accurate and complete 3D models of varied cardiac anatomies need to be available. As will be discussed in the first chapter of this section, these models are very useful for making 3D measurements of volumes or distances across different image planes. On top of these utilities, the ability to create true anatomical models and utilize real cardiac anatomies for education and testing, adds unique values for the engineer trying to design a particular cardiac device. To that end I will discuss the advantages and disadvantages of these methodological approaches and how they can impact the final products usefulness.

Methods for 3D Modeling of Human Anatomy

To obtain 3D models of human cardiac anatomy we utilized our human heart library of over 270 hearts. These hearts, which have been previously perfusion fixed via methods described in Chapter 3, were MRI and/or CT scanned in order to obtain high resolution scans to reconstruct the structural and vascular anatomies.

For the MRI scans, following fixation, the hearts were embedded in a 7% agarose gel and scanned in a 3T MRI unit (Siemens Trio, Erlangen, Germany) using MPRAGE scanning sequence. This resulted in images with 0.5mm x and y pixel resolution and a slice thickness ranging from 1mm to 1.6mm depending upon the size of the heart. The resultant scans produced dicom files sets that were then imported into 3D reconstructive software (MIMICS, Materialize, Leuven, Belgium), which allowed for discrete segmentations of these images. The segmentation process involves carefully selecting the anatomy of interest (e.g. the atrial septum, or mitral valve [Ch. 3]) and producing a 3D model of the anatomy (Fig. 4.1) and here I will briefly describe the software utility and progression of creating these models.

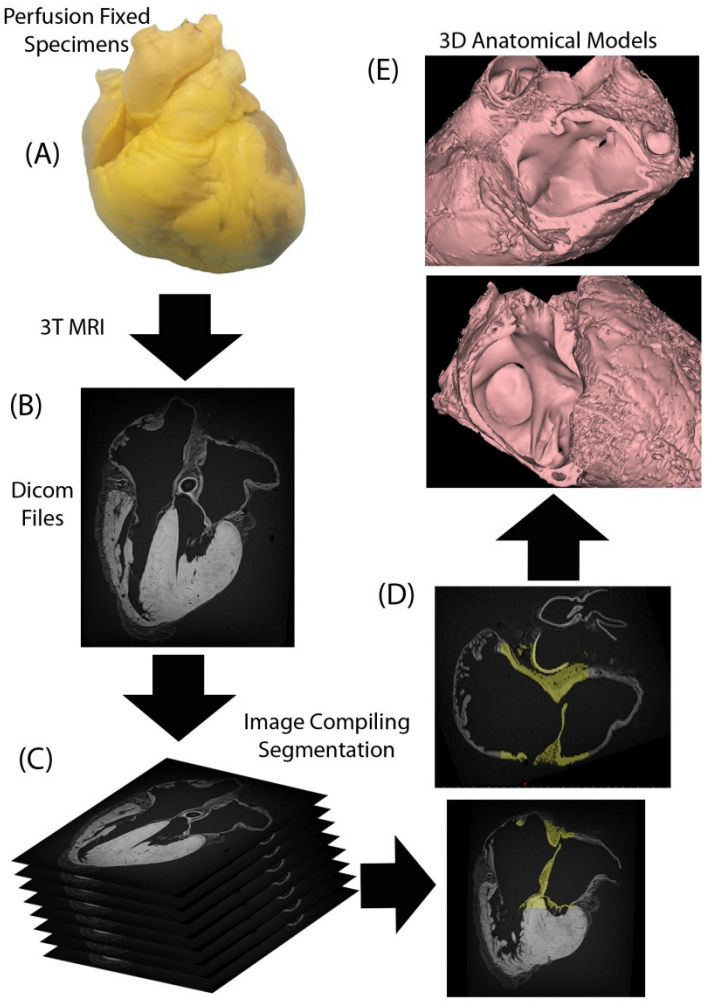

Figure 4.1: Stepwise progression to obtain 3D images of the heart. A) Human hearts are obtained and fixed in formalin. They are scanned with a 3T MRI and B) image slices between 1 and 1.6mm slice thickness are produced. C) Utilizing MIMICs software, the image stakes are compiled into a series of voxels and D) the particular anatomy of interest is selected. E) From the selection 3D models are created and allow for manipulation of the object, measurements or even printing of the object.

From the CT or MRI scans, the images were imported into MIMICs as a series of voxels with various grayscale numbers associated with each voxel. The voxel gets its dimensions from the patient scan sequence values for pixel size and slice thickness. The grayscale associated with each voxel was directly correlated with its Hounsfield units for CT scans (a term named for the inventor of the CT scanner) [77]. Ultimately the Hounsfield units are associated with the radio-opacity of the material being scanned (e.g. air will show up darker than denser material such as

calcium deposits that generally show up as white). Based on these values, different voxels can be specifically selected and segmented out from the rest of the voxels. Once the voxels associated with the given anatomy of interest has been fully selected, then the program will create a triangle mesh connecting all of the selected voxels together as the best possible fit. This creates a 3D CAD model of the anatomy selected. Because of the retention of the voxel size from the patient scan, assuming the anatomy is properly segmented out, the modeled anatomy will have the same dimensions as the actual anatomy.

From these 3D models, measurements of distance, surface area, and volume (to name a few) can be made across the entirety of the selected anatomy. I found this method to be extremely useful in that the physical measurements taken from cadaveric hearts are generally limited to 2D measurements without the use of specialized equipment (ie. a 3D microscribe or point plotter). In the next section I will discuss the usefulness of these models in the realm of percutaneous cardiac device designing and testing and follow that up with how the models can be used to better understand anomalous anatomies and also those associated with both direct and medical imaging techniques.

3D Modeling of Human Cardiac Atria for use in Bench Top Testing

Stephen A. Howard
Christopher D. Rolfes
Mark A. Benscoter
Paul A. Iaizzo

Three dimensional modeling has been considered to be very useful for medical device testing. As will be discussed in the next chapter, today medical device development requires large quantities of detailed of pre-clinical and bench top testing to 1) assess safety, 2) assess the utility of the device; 3) to understand how the device will wear, and 4) and verify that it can be easily and reproducibly deployed by the end users. Most recently, the FDA, in conjunction with medical device and drug companies, are trying to accelerate the use and advance computational modeling as a potential means to make device development more cost effective. The hope is that it will also develop an accurate way to perform initial testing and verification of devices to reduce the time to regulatory approval[78]. With this effort, the need for clinically relevant anatomical models is becoming an even greater need.

To that end, we currently utilize reconstructive software such as that described above to produce anatomical models of relevant patient scans. With this technology we have produced multiple types of bench top testing devices to better validate and improve cardiac therapies.

CT Scans

CT scans were made available through a clinical study of an investigational device. These scans are obtained with patient consent for use in research and had prior IRB approval. As such the scans can be utilized for research and development procedures. Within the patient CT database made available for this research, there were a number of patients that were diagnosed

with atrial fibrillation (AF). Those with this diagnosis were further separate into two groups: those with paroxysmal AF and those with persistent AF. The scans were contrast CT images wherein the left and right atria were brightened by the presence of contrast media in the chambers. This allowed us to segment out the blood volumes of the atria which in turn will give the internal wall topography within the two chambers (Fig. 4.2).

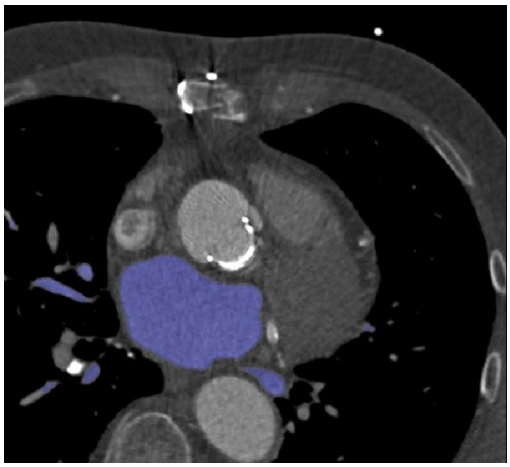

Figure 4.2: Single slice of a CT scan where the left atrium has been isolated and segmented out from the rest of the anatomy. Using MIMICs software we can create 3D models from the image slice data.

Model Creation Method

As part of my thesis and an internship, models of the left atrium (LA) were produced from each obtained patient scan using the procedure as described above. The anatomies of the pulmonary veins, LA and orientation in respect to the fossa ovalis were generated and then measured. Of this population of patient scans, those with abnormal, difficult or odd shaped anatomies were selected for 3D printing, for bench top testing purposes. Similarly representative samples from normal, paroxysmal AF and persistent AF population were generated. The primary objectives of creating these models were to 1) have anatomically correct anatomies into which catheters and devices could be placed, so to assess the maneuverability of AF ablation equipment within the left atrium and 2) to have models in which end users of the products could then utilize

and manipulate prototypes and current devices as a means to determine whether or not they fulfill the needs of the user.

After the blood volumes were segmented out and reconstructed, a shell was created around the volume, which effectively created the architecture of the endocardium. With the structures of the right and left atria put together, portions of the anterior and superior walls of the atria were removed to provide better visualization of the endocardium. The models were subsequently transferred into CAD software (SolidWorks, Waltham, MA). In the software, the fossa ovalis was located and a hole was extruded into the model, thus creating a transseptal hole for catheter access. This access would allow catheters to cross into the LA from the RA. Additionally, a tube was created off of the IVC to confine the sheath and catheters more similarly to how it would be held in the body. To finish the bench models, legs were attached on the underside of the model so to hold it in an anterior-posterior position and also to allow it to be placed on a flat surface (Fig. 4.3).

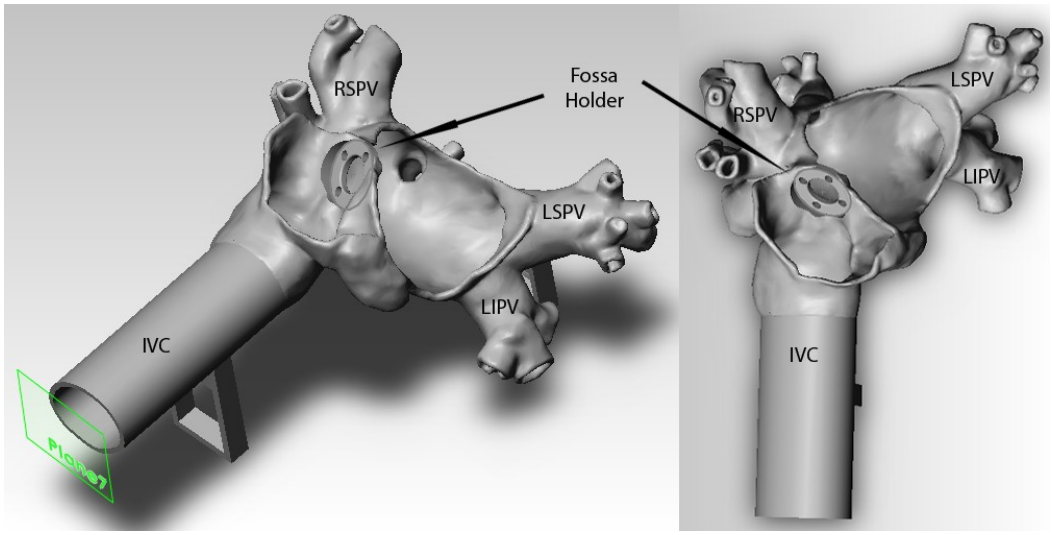

Figure 4.3: CAD model of a LA and RA with a transseptal location and extended IVC. This model was created from 3D reconstructions of anatomy via MIMICs software and imported into SolidWorks to add on additional features like a holder for a simulated fossa ovalis and legs to hold the anatomy in an anterior-posterior orientation and to fix it to a flat surface.

These computer genterated models were then printed with polylactic acid (PLA) in a 3D printer (Stratasys, Minneapolis, MN). The models that were printed had two different transseptal style holes. One model, as pictured in Figure 4.4, had two holes in the atrial septum with one placed as a high puncture location and another in a more inferior location. This allowed for the two different approaches to be tested with catheters and sheaths. In the second model iteration, as pictured in Figure 4.3, the fossa was completely removed and a holding fixture was put in its place. This holding fixture has 4 smaller holes surrounding a larger hold. The smaller holes allowed for magnets to be embedded into the fixture and another fixture was created to mate with it and sandwich a silicone membrane between the two holders. This silicone membrane simulated the fossa ovalis since it had similar tenting properties and mobility of a native fossa, which greatly improved the relative anatomy of this particular model.

Figure 4.4: Stereolithography model printed from CAD files created from human anatomy. This particular model has a left common pulmonary vein and was an interesting anatomical specimen. The model facilitates bench top testing by providing clinically relevant human anatomy and two separate transseptal locations to assess the feasibility of device delivery into the left atrium.

Conclusions

The two 3D model approaches presented here allow for the unique assessments of human cardiac anatomies at different levels of accuracy. Both the CT and MRI images offer approximately 0.5mm pixel size and 1-2mm slice thickness, although the MRI of human heart scans presented in the previous section offers a higher level of resolution and greater fine details in anatomies when compared to the whole body CT scans (described in the previous section). The reason for this, is that there is a higher degree of tissue contrast when employing MRI compared to that CT. Likewise, the movement artifact seen in the patient CT scans decreases its relative accuracy. So for the purposes of this thesis, the MRI images of the static hearts provided very accurate anatomy of the atrial septum and the patient CT files did not provide great tissue differentiation due to the low tissue contrast. However, the CT scans did offer anatomically correct placement and orientation of the anatomy and surrounding structures which is important when considering a percutaneous approach of a cardiac therapy.

Novel Imaging of Atrial Septal Defects in Isolated Human Hearts

Published in *Journal of Cardiovascular Translational Research* 2013 Vol. 6 No.2. pp.218-20

Stephen A. Howard, BA[1,2]

Jason L. Quill, PhD[1,2,5]

Michael D. Eggen, PhD[1,2,5]

Cory M. Swingen, PhD [4]

Paul A. Iaizzo, PhD[2,3]

Departments of Biomedical Engineering[1], Surgery[2],

Integrative Biology and Physiology[3], and Medicine [4]

University of Minnesota, Minneapolis, MN, USA

Medtronic, Inc., Minneapolis, MN, USA[5]

Keywords: Congenital defects; magnetic resonance imaging; patent foramen ovale; oval foramen; persistent patency; atrial septal defect

Within the adult population living with congenital heart defects, approximately 20% have an atrial septal defect, which suggests that only 0.4%-0.05% of the entire adult population has an atrial septal defect (ASD). In patients with a left to right atrial shunt, treatments may include closure of the defect with a transcatheter device and/or surgical repair. From the perspective of a physician or engineer, it is vitally important to understand the anatomical nuances of such defects, not only to offer the most optimal treatment for the patient, but also to call attention to the potential anatomy of ASDs which may go undetected. To do so, we reanimated two human hearts deemed not viable for transplant from 56-yr-old and 68-yr-old males. Neither patient history reported any heart conditions that would suggest an atrial defect, yet an ASD was found in each heart. Here we present sets of images, videos and 3D reconstructions that provide a clearer view of the anatomy of ASDs in functional human hearts. With an enhanced understanding of 3D functional aspects of ASDs, physicians can make improved decisions regarding treatment options and engineers can optimize device designs.

Introduction

One of the prominent features in the right atrium is the fossa ovalis, which helps to separate the left and right atria during normal function of the heart. An atrial septal defect (ASD) is a congenital defect in the heart that creates a shunt for blood to pass from the left to the right atrium across the interatrial septum. This can be caused by an incomplete overlap of the flap valve of the fossa ovalis and the superior rim or by other abnormalities causing the fossa to be fenestrated. It should be noted that an ASD is different from probe patency of the fossa ovalis where there is overlap of these structures but incomplete fusion of the two together (for more information on the atrial anatomy see ‘Standardized review of atrial anatomy for cardiac electrophysiologists’ in this issue).

Within the adult population living with congenital heart defects, approximately 20% have an ASD, which suggests that only 0.4%-0.05% of the entire adult population has an ASD compared to a probe patency of the septum which is prevalent in about 27% [15,16,79,80]. To diagnosis an ASD, generally a contrast echocardiogram will be performed. Since this is not a common procedure for healthy individuals, those with asymptomatic ASDs and no reason for an echocardiogram may go undiagnosed. Yet for those in which high amounts of shunting are observed, treatments may include closure with a transcatheter device and/or surgical repair. From the perspective of an engineer or physician, it is vitally important to understand the anatomical nuances of such defects, not only to offer the most optimal treatment for the patient, but also to call attention to the potential anatomy of ASDs which may go undetected. To do so, we have uniquely employed both magnetic resonance imaging (MRI) and Visible Heart® imaging modalities to investigate the functional anatomies of ASDs in reanimated human hearts [74].

Methods

Two human hearts deemed not viable for transplant were reanimated using Visible Heart® methodologies [74,81]. The hearts were from 56yr old and 68 yr old males and neither patient history reported any heart conditions that would suggest an atrial defect. Upon investigation of the specimens it was determined that both had an ASD, which was defined as a secundum defect due to the incomplete overlap of the flap valve with the superior rim of the fossa ovalis. The first heart was continually perfused with a clear Krebs-Henseleit buffer which allowed intracardiac imaging while functioning *ex vivo*. In the absence of blood, conventional endoscopes were used to directly visualize the endocardial wall movement as well as the functional anatomy of an ASD (Movie 1)[74]. In the second heart, an MRI-safe apparatus was used to reanimate the

isolated human heart within a 1.5 Tesla MRI unit, using previously reported methods [81,82]. Cine imaging was performed using a steady-state free precession sequence (True-FISP) in order to visualize motion of the heart with high temporal and spatial resolution. Turbulent blood flow jets (due to the movement of blood from the left atrium to the right atrium) through the ASD and a shunt were observed using contrast-enhanced imaging (Movie 1).

Subsequently, these two human hearts were pressure fixed in 10% formalin to retain dilated chambers following fixation, and then static images were taken with an endoscope to again assess the sizes and shapes of the ASDs (Fig. 4.5). Morphologic MRI scans were performed on these specimens to allow for 3D model reconstructions from the image stacks; these models also show the relative locations and anatomy of the ASDs within these hearts (Movie 2, Fig. 4.6). Quantitative measurements of the 3D models indicated that the ASDs were semi-oval in shape with openings of about 12 x 4 mm for the first heart and 12 x 5 mm for the second. The presence of either of these defects, if observed clinically, would have made the patient a potential candidate for closure using an ASD occlusion device [27].

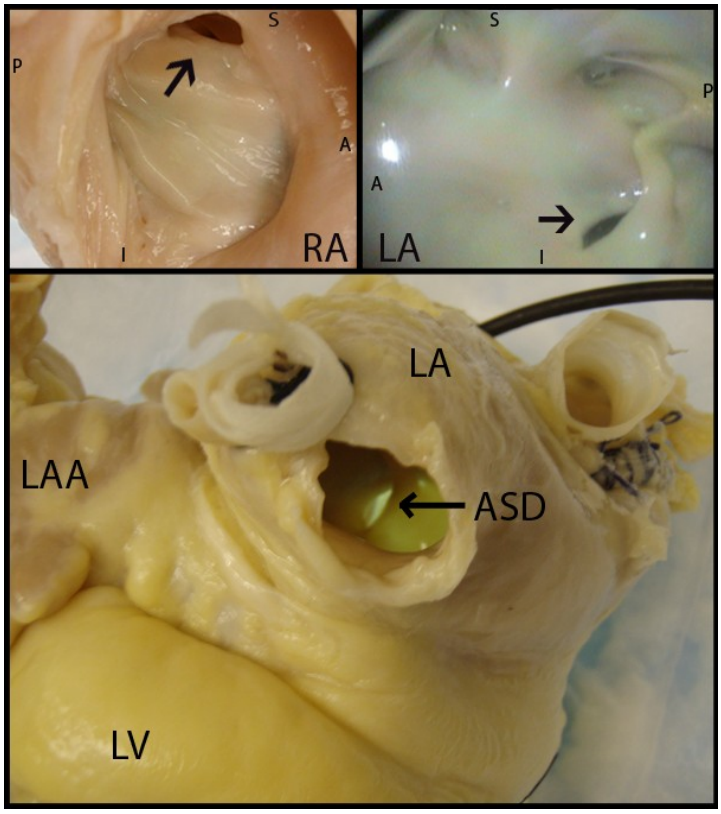

Figure 4.5: Post-fixation images of an atrial septal defect (ASD) in a human heart. The defect is clearly viewed and can rightly be described as an ASD due to the insufficiency of the flap valve to cover the superior rim of the fossa ovalis, which is commonly called a secundum defect. *Top panels*, images of the ASD (*arrow*) from the right and left atrium, respectively. The superior (*S*), inferior (*I*), anterior (*A)*, and posterior (*P*) aspects of the fossa are indicated on each image. In the image from the LA, an interesting connection can be seen between the flap valve and the wall of the left atrium, which is subsequently modeled in the lower right panel of Fig. 4.6. *Lower panel*, external image of the heart in which the ASD can be easily viewed by looking through the pulmonary vein. In this image, a light source is placed within the right atrium to show the defect. *LA*, left atrium; *LAA*, left atrial appendage; *LV*, left ventricle; *RA* right atrium

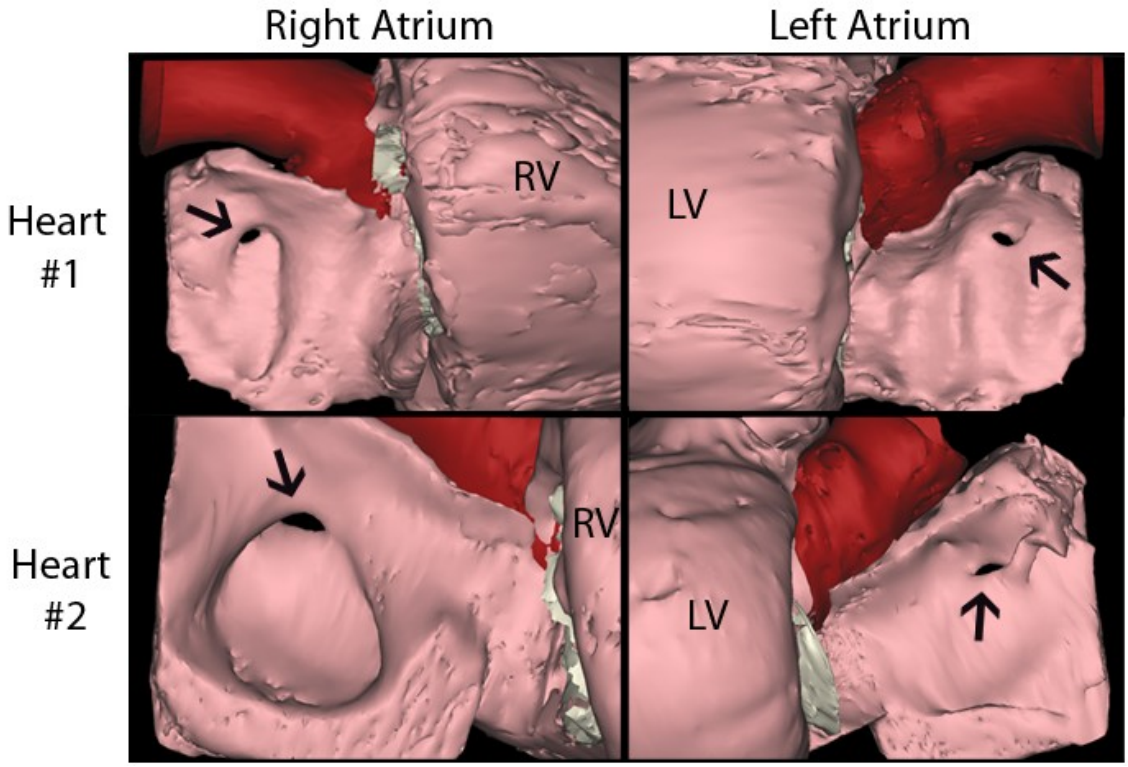

Figure 4.6: Three dimensional models of the atrial septal defects (ASDs) in heart #1 and heart #2. In all images, the free walls of both atria have been removed for better visualization of the ASDs (marked by *arrows*). The ASDs can be seen on both the right and left side of the atrial septum and the connection noted in Fig. 4.5 can be seen in the bottom *right panel.*

Conclusions

The anatomies presented in this paper demonstrate a unique view of ASDs in functional human heart specimens. It is of interest to note that neither of the patient's clinical histories revealed any indications of an ASD or related symptoms. In that respect it seems reasonable to believe that there may be other individuals who have a small ASD and yet go undiagnosed due to the lack of clinical indications. This suggests that ASDs could be more prominent within the population than previously reported. Through the use of direct videoscopic visualization, 3D modeling, and ECG gated MR imaging modalities within functional isolated human hearts, we captured a unique set of images that allow for a better understanding of ASD functional

anatomies/defects. With an enhanced understanding of 3D functional aspects of ASDs, physicians can make improved decisions regarding treatment options and engineers can optimize device designs.

Movie Captions

Movie 1: Endoscopic image of the atrial septal defect (ASD) from Heart #1 as seen from the right atrium (RA). Next the cine of the contrast-enhanced MRI image of the ASD in Heart #2. The atrial shunt is highlighted with an arrow, and the contrast injected into the left atrium can be seen jetting through the defect from the left atrium (LA) into the right atrium.

Movie 2: Rotational views of the 3D reconstructed hearts in both an anatomically correct manner as well as about their short axes. The final portion of the video shows a close-up of the atrial septal defect (ASD) relative to the heart's anatomy.

Direct Visualization of an Iatriogenic Septal Defect in a Reanimated Human Heart

Stephen A. Howard [1,2]
Ryan P. Goff[2,5]
Paul A. Iaizzo[2,3]

Departments of Biomedical Engineering[1], Surgery[2],
and Integrative Biology and Physiology[3]
University of Minnesota, Minneapolis, MN, USA

Corresponding Author:
Stephen A. Howard
University of Minnesota
B172 Mayo, MMC 195
420 Delaware Street SE
Minneapolis, MN 55455
612-624-8742
howa0255@umn.edu

Keywords: Atrial defects; 3D modeling; Atrial Fibrillation; heart catheterization; persistent patency; iatrogenic atrial septal defect

Introduction

Access to the left atrium is required for a number of cardiac therapies, including: ablations pulmonary vein isolations, left atrial appendage occlusions, mitral valve repairs and/or valve replacements. Generally these procedures require a transseptal puncture to enter the left atrium. Doing so can create holes between the two chambers known as an iatrogenic atrial septal defects (IASDs). Such defects can allow shunting between the two atria. However, in most patients it is generally considered that these will result in transient left to right shunts and these IASDs will close within a timely fashion without clinical consequences[83]. Nevertheless, post-procedurally IASDs have been seen in upwards of 87% of patients 1 day following the procedure and have been noted to exist up to 18 months or later in 15% of the patients[1].

Methods/Results

Our lab was fortunate to receive a human heart deemed not viable for transplantation, for research purposes. The donor was a 72yr old female who terminally suffered an intracranial hemorrhage. Previously, this patient was diagnosed with atrial fibrillation (AF), with two known bouts reported. Importantly for this report, this the patient underwent AF ablation procedure 2 months prior to organ donation. Our laboratory received the heart 6 hours post-cross-clamp, it was then prepared for reanimation as previously reported utilizing Visible Heart methodologies[74]. With the heart functioning in a 4-chamber working mode, we were able to directly visualize two distinct IASDs in the atrial septal wall and both were large enough to pass a 7F catheter through. We presume that both were from the ablation procedure 2 months prior (Fig. 4.7, Movie 1). Along with the IASDs, the scar tissue formation as a results of LA ablations were also observed from what looks to be part of a pulmonary vein isolation procedures, with scar lines seen on the posterior wall of the LA (Fig 4.8).

Conclusion

Although most of the procedures involving a TSP may have the inherent risk of an IASD, it is a consequence that needs to be weighed against the benefit of the procedure and determine whether or not the defects warrant a subsequent placement of a closure device. The post-procedural defects as observed and described here within this reanimated human heart, need to be considered when performing a clinical procedure. Although such are known potential complications, the direct visualization of such in this reanimated human heart specimen may provide a novel clinical insights as to what these induced defects may functionally appear as and how they compare to previously published ASD anatomy[14]. Furthermore, this unique look at IASDs may provide medical device developers an important perspective when developing transseptal therapies.

Figures and Legends

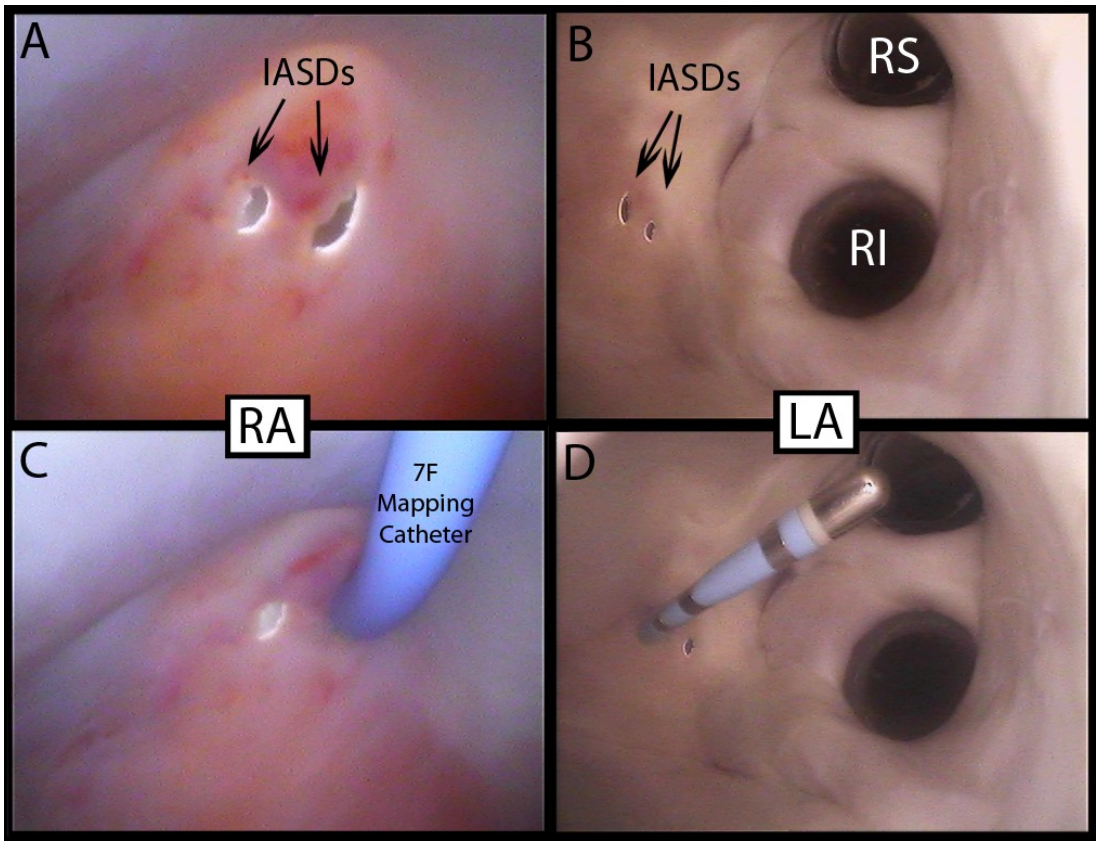

Figure 4.7: Two iatrogenic atrial septal defects (IASDs) imaged in a functional heart from the right atrium (RA) and the left atrium (LA) in panes A and B respectively. In panes C and D show a 7F mapping catheter going through the most anteriorly positioned IASD. Cannulas can be seen in frames B and D where the right superior (RS) and right inferior (RI) pulmonary veins enter into the atrium, and in both sets if images, the top of the image is the superior aspect of the anatomy.

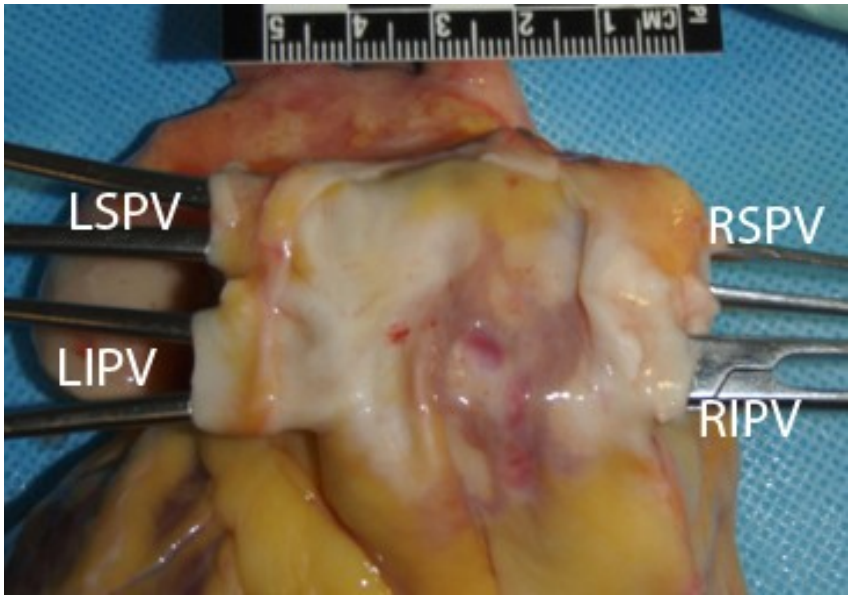

Figure 4.8: Cardiac ablation lines seen form the posterior aspect of the LA. The two tissue clamps are seen going through the superior and inferior pulmonary veins. [LSPV, left superior pulmonary vein; LIPV, left inferior pulmonary vein; RSPV, right superior pulmonary vein; RIPV, right inferior pulmonary vein.]

Movie 1: The left side of the video displays the fossa ovalis from the right atrium (top left) and left atrium (bottom left), while the right side shows an external view of the functioning heart. As the movie progresses, a 7F catheter can be seen coming from the superior aspect of the anatomy and advancing through the iatrogenic atrial septal defect and into the left atrium. In the left atrium the catheter is able to reach the pulmonary veins with its steerability.

Chapter 5: PFO Size, Prevalence and Morphology

Introduction

A probe patency that exists in the atrial septum is referred to as a patent foramen ovale (PFO). This defect is caused by the incomplete fusion of the septum primum to the septum secundum within the first 2 years of life. This patency is established *in-utero* as a blood shunt to allow some of the oxygenated blood from the mother to effectively bypass the lungs and be directed into the systemic blood stream[84]. When the baby takes its first breath, what will happen is that the pulmonary artery pressure will decrease and subsequently decrease the right ventricular and atrial pressures. This will create a larger relative pressure in the left atrium over the right atrium and effectively close this flap valve of the two septa.

If this patency exists later into life it is described as a probe patency of the foramen ovale, or a PFO. This defect has been seen in approximately 25% of the population and the prevalence declines as the age of the patient population increases [16]. In general this defect allows for blood to pass only from the right to the left atrium. This is due to the location and orientation of the septal overlap. In rare circumstances or in instances of concomitant cardiac congenital defects, the pressure on the right side can become higher and allow shunting to occur from right to left [85,86]. There has been a reported case of thrombus crossing this defect and getting into the arterial blood stream which was visually confirmed with echocardiographic imaging. This is one of the potential issue related to right to left shunting and many times the reason that a physician will close such a defect [19].

Along with this reported case of a thrombus crossing the septal defect, other clinical implications have been associated with the presence of a PFO. A number of studies have been cited to show that in patients with cryptogenic stroke compared to those with known stroke causes, there is a higher prevalence of PFOs (33.9% to 12.3%) [87]. Similar groups have reported similar findings from populations of patients with and without stroke (10% to 40%, with a subgroup with no identifiable causes being 54%) [88]. PFOs have also been associated with migraines and aura[86,89], and transient ischemic events [90,91].

Due to the association of PFOs with clinical events, atrial septal occluder devices have been used to close such defects. As was shown in chapter 1, there are a number of these devices that have been used for closing PFOs (albeit, "off-label"), including the Amplatzer Septal Occluder®, Gore® Helex®, and STARFlex [41]. Clinical trials have been performed to assess the safety and efficacy of closing PFOs as means of stroke prevention in cryptogenic stroke population including the RESPECT, CLOSURE I, and PC Trials[92,93]. Most of these studies have been meet with criticism on both sides in that some think it is putting the patient in more danger than the potential help it is giving [93–96].

Regardless of the conventional wisdom surrounding whether to close or not to close PFOs, these procedures are being performed currently and devices are being created to specifically address PFO anatomy [97–99]. This means that the anatomy of PFOs needs to be fully understood including the morphology as well as the physiology. The basic anatomy of PFOs has been studied by many different groups. Most of the data that has been published comes from cadavers[16] or echocardiographic studies[100,101]. From each study, similar data is presented, the prevalence is generally 25% of the population[16,102], the diameter of the PFO ranges from 1-19mm in diameter [16], and the tunnel length is on average 11mm-14mm [100,103].

Although 3D assessment of PFO anatomy has been described and reported [2], the size of the PFO has not been documented by means of these methods. With the advancement of 3D echo more of this data is being collected[104,105], but full 3D models of PFO have not been created and measured, including the internal anatomy of the PFO. Because of the limitations of imaging resolution as well as movement artifact, MRI, echocardiograph and CT images are not perfect at producing images that are easily measureable and able to obtain data on a sub-millimeter scale in patients. This means that there is still a need for good 3D anatomy data regarding the size and variability associated with PFO structure. To begin to address this need we utilized a library of 179 human hearts to determine PFO prevalence, size and other factors associated with this defect. A subset of these hearts with PFOs were scanned in a 3T MRI to obtain images that could subsequently be used to create 3D models of the atrial septal anatomy and compare to the physical measurements of the hearts.

Methods

Heart Measurements

From a specimen library of over 280 human hearts that were obtained and perfusion fixed by methods described in chapter 3, we utilized 179 specimens that were 1) available for measurements and 2) had the required anatomy to be measured (i.e. intact atrial septum and/or PFO). Within each specimen, the height, width, and thickness of the floor of the fossa ovalis was measured (Figure 5.1), the first two measurements made with a standard caliper, and the last with a c-clamp micrometer.

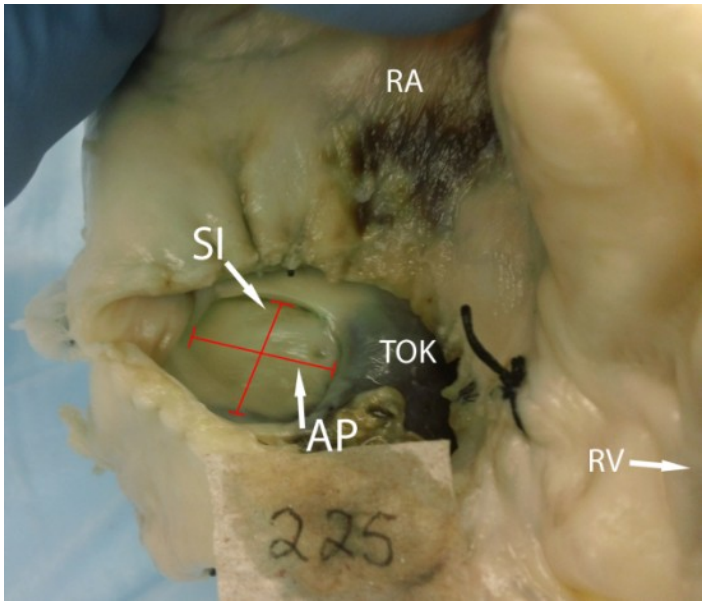

Figure 5.1: Figure of superior to inferior (SI), and anterior to posterior (AP) orientation and measurements of the floor of the fossa ovalis. The fossa ovalis is viewed through an incision site located at the entrance of the inferior vena cava into the right atrium. The adjacent structures are listed to add to prospective: (RA) right atrium, (RV) right ventricle, and (TOK) triangle of Koch.

If the specimen had a PFO or another type of atrial septal defect, it was noted and measured. The measurements of the PFO included the tunnel length, as defined as the distance of overlap between the septum primum and septum secundum. Also the opening to the entrance of the PFO from the RA and LA were approximated (Fig. 5.2). All of these data were taken and compared to their corresponding patient history. Each of the hearts had some sort of medical history, and the completeness varied from specimen to specimen. However, the sex, age, weight, height, and medical histories (specifically related to hypertension (HTN), atrial fibrillation (AF), stroke, transient ischemic attach (TIA), and cerebral hemorrhage not associated with accidents) were obtained if possible.

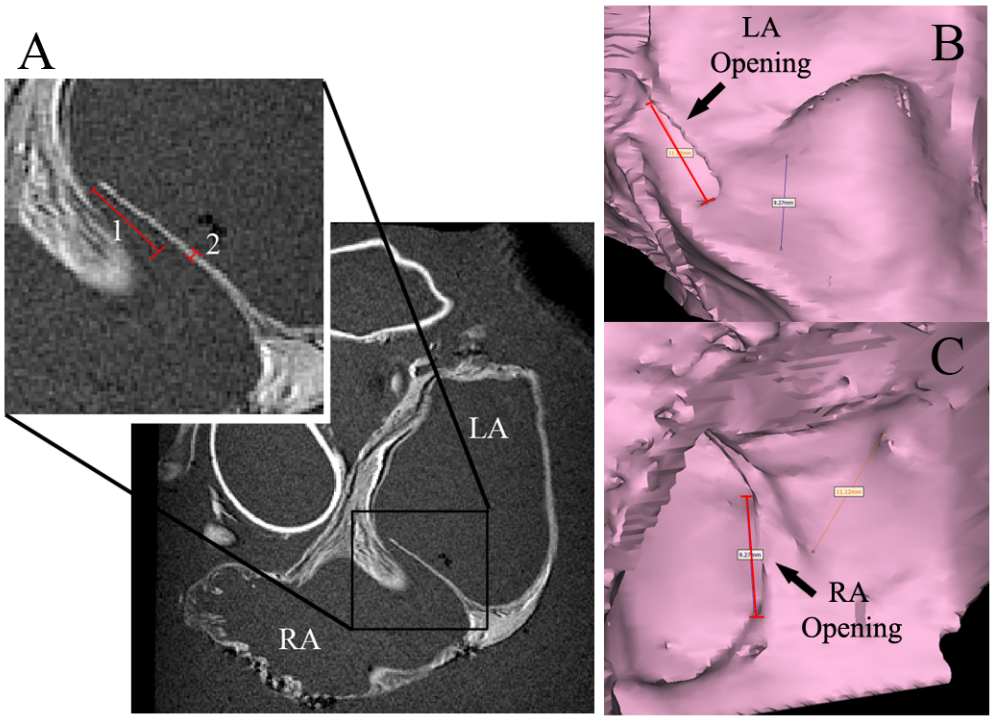

Figure 5.2: Measurements recorded in the physical and 3D anatomical models. (A) MRI slice showing a probe patent atrial septum. The length of the PFO tunnel (1) is defined by the shortest distance between the left atrial (B) and right atrial openings (C). The thickness of the septum primum (2) was also measured, but only in the physical models due to the resolution limitations of the MRI image.

3D Measurements

Following this data collection, a selection of hearts with PFOs were scanned to look at the 3D morphology of the defect. Nine hearts were MRI scanned and deemed to have scans that were good enough to produce 3D models. Examples of why a scan would be excluded include low-resolution scans, anatomy where the PFO was indistinguishable from the atrial septal anatomy, and incomplete septal anatomy (e.g. only half of the fossa ovalis present). From the scans the files were imported into MIMICs anatomical reconstruction software and the atrial septal anatomy was segmented out and created into a 3D CAD model. Using the software, we were able to make the same measurements that were performed on the physical specimens and in addition to that, the septa overlap area was accurately measured. To obtain the area measurement,

the space between the septa were reconstructed with the software and limits of LA and RA PFO openings were placed on the model to re-create the area of the PFO (Fig 5.3).

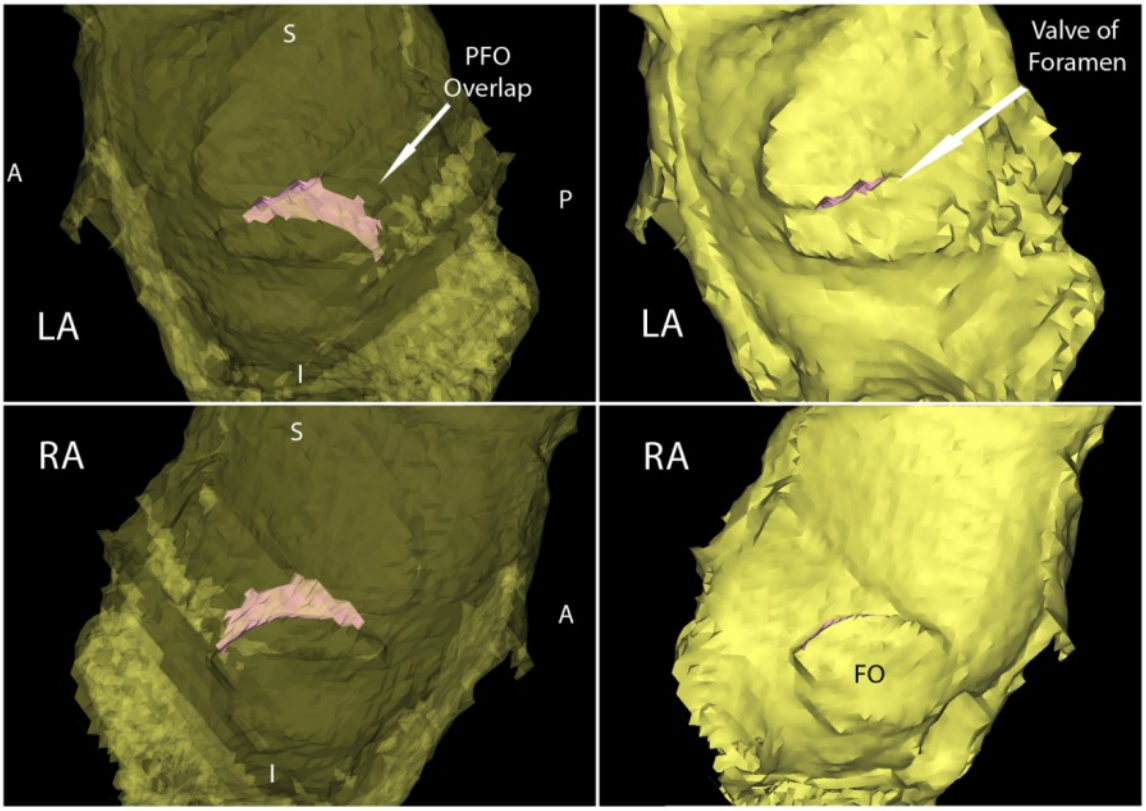

Figure 5.3: Model of the PFO overlap area. These 3D reconstructions show the PFO overlap area modeled from a left atrial (LA) and right atrial (RA) aspects. The images on the left show a semi-transparent view of the septum which helps to fully appreciate the overlapping area of the PFO. The orientation of the septum is given by the superior (S), inferior (I), anterior (A) and posterior (P) aspects of the septum.

Images of these models were taken perpendicularly to the floor of the fossa ovalis (as shown in Fig. 5.4). These images were loaded into ImageJ software with a relative distance marker to obtain the area of the overlap[106].

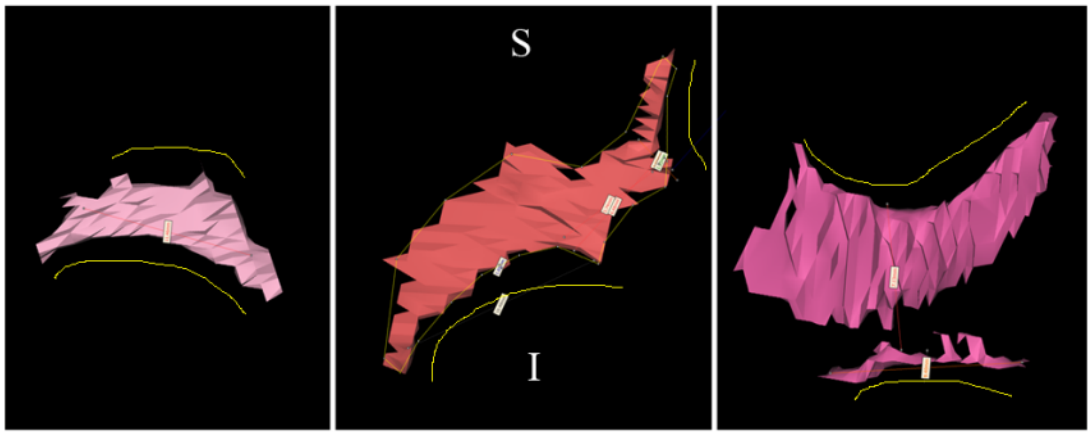

Figure 5.4: Three dimensional rendering of the PFO overlap area as defined by the left and right atrial opening of the defect. The area of each of these overlaps was calculated in ImageJ and the openings into the left and right atria are outlined with a yellow line (top and bottom respectively). The orientation of the defects is also indicated with superior (S) and inferior (I) markers.

Statistics

In this analysis all data are represented as the mean ±SD unless otherwise mentioned. To test for significance, the Student's T-test was utilized for one to one comparisons, and a Chi test was performed when looking at differences in disease prevalence. Significance was determined if the p-value<0.05.

Results

Physical Heart Measurements:

From the selection of 179 hearts, not all of the hearts had complete data associated with them due to either inaccessibility to the anatomy of interest (eg. unable to gain access into the LA for measurements or incomplete medical history files). The data from the physical measurement of the heart specimens showed some interesting data. Within this population of hearts there were 26.1% hearts that had a PFO, and 1.7% had an atrial septal defect (ASD). The baseline characteristics of the non-PFO and PFO groups are summarized in Table 5.1. This data showed a significant difference between the two groups with regards to patient weight (172±42lbs to

189±51lbs, p=0.03) and BMI (26.9±5.8 to 29.9±7.8, p=0.006) with the PFO group being larger in both cases.

Analyzing the prevalence of various disease states between the two populations we found no significant differences, even though the non-PFO population seemed to have almost a 5 times greater prevalence of a diagnosis of AF.

Table 5.1: Summary of Clinical Characteristics between PFO and non-PFO.

	PFO	No-PFO	P-value
n=	43	124	
Males (%)	41.3	46.8	ns
Age	58.5±12.8	60±16	ns
Weight (lbs)	189.4±50.5	171.9±42.4	0.03
Height (in)	66.8±3.7	67.1±4.0	ns
BMI	29.9±7.8	26.9±5.8	0.006
Medical History			
AF (%)	2.2	10.9	0.07 (ns)
Stroke (%)	11.1	5.1	ns
TIA (%)	1.5	2.2	ns
Cerebral Hemorrhage * (%)	37.0	30.7	ns

*Not including deaths involving accidents or self inflicted wounds

Further comparisons were made to determine the differences in the anatomy of the fossa ovalis. Between the two populations, the SI and AP diameters of the fossa ovalis were significantly larger and the septa were thinner in the PFO population (Table 5.2). Also the length of the PFO tunnel varied within that subgroup with a range of 2-20mm with an average of 9±5mm in length. There were no significant differences between the opening sizes of the left and right atria, although within the population of hearts the size of the PFO opening was on average

4.7±3.7mm difference from one side to another. Additionally, there were no significant differences in the PFO anatomy within the patients that presented with various clinical conditions (e.g. stroke or hypertension).

Table 5.2: Size of the fossa ovalis and PFO within the two patient subgroups.

	PFO	No PFO	P-value
SI (mm) [Range]	22.3±5.7 [38.8-13.8]	18.3±6 [38-2.1]	0.001
AP (mm) [Range]	18.8±4.7 [30.7-6.6]	15.5±6 [39.6-6.7]	0.0004
Thickness (mm) [Range]	0.51±0.18 [1.01-0.18]	0.67±0.30 [1.91-0.19]	0.0016
tunnel length (mm) [Range]	8.9±4.5 [19.6-1.6]	-	-
RA side opening (mm) [Range]	9.4±4.5 [20.9-2.5]	-	-
LA side opening (mm) [Range]	10.2±4.0 [18.1-4.1]	-	-

3D Models vs. Physical Measurements:

Nine specimens from the PFO subgroup above were reconstructed and 3D models were created and measured to determine the validity of the measurements. The differences in the measurements are shown in table 5.3. No significant differences were found between the two measurement methods except for the area of the PFO overlap. The overlap was calculated using the 3D models as described above, however for the physical measurements, a surrogate for the PFO area was performed. The PFO was assumed to be approximately the shape of a trapezoid with the distance between RA and LA being the sides of the trapezoid and the length of the tunnel being the height. By using the following equation we were able to calculate and approximate area of the PFOs:

$$Trapezoid\ Area = \frac{(RA\ opening + LA\ opening)\ x\ Tunnel\ Length}{2}$$

Table 5.3: Comparison between 3D and physical measurements of a subset of the PFO population.

N=9 viable specimens	3D Model Measurements	Physical Measurements	P-value
SI (mm)	22.5±5.5	21.5±7.3	ns
AP (mm)	17.2±4.6	17.3±5.3	ns
tunnel length (mm)	8.1±4.0	8.6±4.7	ns
RA side opening (mm)	11.5±3.9	9.9±6.4	ns
LA side opening (mm)	10.0±5.6	10.4±4.0	ns
PFO Overlap Area (mm^2)	85±35	55±36	0.003

Assessing the differences between the two area measurements, it seems clear that the physical measurements of the hearts seem to underestimate the area of the PFO (Fig. 5.5). Based on the best fit linear regression, on average the physical measurement calculation underestimated the PFO area by approximately 30 mm^2. However when assessing the PFO tunnel length, there seemed to be no trends and no significant difference between the two means of measurement. Thus suggesting that the physical method was a good analog for the 3D measurement (Fig. 5.6).

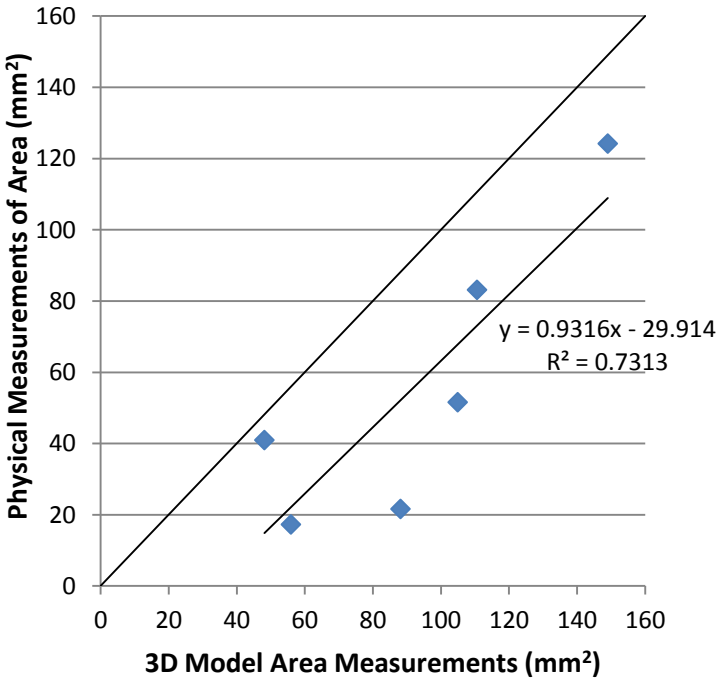

Figure 5.5: PFO area of 6 different hearts. This graph compares the two different means of area measurements, 3D measurement and trapezoidal calculation from physical measurements.

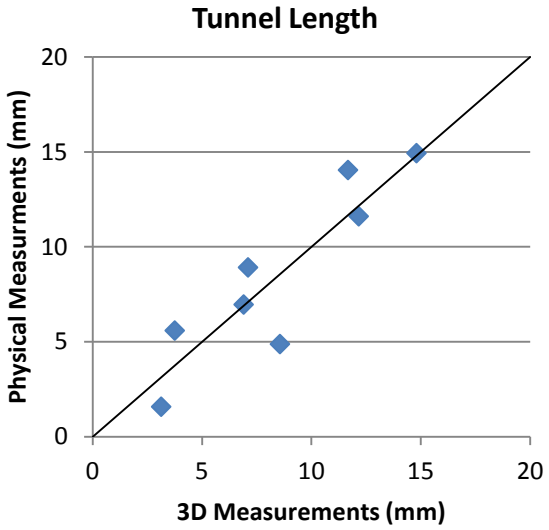

Figure 5.6: PFO tunnel length of different hearts comparing the 3D model measurements to the physical measurements.

Discussion

These data collected in this study correlate well with previously reported literature regarding the PFO prevalence (26.1% in this study and about 25% in other studies [16,102]) and tunnel length of 8.9±4.5 although it is slightly on the lower end of the reported values of 11mm-14mm [100,103]. One nuance that has been presented here is that the data pertaining to the thickness of the septum primum has not been reported to the best of our knowledge in patients with PFOs even though the thickness of the septum secundum has [103,107]. This is likely due to the size of the relative structures and the resolution of the imaging modalities used. In many cases, the pixel resolution of clinical imaging modalities are on the order of 0.5-1mm [108,109], so to measure the thickness of a sub millimeter structure can be a big source of error. With this data the thinner septum that is seen in these PFO patients should be considered and understood when considering the use of an atrial septal occlusion device.

This paper also begins to address the anatomical variation within the PFOs in the region that is unseen by many imaging modalities. The septal overlap area is another value that is not reported in the literature, primarily due to the lack of sufficient 3D imaging capabilities and likely the amount of work needed to recreate 3D models and derive the area from heart scans. The closest that we have found presented in the literature comes from Tanaka et al. where they present the cross-sectional area of PFOs in 50 patients but the cross section is taken perpendicular to the plane of the floor of the fossa ovalis and not parallel like presented here [3]. Similarly their data suggested that the entrance (RA side) to the PFO was greater than the exit (LA side). However our data showed that on average there was a slightly larger opening on the LA side, however the data was not significantly different from one another. Although they measured area and in this study we measured the length of the opening, it is reasonable to believe that there should be a correlation between the two values. Finally, while comparing the 3D measurements to the physical measurements, there was no difference between the measurement of the tunnel length

nor the left and right atrial PFO opening lengths. The advantage to using the 3D modeling was the ability to obtain the area of the PFO overlap which could likely be a factor for cryptogenic stroke since tunnel length itself is being thought of as a potential factor [100,107].

Conclusions

The creation of 3D CAD models to understand atrial septal anatomy is meticulous and time consuming and the resolution that can be obtained from a patient CT or MR scan may not be of high enough resolution to fully understand and appreciate the intricacies of PFO anatomy. For these reasons, this method of atrial septal modeling while beneficial for understanding the underlying anatomy, currently is not practical or cost effective to perform on every patient[2]. The scans that we have employed to obtain this data are very high resolution data from static hearts which reduces noise and movement artifact from patient scans. Because of this we are able to produce these models and understand the variability in the anatomy and begin to understand how these anatomies differ one to another.

The data presented here gives engineers and physicians a better idea of what sorts of morphologies can be expected in regards to PFO anatomy. Also the physical measurements of cadaveric hearts will offer good indications of the linear anatomical measurements, but the 2D and 3D anatomy of the PFO is not well characterized by such methods. When designing devices for a closure procedure or closing a PFO, these factors of the anatomy must be considered and fully appreciated to obtain the best outcomes for the patient.

Imaging Patent Foramen Ovale in the Visible Heart® and Virtual Reality

Stephen A. Howard
Dane Coffey
Arthur Erdman
Paul A. Iaizzo

Introduction:

Utilizing the Visible Heart apparatus and methodologies, we were able to directly visualize patent foramen ovale (PFO) in multiple human hearts. In some cases we were able to visualize the tunneling of the PFO via a catheter passing through the septum, in other cases, a contrast medium (either food coloring dye or microbubbles from agitated saline) was injected into the heart to show the patency. These videos and images illustrate the functional anatomy of the defect and begin to assess the variability from patient to patient.

To further show the complexity of the anatomy, three dimension (3D) models were created from MRI scans of these and similar hearts and imported into a virtual reality (VR) simulator at the Medical Devices Center at the University of Minnesota. Videos of these models were created to illustrate the uniqueness of the PFO morphology in 3D. From both of these imaging modalities, educational material was created that can help to teach engineers, physicians, as well as patients, what the defect looks like and what it means for potential treatment options.

Methods/Results

Visible Heart Images

Using the Visible Heart methodologies as described in chapter 3, human hearts were reanimated and a few of them had a PFO present. With these specimens we were able to confirm

the presence of a PFO visually by passing an electrophysiological (EP) catheter through the septum (Fig. 5.7). Other instances the PFO was not observed until a transseptal puncture was performed on the septum and the PFO was more clearly visualized (Fig. 5.8).

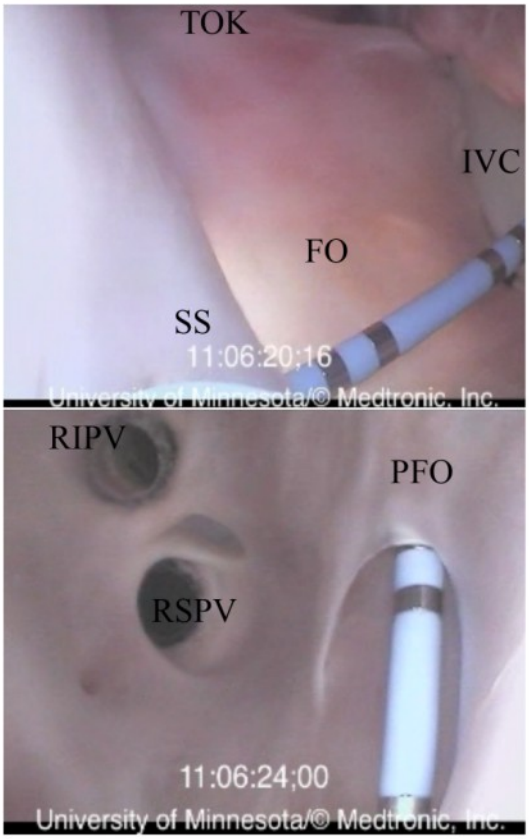

Figure 5.7: Videoscopic images taken in the right and left atria (top and bottom respectively). An electrophysiological mapping catheter was passed through the septum by means of the patent foramen ovale (PFO) as it is seen extending from the inferior vena cava (IVC) in the top image, crossing superiorly through the defect next to the septum secundum (SS) and out the left atrial opening in the bottom image. Neighboring structures are labeled for orientation purposes: right superior pulmonary vein (RSPV), right inferior pulmonary vein (RIPV), fossa ovalis (FO), triangle of Koch (TOK).

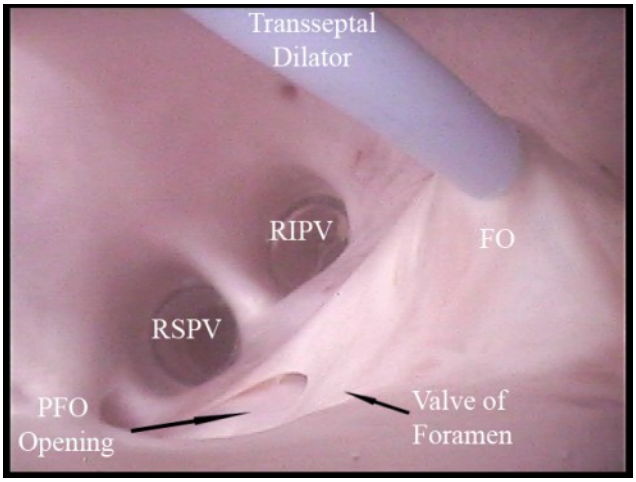

Figure 5.8: The presence of a PFO in this heart was visualized following a transseptal puncture procedure. The valve of Foramen was pushed into the left atrium further which exposed the tunnel of the PFO.

The case of the PFO being found following the transseptal procedure illustrates an interesting point. If a transseptal procedure is to be performed on someone with a PFO, there could be an increased risk of dislodging a thrombus from the tunnel while performing the transseptal procedure. The motion and disruption of the atrial septum could theoretically provide enough force to dislodge a thrombus and produce an emboli in the arterial blood supply. Similarly, there have been reports of physicians utilizing the PFO as an LA access point and this procedure could push such thrombi into the LA. However, it is generally thought that the angle at which the catheter comes out of the PFO limits the range of motion and increases the difficulty of the procedure and thus a TSP is favored over this method [110].

Echocardiography Imaging of PFOs

Detection of a PFO in a patient is generally performed using ultrasound imaging and a contrast medium, usually consisting of agitated saline which creates tiny microbubbles [20]. With permission and confidentiality directly from a patient an example of this procedure is illustrated in figure 5.9. To perform this test, the agitated saline is injected into the venous blood supply and the sonographer holds a 4 chamber view of the heart to determine if any of the contrast medium

makes its way into the LA. If there are no bubbles present in the LA, the patient will be asked to perform a Valsalva maneuver where by forcefully trying to exhale while holding their breath, as to compress the thoracic cavity and effectively increase the relative RA pressure compared to the LA pressure. In the presence of a PFO, this will cause a right to left shunt and cause bubbles to be seen on the left side of the heart (Fig. 5.9).

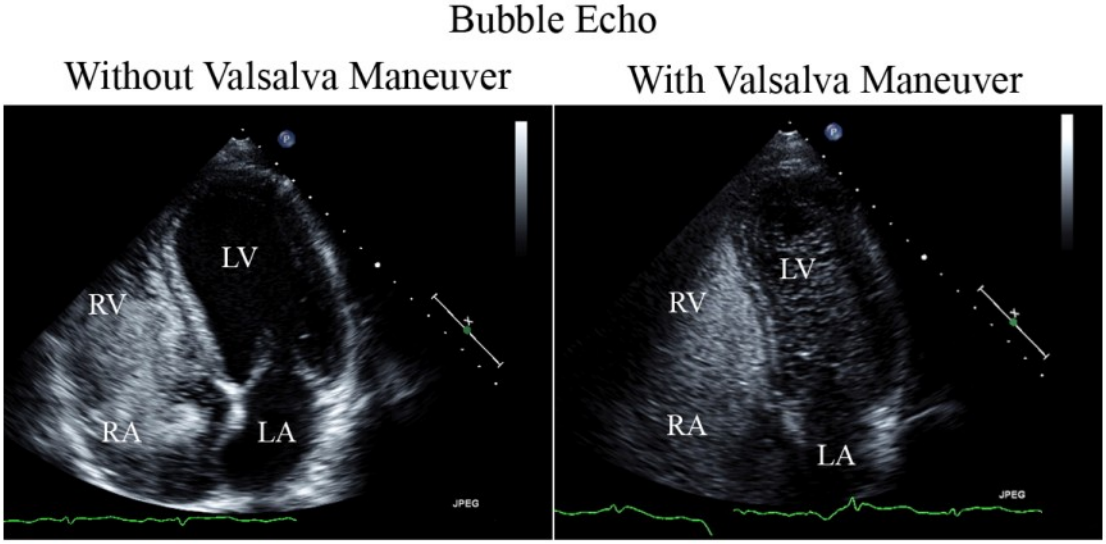

Figure 5.9: Clinical images of a bubble echo test. The image on the right clearly shows the right side of the heart being filled with contrast medium, but nothing is present on the left side. When this procedure is performed again while the patient performs a valsalva maneuver, the bubbles are seen on the left side of the heart. Right atrium and ventricle (RA and RV) as well as the left atrium and ventricle (LA and LV) are labeled in the image above.

In the Visible Heart® prep, this imaging was reproduced by using a transthoracic ultrasound probe on the epicardium of a reanimated human heart (Fig. 5.10). Due to the limitations of the setup, we were unable to perform a valsalva maneuver on the heart and instead, created a persistent patency of the PFO by placing an EP catheter across the defect (Fig. 5.7).

Figure 5.10: Bubble echo test performed on an ex-vivo fully functioning human heart with a PFO. The before, during and after shots of the injection of the agitated saline are sequentially presented above with the right atrium (RA), left atrium (LA) and aorta (Ao) viewed. The presence of the microbubbles in the LA following the injection confirms the presence of the PFO and right to left shunt in this heart.

Virtual Reality Imaging of PFOs

In collaboration with the Medical Device Center at the University of Minnesota, we were able to utilize 3D reconstructions of human hearts with PFOs in a virtual reality (VR) simulator. The benefit of using one of these simulators is that the anatomy can be investigated with the help

of stereo imaging to demonstrate the depth of the anatomy. In conjunction with the 3D computer models of the human anatomy, the VR system can allow for engineers to measure the anatomy and simulate the implant of prototype percutaneous devices without compromising the actual human anatomy or utilizing costly animal models.

For the use of this thesis we were successfully able to import and navigate through 4 different models of atrial septal defects. Unfortunately due to the constraints of this thesis and its 2D existence, it is incompatible with the stereoscopic images that were produced and the videos created showing a tour through the septal defects in 3D. However, a step-wise progression of the video can be seen in figure 5.11 as it progresses from the Right atrium (Fig. 5.11a) to the left atrium (Fig. 5.11n).

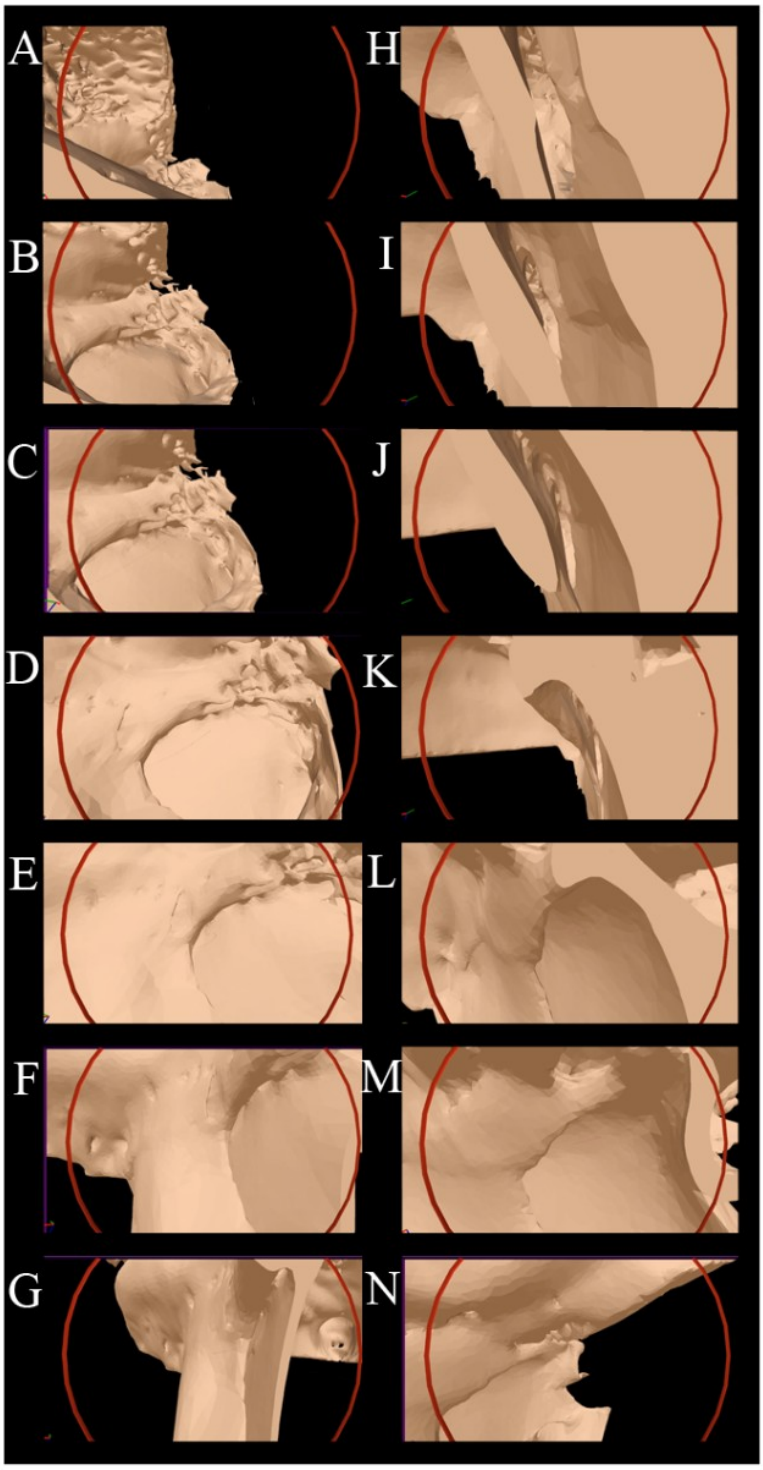

Figure 5.11: Stepwise progression of VR video footage going through the PFO of a computer modeled human heart. The clips start in the right atrium where the location of the tricuspid valve can be seen in the upper left corner. As the clips progress the fossa ovalis comes into view (D). Then the video continues down and through the tunnel of the defect (H-K) where finally it emerges into the left atrium and looks back onto the LA septum (L-N).

Conclusions

The models and images of the PFO anatomy are valuable educational and testing models of true human anatomy. By utilizing the imaging modalities discussed here, we were able to successfully navigate catheters across the PFO and visualize them during other cardiac procedures. When this knowledge is added to the 3D modeling and VR capabilities, a truly unique look at the defect is seen and a greater appreciation for the variance in structure can be seen.

Due to time constraints and limited capabilities the models have not been utilized to date for medical device testing and computer simulated implantation. However, with the anatomies in place and loaded into the VR system, such testing and device design can take place as the next steps. It is no doubt that these images and models are highly useful for these purposes and now that they have been brought into the system, they will benefit cardiac device engineers and physicians.

Section Summary

Understanding cardiac anatomy and potential congenital or iatrogenic malformations is essential for physicians and engineers alike. However, the baseline knowledge of these conditions can only go so far and more advanced imaging modalities need to be employed to understand the anatomical morphology and physiology. In this section I presented a number of papers presenting direct visualization of such anatomy and their associated congenital and iatrogenic anomalies. Due to patient variability and differences in cardiac anatomy, these structures only present limited views into the potential anatomy, but the stark differences from the figures in anatomy textbooks suggest that these images are very important for understanding how the anatomy can present itself in a patient.

The methods of visualization and 3D imaging present a novel and unique view of cardiac anatomy. By utilizing computer modeling, anatomical features and abnormalities are better understood as to their complexities and clinical presentation. The combination of both the modeling and direct visualization methods help to concrete the idea of the structure and function of the anatomy and in some cases can begin to show how those with these anomalous structures may never be aware of the congenital condition.

The 3D modeling also provides a means to understand the morphology and physiology of the atrial septal anatomy, and how medical devices can interact with the anatomy. By these computational methods, these models can be utilized in device testing and validation work and supply accurate anatomical models. Bench top testing (as will be discussed in chapter 6) is essential for creating cardiac medical devices. In many cases the design stems from the specific anatomy. By having this ability to re-create these 3D models with accurate human cardiac

anatomy from patients with known clinical conditions (ie. atrial fibrillation), the devices can be tested in anatomically relevant models. These models begin to tell the story of the anatomy that can be studied to appreciate how biomedical devices can interact with the cardiac structures and potentially get a glimpse into potential failure modes. Additionally, study of these models allows us learn to design devices specifically tailored to the particular cardiac morphologies of interest.

Finally, taking a step back from the bench top testing, these models will be abundantly useful for *in-silico* testing. As presented, virtual reality simulation of the cardiac anatomy can be utilized and allow for medical device engineers to test their devices computationally, which generally is much cheaper and faster than animal and sometimes bench top testing. With a larger push from the FDA to incorporate more computational modeling into medical device submissions[111], these anatomical models need to be available, accurate and fully definable and understandable in regards to the anatomy and anomalous structures.

Section III: Designing Percutaneous Cardiac Devices

Section Preface

Medical device design requires many different steps starting from identifying the initial clinical need and resulting in a final product. In the previous section I discussed the importance of visualizing the anatomy, not only from an educational stand-point, but also from an engineering one. The anatomy needs to be understood, as well as the consequences that the medical device has on the anatomy, and clinical outcomes.

A major portion of medical device design involves product testing and validation, whether in bench top or pre-clinical models. Most devices require many iterations of testing to alter the design and to ultimately attempt to create the best device for that particular clinical need. This process may take many years before a fully functional final product is suitable for human use, but the step-wise process of taking a device from conception to market should be followed to better ensure the safety and efficacy of the product. In this section I present a paper looking at this process specifically tailored towards producing prosthetic valves for cardiac valve replacement, the fundamentals of which can be applied to the design of other medical devices.

The last part of this section discusses the use of an ex-vivo testing model, the Visible Heart, and specifically a means to test the impact of a particular transseptal access sheath on the atrial septum. This section will look at obtaining tenting forces of the fossa ovalis to fully understanding how the tissue reacts to medical device therapy which is essential in device design. So I present work that tries to understand these biomechanical properties in a fully functioning heart.

Chapter 6: Successful Development and Regulatory Approval of Replacement Cardiac Valves

Stephen A. Howard[1]

Michael G. Bateman PhD[1,2]

Timothy G. Laske PhD[2]

Paul A. Iaizzo PhD[1,3]

[1]Departments of Surgery and Biomedical Engineering, University of Minnesota

[2]Medtronic, Inc.

[3]Department of Surgery, Institute for Engineering in Medicine, Lillehei Heart Institute, University of Minnesota

Published in Heart Valves: From Design to Clinical Implementation 1st Edition. Iaizzo PA (eds) 2013. New York: Springer.

Abbreviations

DFM	Design for manufacture
FDA	Food and Drug Administration
FMEA	Failure modes and effects analysis
HDE	Humanitarian device exemption
IDE	Investigational device exemption
IFU	Instructions for use
IP	Intellectual property
USPTO	Unites States Patent and Trademark Office
VOC	Voice of customer
ISO	International Organization for Standardization

Introduction

Throughout the twentieth and twenty- first centuries there have been rapid advancements in the field of surgical and interventional cardiac valve replacements, due to concurrent progress in both cardiac medical technology and surgical techniques. Surgeons can now implant devices developed from novel biocompatible materials in a motionless and bloodless operating field via the use of heart-lung bypass machines and cardioplegia solutions. To date, these techniques for surgical and minimally invasive valve repair and replacement are now accompanied by percutaneous replacement techniques (i.e., performed without bypass and delivered to the beating heart). Nevertheless, the availability of these implantable devices and surgical tools is accompanied by stringent and necessary testing and approval requirements. The modern day process of product development, from the initial steps of brainstorming and idea generation to bench top and clinical testing, continues to be refined. Today this is huge business and today has been valued to be a $307 Billion market for medical equipment and supplies in 2012 [112], which in itself is an impetus to drive the development of novel technologies in the field of cardiac devices.

Background

Via advances in the management of the surgical patient, the allowable times for cardiac surgery have increased along with the complexity of the procedures that have and can be attempted. Thus, innovations have flourished as this rapidly changing field has, in turn, stimulated growth in prosthetic valve design. With companies such as St. Jude Medical forming around the development of a bileaflet mechanical heart valve. Today, medical device development companies are generating a multitude of novel systems that are being used to correct a wide variety of cardiac valve pathologies. Furthermore, numerous valvar therapy innovations are submitted to the United States Patent and Trademark Office (USPTO) every year. For example, searching the database of US patents via a Google patent search (http://www.google.com/patents) for the term "cardiac valve" returns 3,850 visible patents as of July 2012 [113] . Note that when limiting the search to previous decades, it is apparent that innovation and/or production of patentable ideas with regard to cardiac valves have been increasing exponentially (Fig. 6.1). It should also be noted that this list does not include the large number of international patents that exist. Rather, it demonstrates the dramatic acceleration of device innovations related to the assessment of cardiac health and the treatment of cardiac pathologies [114] .

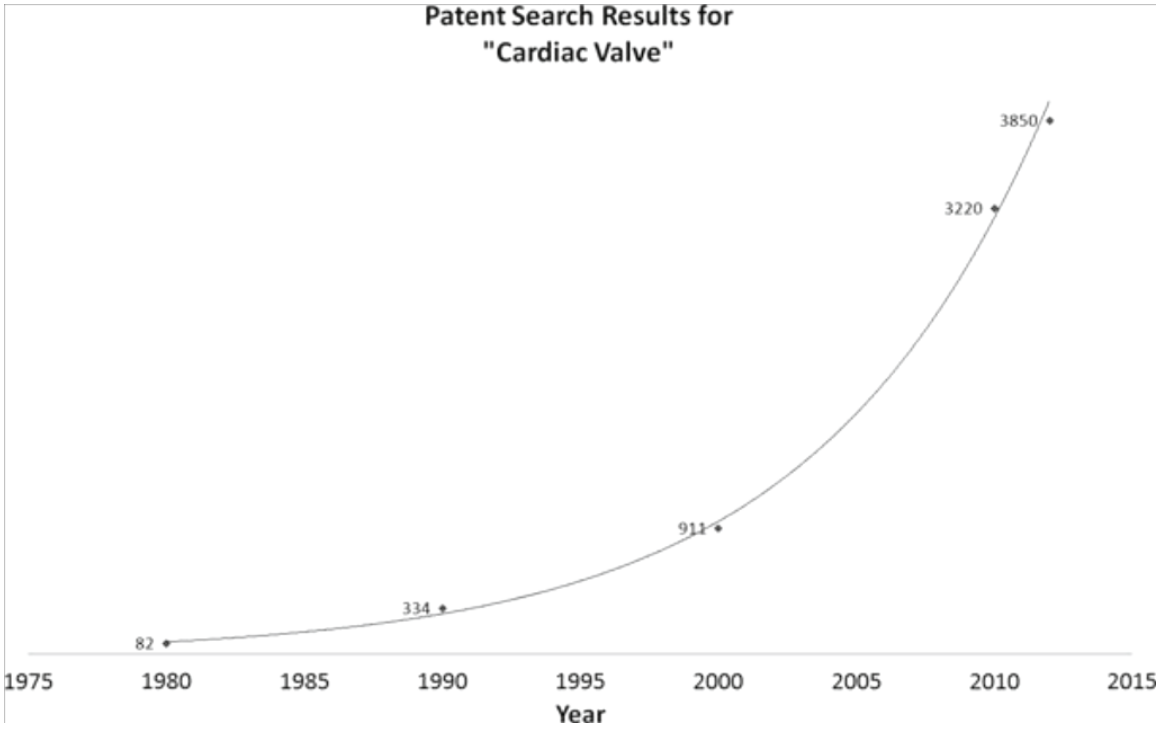

Figure 6.1: Patent results for the term "cardiac valve" within a US patent database

Market-Released Cardiac Valves

The most commonly used devices currently available for valve replacement or repair are listed in Table 6.1. It should be noted that detailed explanations for some of these novel percutaneous valve replacement systems are highlighted as the next generation of technologies in Ch. 7, 8, 9, 10, and 11. Additionally, detailed descriptions of various valve pathologies are described in Ch. 6.

In general, the development of surgically implanted prosthetic heart valves for the treatment of valvar stenosis and regurgitation has fallen into two distinct categories: mechanical and tissue valves. Yet, both of these approaches require removal of the diseased valve leaflets and utilize a rigid circular annulus that is sewn into the native valve annulus to support the prosthetic

valve. The most common mechanical valve designs employ one of the following: a ball and cage design (such as the Starr- Edwards Silastic ball valve), a tilting disk design (such as the Medtronic Hall valve), or a bileaflet design (such as the St. Jude bileaflet valve). To date, surgically implanted mechanical valves have shown exceptional performance and have also displayed excellent durability. However, patients who have received these implants are required to take anticoagulant medications to minimize the risk of clot formation associated with the biocompatibility and non-physiological fluid flow properties that often occur with these prostheses. These anticoagulation therapies then impose limits on the patient's life, as they must always remember to take their medications and avoid activities that could potentially cause bleeding or bruising, including physical contact sports.

To address these challenges, tissue leaflets were subsequently incorporated into replacement valve designs, to better mimic the native cardiac anatomy and minimize the need for anticoagulation requirements. The two most common approaches to this solution include the direct xenotransplantation of a treated porcine valve (such as the Medtronic Mosaic valve) or the construction of leaflets from treated porcine or bovine pericardium (such as the Carpentier-Edwards PERIMOUNT Magna Ease valve). Clinically, the use of tissue valves has been shown to require minimal or no anticoagulation treatments, and currently such valves have exhibited very good performance in humans for 10–15 years. However, their long-term durability— 20 years or more—is still under question, and the nature of the material employed within their designs may lead to the possibility that these replacement valves will also elicit calcifications and thus become stenotic again. Note that although both surgically implanted valve technologies show individual merits, they both require highly invasive surgical procedures for successful implantation. Consequently, there have been major efforts to develop percutaneous valve replacement systems, whereby the technological advancements behind surgically implanted tissue valves have been

combined with stent designs and delivery technologies. To date, such systems utilize the percutaneous endocardial delivery of a metallic frame, positioned across the valve annulus that, when deployed, replaces the diseased leaflets with tissue leaflets sewn into the center of the frame conduit. Note that these transcatheter-delivered valve replacement therapies are described at length in Ch. 7, 8, 9, 10, and 11.

Table 6.1: Examples of market-released cardiac devices used to treat cardiac valve pathologies

Prosthetic valves
• Mechanical valves
• Tissue valves
○ Surgically implanted
○ Transcatheter delivered
Valve annuloplasty rings
• Surgically implanted
• Transcatheter delivered
Valvuloplasty balloons

Valve annuloplasty rings are almost exclusively used for the treatment of annular dilation and consequent valvar regurgitation of the atrioventricular valves. The majority of annuloplasty products on the market are focused on mitral regurgitation due to the severity of the pathologies in relation to tricuspid regurgitation. Most surgically implanted annuloplasty rings are sewn to the valve annulus, which is saddle-shaped and composed of a dynamic junctional zone of fibrous and muscular tissue between the atrium and ventricle. To accommodate different patient anatomies and physiologies, there are a variety of several ring size, shape, and material property options available to the surgeon, including rigid complete rings (such as the St. Jude Rigid Saddle Ring) and partial flexible bands (such as the Cosgrove- Edwards annuloplasty system)[115]. As with prosthetic valves, there has recently been a push to develop transcatheter-delivered annuloplasty devices to treat mitral valve regurgitation. These devices aim to mimic surgical annuloplasty devices by reducing the mitral annulus in order to achieve better apposition of the native mitral leaflets, utilizing the close proximity of the coronary sinus to the mitral annulus.

The advantages and disadvantages of transcatheter-delivered annuloplasty rings are also discussed at length in Ch. 8. Valvuloplasty balloons have been developed and utilized to treat patients with stenotic heart valves, by inflating a balloon that has been percutaneously positioned across the valve annulus to enlarge the valve opening and improve valve function and blood flow. The technique of balloon dilatation of the stenosed mitral valve was first described in 1984 by Inoue, and was soon adopted into clinical practice replacing older surgical closed valvotomy procedures[116]. These procedures are often used to avoid or delay open-heart surgeries and/or valve replacements. Again, each of these device categories has been developed to treat a specific form and/or stage of cardiac valvar disease. However, it should be noted that the modern cardiac surgeon or interventionalist will often use a combination of these approaches/devices to treat a given pathology. For instance, a surgeon may utilize a valvuloplasty procedure to open a stenotic valve before delivering a transcatheter aortic valve replacement.

Typical Anatomy of a Cardiac Device

As noted above, much has recently changed in the fields of cardiac valve replacement and repair. Specifically the improvement of established therapies, the development of novel devices, and the dramatic increase of associated regulatory issues. Currently, in order for any device to be considered acceptable for clinical use, it must demonstrate a number of essential characteristics. The following section will outline the key criteria that need to be fulfilled when developing a cardiac device with a focus on implantable devices.

Functionality

It is vital that any product performs to the standards set by the manufacturer's claims. Many medical devices are born from the desire to satisfy a previously unmet clinical need. To be successful, a new product must elicit this functionality, at or above the currently available solutions and techniques. The functionality of a cardiac device also encompasses its ability to perform the desired task without compromising any other biological process. For example, a transcatheter-delivered aortic valve replacement should not compromise the function of the mitral valve or the vasculature through which it is delivered to the heart. These specifications are often outlined by regulatory committees such as the International Organization for Standardization (ISO), as seen in Table 6.2 describing the operational specifications for cardiac valve prostheses.

Table 6.2: Specifications for a prosthetic cardiac valve (ISO 5840:2005(E) [117])

Has reproducible function
• Allowing forward flow with acceptably small mean pressure difference
• Preventing retrograde flow with acceptably small regurgitation
• Remaining fixed once placed
• Having an acceptable noise level
• Maintaining its functionality for a reasonable lifetime, consistent with its generic class
• Maintaining its functionality and sterility for a reasonable shelf life prior to implantation
Is biocompatible
• Resisting embolization
• Resisting hemolysis
• Resisting thrombus formation
Is compatible with in vivo diagnostic techniques
Is deliverable and implantable in the target population

For implantable cardiac devices such as transcatheter and surgically implanted valves, the question of functionality typically includes the pathway in which the device is delivered. For example, surgically implanted devices require a suitable method of fixation to the heart, such as the sewing ring of a prosthetic heart valve. However, these parameters can be greatly complicated when one chooses to deliver such devices through minimally invasive techniques, such as through

the wall of the heart (typically the apex) or through the vasculature without placing the patient on cardiopulmonary bypass. Hence, not only must the delivery system be able to position the device in its intended anatomical location, but additionally it must not induce any adverse effects on the patient. For instance, the patient populations in need of aortic valve replacements will often present with calcified aortic arches. A calcified aorta can be problematic when delivering a device from the femoral artery, since the delivery system must not dislodge the calcifications nor puncture the aorta, both potentially fatal incidents.

Another excellent example of device functionality involves the development of transcatheter-delivered heart valves to treat patients with highly stenotic aortic valves. Note that these technologies are described at length in Chap. 10, along with a discussion of the potential benefits and detriments of device functionality with regard to both the implanting physician and the patient. To date, companies developing these new transcatheter-delivered technologies have been very specific in their description of the patient populations for which the valves are designed, as well as the conditions under which the valves should be implanted. As such, they create extensive documentation of instructions for use (IFU). By doing so, they develop guidelines for acceptable usage of the device and attempt to ensure that the devices are used only in situations that correspond to the conditions under which the device was critically designed to function. Although device manufacturers set guidelines in the IFU regarding how the device is to be utilized, in rare instances a physician may choose to use it otherwise (e.g. use an aortic valve device to replace the pulmonary valve). This action is called *off - label use*. Off-label use is something that does occur and, in many instances, has saved numerous lives. However, even if a physician has used the device for a particular purpose outside of the IFU, in no way can the device manufacturer encourage or advertise this use unless it has gone through animal and

clinical testing for that particular use (see Chap. 17 for additional details regarding pre-clinical testing).

Biocompatibility

Biocompatibility related to medical devices is generally defined as the ability of a material to perform with an appropriate host response in a specific application[118]. In 1987 Williams described how the biocompatibility of a material can be qualitatively evaluated to assess its relative performance when implanted. The succinctness of this term is often misleading when applying the principles of biocompatibility to cardiac devices, due to the large number of different materials that are commonly used to manufacture such modern devices. For example, tilting disk valve prostheses such as the St. Jude Masters series (St. Jude Medical, MN; Fig. 6.2) are manufactured from a variety of materials including pyrolytic carbon for the disks and Dacron® for the sewing cuff. One needs to consider that each of these materials may elicit different responses from the host body. Hence, they need to be individually assessed and quantified before the cardiac device is implanted. Examples of such tissue responses can be seen in Table 6.3.

Table 6.3: Potential patient-device interactions causing clinical complications [119]

Adverse local tissue interactions
• Inflammations
• Toxicities
• Carcinogenic responses
• Calcifications
• Embolization or lymphatic spread of material fragments
Induced device migrations: encapsulation or a foreign body response
Inappropriate or altered healing responses
Associated infections
Thrombosis
• Thrombotic occlusion
• Thromboembolism

Figure 6.2: St. Jude Medical bileaflet valve

Figure 6.3: Braunwald-Cutter valve

The mechanisms related to how the host or patient may respond to different components of a cardiac device must be extensively evaluated to ensure that the correct materials are selected for the final device design. This evaluation can be complicated by the fact that it is hard to replicate, in vitro, the range of human immune responses that may exist. To address this, all cardiac devices must also undergo rigorous animal testing, yet it is important to note that this too can sometimes provide misleading results on species-specific bioreactivities. An example of this can be seen in the design and development of the Braunwald-Cutter heart valve ball and cage prostheses (Fig. 6.3), whereby cloth-covered cage struts were designed to encourage endothelialization and subsequently decrease any chance of thrombolytic events [120]. Extensive testing in the mitral position of pigs, sheep, and calves showed promising results, thus the device was approved for human clinical trials. However, the device did not elicit the same host responses when implanted in humans; rather it resulted in aggravated wear on the cloth cage struts and,

more critically, the formation of debris embolization. It should also be emphasized that host responses are not limited to immune reactions. For example, implanted tissue heart valves remain susceptible to accelerated prostheses leaflet calcification. More specifically, it has been reported that this type of calcification is initiated by reactions between the extracellular fluid and the leaflet membranes, creating calcium phosphate mineral deposits [121]. As a result, much research is ongoing to enhance leaflet materials and minimize bioreactivities, including calcification inhibitors on the valves that limit mineral deposition on the implanted materials. Furthermore, a device's material can also display unexpected interactions with the host, as evidenced by the earliest versions of the Starr-Edwards caged-ball mechanical heart valve. The valve design used a silicone ball that was found to absorb lipids from the blood and thus swell [122]. In addition to resultant poor valve function, this also caused the silicone balls to become brittle; in turn, this increased the possibility of ball fracture and consequent embolization of small fragments into the arteries downstream of the valve position.

Durability

As well as exhibiting the appropriate level of biocompatibility, any device implanted into a human heart must also display sufficient durability and longevity. It should be emphasized that this poses a unique problem in the field of implantable cardiac devices, due to the extremely large number of cycles that such prostheses are expected to endure. Furthermore, there are potentially life-threatening implications due to device failures. One needs to consider that the heart is itself a highly dynamic organ which can elicit three to four-fold increases in cardiac output (internal pressures); hence, the mechanical stresses on an implanted device can increase four to six fold during exercise.

The relative durability of any cardiac device is further challenged by directly interacting with the turbulent and pulsatile flows of blood, which is the case for prosthetic cardiac valves. More specifically, the flow of blood through mechanical prostheses, particularly tilting disk valves, can lead to a particular type of erosion called *cavitation* whereby gaseous bubbles form and violently collapse on the surface of the valve disks due to the sudden temporary decrease in pressure during closure. This phenomenon has resulted in fractures of the valve disks and was originally observed in the 1980s, in association with the failure of the Edwards-Duromedics valve (Edwards, CA) [123]. Subsequent tilting disk valves, such as the St. Jude bileaflet valve, have been designed to critically reduce this particular material erosion by reducing the area of the tilting disks.

As with other cardiac devices, prosthetic valves are expected to endure a large number of cycles (millions) in their lifetime. For example, in order to minimize the possibility of failure when embarking upon a human clinical trial, the International Organization for Standardization (ISO) has set up a series of strict guidelines for the performance of prosthetic heart valves. The current ISO guidelines require rigid devices, such as tilting disk mechanical valves, to remain functional for a minimum of 400 million cycles (approximately 10 years in vivo), and flexible devices, such as tissue valves, to remain functional for a minimum of 200 million cycles (approximately 5 years in vivo). This testing must be done under the following minimum performance conditions: beat rate = 70 cycles/min, simulated cardiac output = 5.0 L/min, mean aortic pressure = 100 mmHg and systolic duration = 35% (ISO 5840: 2005(E)). Today, no new valve design can progress to a clinical trial before demonstrating these levels of durability over a suitable sample size. Even today, in the newly emerging field of prosthetic valves, there is little long-term clinical data regarding overall durability. However, a recent study by Mykén et al., examining the St. Jude Bicor® stented tissue valve shows promising data on the relative durability of surgically implanted tissue valves over 20 years post implantation [124].

Design for Manufacture

During the cardiac device design process, the design team must not neglect the fact that the new device will eventually need to be manufactured in an efficient and cost-effective manner. Such methodology is known as *design for manufacture* (DFM) and emphasizes that an economically successful design should also ensure a high quality product, while minimizing manufacturing cost. By utilizing manufacturing cost estimates, the DFM process proactively helps to guide and prioritize cost reduction efforts involved with device design. Thus, DFM should consequently have significant effects on product lead times, development costs, and final product quality.

As such, DFM specifically requires inputs from a multidisciplinary team. In other words, the overall process needs to draw upon the expertise of manufacturing engineers, cost accountants, and production personnel in addition to inputs from the core design team [125]. Yet, when applying these principles to cardiac device design, it is imperative to understand that the quality of care impacted by the device must not be compromised by the need for a more cost-effective manufacturing process. One needs to consider that production costs can be controlled by using existing technologies and established manufacturing techniques. In today's medical device industry, numerical methods of design and testing, also known as *in silico testing* , can be used to streamline the DFM process (examples are presented in Ch. 17).

Device Development

In many cases, a novel medical technology often begins as a rough sketch (e.g., on the back of a napkin or on an iPad), thus launching the iterative process of device development and potentially culminating in the evolution into a marketable product. Often these ideas develop

from collaborations between physicians and scientists, but they can also be the product of an inventive individual. Nevertheless, innovations that come from creative minds are generally sorted into two categories—sustaining or disruptive. *Sustaining* innovations within the realm of medical devices are generally considered as improvements to current therapies (i.e., bileaflet mechanical valve vs. a single tilting disk). *Disruptive* innovation comes about when the device revolutionizes the market or initiates its own market (e.g., transcatheter delivered valve replacements vs. surgical implantation).

Today, it is generally considered that most new medical devices, either sustaining or disruptive, are not created by large companies but by small start-up companies. Such small companies are either funded by a venture capital firm or an angel investor (investment from a single person), and are typically focused on developing one primary product. On the other hand, larger companies will generally focus on improving current market-approved products and thus foster sustaining innovations rather than developing new cardiac devices. The rational for larger companies not to develop new devices generally comes from the risk inherent to device development. Nevertheless, there are many different ways in which a medical device may fail to make it to market, and smaller companies are willing to take that risk; many times the company will not survive. For a larger organization, this risk may not be worth pursuing until the device and its company have overcome certain barriers such as initiating animal and clinical trials. In certain cases, a larger company may invest in a smaller start-up, but it may choose not to fully purchase the company until testing has been completed (or at least is underway). Once the smaller company has arrived at this point, larger companies may look to purchase the smaller company; however, the overall valuation will have gone up. Academic institutions can also foster device innovation using grants or federal funding, but very few of these have the general capability and resources to develop a device beyond conception (or early prototyping).

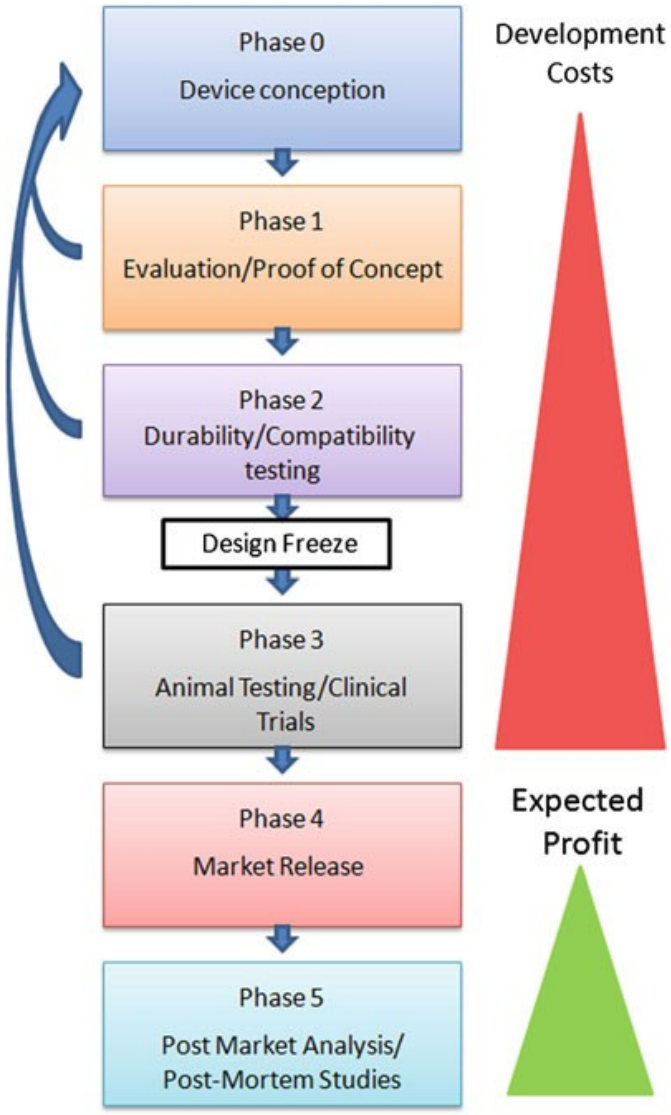

Figure 6.4: Flow chart of device development process. The six phases of device design are shown as well as the expected cost and profit with marketing a medical device

The Commonly Described Six Phases of Device Development

There are a number of different systems that describe the steps taken for the development and testing of any cardiac device. One of these, in particular, involves breaking the process up into six phases of development, as shown in Fig. 6.4. Importantly, throughout each of these

phases, a number of different elements need to be checked and rechecked in order to create a successful device. For example, during *voice of customer* (VOC) research, one should obtain input from numerous consumers of the potential product, including professionals that implant the device, patients, and payers and caregivers. This will help insure that the concept/device fulfills the needs of all those considered as future customers. Business feasibility and marketability will also drive the device design process, in order to be as cost-efficient as possible. Note that the initial stages of research and design are generally the least expensive portion of designing a device. When animal studies need to be undertaken, especially with chronic implant studies, the development costs dramatically increase. Yet, the subsequent human clinical trials have the greatest associated costs, in many cases costing millions of dollars to complete testing (see Ch. 17). Finally, it is critical that the device developer maintains extensive research into retaining *intellectual property* (IP) rights associated with their device. The continually changing design should be determined to be novel, non-obvious, and useful and can therefore warrant a new or continuation patent application.

Phase 0 is often noted as the planning phase during which much of the groundwork is completed, including developing prototype devices, creating a product platform, assessing market opportunities (determining if it will be worth pursuing financially), and identifying product constraints associated with IP.

Phase 1 is considered the concept development phase. This is when the development/ refinement process, as well as bench top testing, of the device begins. For example, feasibility studies are performed to determine whether the product is technically possible to manufacture and create, as well as to estimate the potential market size. Ultimately, the market size will determine the profitability potential of the device. It should be noted that there remains a special need for

pediatric-sized cardiac devices, partly because they are often considered non-profitable to manufacture at small volumes and are thus generally developed as a humanitarian effort.

Phase 2 occurs after the device design meets the previous criteria from Phase 1. This is where further bench top tests are performed for both accelerated failure and required function of the devices. In vitro work or acute animal studies can also be initiated to assess potential biocompatibility. The end of Phase 2 generally involves a design freeze where nothing can be changed on the device without going back to Phase 1 or 0.

Phase 3, which is initiated after the design freeze, assures that testing will provide an accurate assessment of the device function within a living organism. Testing often includes chronic implantation in appropriate animal models, which is then followed by regulatory approvals before the onset of clinical trials in humans. Yet, even subsequent to a success clinical trial, final approval for market release of the product is sought.

Phase 4 is initiated when the product is actually market released. Usually this is the phase of the overall process where the company expects to see a return on investment. Yet, profitability is contingent on successful clinical trials, approval of the device for market release by the regulatory body of the country, and the ability of the company to commercialize and market the device, as well as receive payment (reimbursements) for sales.

Phase 5 is considered to be the post-market assessment. Even though a product is fully marketed and approved by a regulatory agency, the company is still required to perform follow-up studies to ensure that the device does not cause any unforeseen issues with patients over time. This in turn also provides the company with additional information for future improvement of their

device. Types of studies that can be performed in this phase include postmortem studies, where the company may receive the explanted device and then analyze its status/condition.

Intellectual Property

At the outset of any device development project, it is critical to look into the published literature and issued patents for similar products/ideas that may be currently protected. Thus, a major part of the product design process is to maintain ownership or licensing agreements of IP relative to the technologies being developed. It is considered that there are a number of ways that developers can keep their IP safe from others infringing on their idea and thus using it for their own. For example, a *trademark* is a name or symbol that is associated with a product or brand in which a company (and only that company) has full rights to use that name or symbol. This prevents others from using the name and associated marketing as a means of promoting their products or services. Similarly, a *copyright* may be granted for any written and/or graphical materials to an individual or group of individuals to protect their work and reduce the risk of it being plagiarized [126]. Another method to protect an idea or product is to keep it a *trade secret* , simply by not divulging any information regarding how a product is made, operates, or performs (e.g., a device running on proprietary software or novel circuitry), and also banking on the notion that no person can reverse engineer the product and thus replicate it. Yet it should be noted that anyone successful in reverse engineering a product may then duplicate the product or procedure (even without knowing the trade secret) with no legal consequences [126].

The most noteworthy way of protecting IP is to file and obtain a device *patent* with broad claims. A patent is a legal document that explicitly describes how a device works or how a procedure is completed, providing enough information that anyone within the field could duplicate the device or process. In the USA patents provide legal protection for 20 years, thus

guaranteeing exclusive marketing rights during that period. However upon expiration, the device can be copied by competitors without legal recourse [126]. Interestingly, within the medical device industry this is often of little concern, due to the speed at which devices are developed and/ or improved, as newly created and updated products may hold new patent protection.

Consequently, it is vital for any product developer to have a solid understanding of how to read patents in order to avoid patent infringement upon the development/ release of their own device. Typically, patents are classified according to device type and use, and will first provide the filing number(s), inventor(s), and the date filed. Next a description of the device/process is presented, generally involving sketches and other images of IP. The most pertinent information is contained within the claims section, which specifically describes what part of the IP is novel and hence what is officially patented and protected by the law. The claims section is generally the portion that legal teams will address when reviewing a patent case.

To obtain a patent, the USPTO requires that the idea must be novel, useful, and nonobvious. As such, the idea must fall into one of the categories of a process, machine, article of manufacture, composition of matter, or improvement of any of the previous [114]. The USA has recently changed to a *first to file* patent system, which is similar to the current European patent procedure. Previously the USPTO granted ownership of a patent to individuals who were the first to invent. This would mean that documentation was vitally important with dates and signatures referencing the date of the initial invention of the idea. While this method has its merits, the USA decided to move to a first to file system which means the patent is awarded to the individual or group of individuals who were the first to file a patent on that particular process, machine, and/or patentable idea. In general, in order to determine if an idea is patentable, one must first search existing patents to see if it has already been invented. In many cases, finding and utilizing patent

information can benefit medical device designers. According to the European Patent Office, there are a number of reasons and ways to use patents to your benefit including to "find out what currently exists and build on it," "keep track of who's doing what," and/or "avoid infringing on other people's patent rights" [127]. To find pertinent patents relative to the cardiac devices you hope to develop, there are many online databases that can be searched for specific information. A few examples of such databases include the European publication server [128], free patents online [129], and Google [113].

Device Prototyping

In the early stages of creating a medical device, it is best to fully investigate all potential options of the device design. Therefore, broad brainstorming and ideation are key aspects of good product design. Using the philosophy that any idea is a good idea, anything from very quick drawings to "off the wall" ideas can be used to generate novel concepts. It is generally accepted that promoting idea generation is important because, even if a particular idea may not be possible or useful, it may spark ideas from someone else to investigate another portion of the project (providing a different angle or approach to solving the problem at hand). Typically, once ideas are abundant the team can then begin to create a list of the best concepts for the proposed device.

Additionally, a very important part of phase 0 in the development process is the creation of quick mock-ups of prototype devices. The goal of these "quick and dirty" prototypes is to create tangible versions of ideas to help others, as well as yourself, fully visualize and understand the product/idea. In other words, a sketch can give one the ability to depict the idea from one particular viewpoint, but to fully appreciate the idea and understand the nature in which it will interact with its environment, a 3D physical rendering is required. A moveable and/or moldable prototype will portray the workings of the device and potential human factor interactions that may

not be apparent in a 2D drawing. Hence, one of the primary purposes of phase 0 is to develop *proof of concept* and to con firm that the idea can be constructed and eventually manufactured into a viable product.

After proof of concept has been attained and market potential assessed, the design team should select a handful of devices that will be fully prototyped and can be shown to customers for feedback. This is considered to be part of phase 1 during which feedback is obtained by collecting the VOC from a large sample size of potential users with varied backgrounds and clinical experiences. The VOC can be obtained through direct questioning, observation, and/or discussions (or use of a prototype) with the customer. Customers may consist of many groups of individuals, including those who will use the device, those who may be on the receiving end of the device, those who would purchase or pay for the device (reimbursement, insurance companies), and those who could potentially profit from the successful device (investors). These groups of individuals will often aid in the design process and hopefully improve the overall design of the product, to fully meet the expectations of all the primary customers. For instance, a user may want the device to be easy and intuitive to use, while the payer's focus is on expense and potential benefit to the patient in order to ultimately reduce healthcare costs (e.g., including a reduction in the number of required future procedures). Those who expect to profit from the product (e.g., a company's chief financial officer) may demand that the costs of product development are minimized. Hence, all of these design criterion and concerns must be proactively considered and addressed by the design team, if their desire is to create a product that satisfies the majority of their potential customers.

In addition to brainstorming, it follows that one needs to track all potential device defects and failures. Note that early on in the development process one needs to consider the risks and

benefits of employing any new procedure that utilizes a newly developed device (Fig. 6.5). Additionally, specific examples and complete descriptions of risk assessment and analyses for a number of different valve replacement technologies can be found in Ch. 8 and 10.

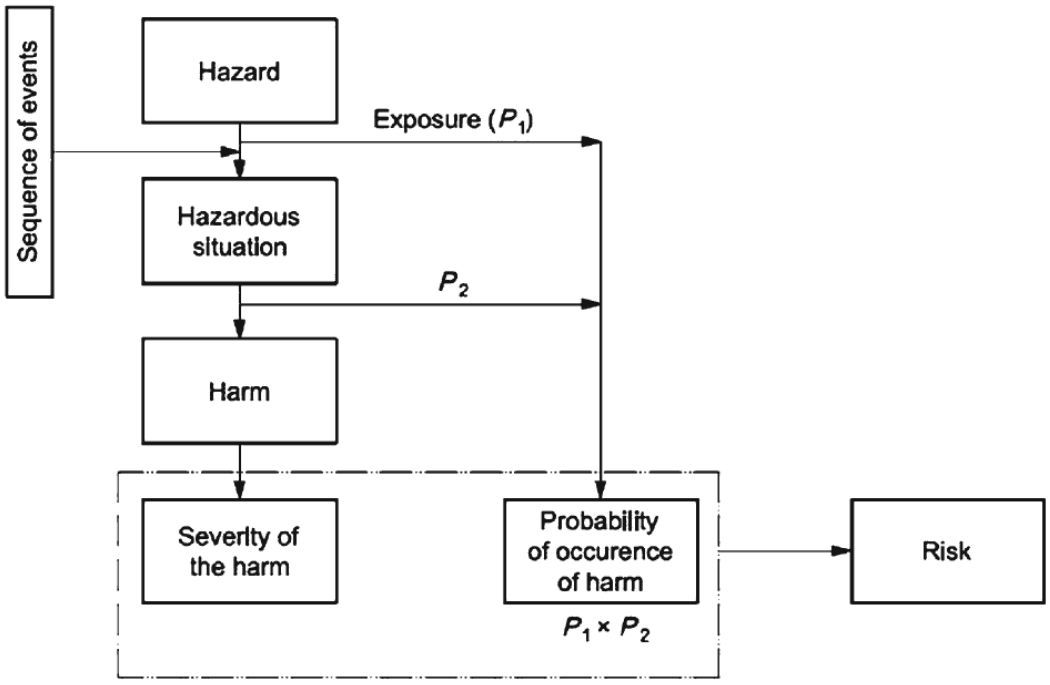

NOTE P_1 is the probability of a hazardous situation occurring.
P_2 is the probability of a hazardous situation leading to harm.

Figure 6.5: An example flow chart for performing risk estimations

In order to complete the risk analysis on a device, one typically employs a *failure modes and effects analysis* (FMEA). These activities are generally defined as a procedure in product development and operations management for identifying potential failure modes within a system, including classification of the severity and likelihood of failure. It is considered that any successful FMEA activity helps the research and development team to identify potential failure modes based on past experiences with similar products or processes. This in turn enables the team

to eliminate such failures with minimum effort and resource expenditure, thereby reducing development times and costs. Figure 6.6 is an example data sheet used for analysis. Complete FMEA on a new prosthetic valve typically creates a 150-page spreadsheet of potential problems, including everything from lea fl et material breakdown to misalignment of the prosthesis within a given heart. Each identified failure mode must be assessed for how likely it is to happen and how severe the impact on the patient could potentially be. If one particular failure mode could feasibly occur in 1 out of every 100,000 patients and have minimal impact on the patient's health, it will not create a drastic design change. Whereas if within the same occurrence rate, a given patient may potentially die from the resulting complications, such a failure mode would need to be addressed.

FMEA number:	Part name: New rigid bileaflet heart valve substitute design	Perpared By:
Design/Mfg. Responsibility:	Part number: 123456	FMEA Orig. Date:
Team members:		FMEA Rev. Date:

Part name & number/function	Failure mode	Potential effects of failure (hazard and/or harm)	Sev[1]	Potential cause(s)/ mechanism(s) of failure	Prob[2]	Design verification	RPN[3]	Recommended action(s)	Reponsibility & target completion date	Actions taken	Sev[1]	Prob[2]	RPN[3]
Leaflet (occluder) P/N 111111 Stops backward flow, opens in response to fluid flow	Rough surface	Loss of biocompatibility resulting in haemolysis, platelet aggregation, thrombus	4	Wrong specification for surface roughness	1	Compare surface to clinically acceptable samples: surface profilometry, SEM, blood flow loop testing	4						
				Inadequate production controls	2	Process validation	8						
	Contaminated surface	Loss of biocompatibility resulting in platelet aggregation, thrombus	4	Inadequate cleaning process	2	Characterize surface chemistry, validate cleaning processes	8						
	Shape of leaflets create poor flow in open position	Turbulent flow resulting in haemolysis, platelet aggregation, thrombus	4	Poor design	2	CFD, Flow visualization	8						
	Fracture	Embolism of small chips resulting in stroke	4	Sharp edges with high stress concentrators	2	Specify appropriate radius of all edges	10						

NOTES [1] Severity rank from Table C.4; [2] Probability rating from Table C.2 or C.3; [3] Risk priority number = Severity rank X probability rating

Figure 6.6: An example of failure modes and effects analysis (FMEA) data matrix used to study a new rigid bileaflet heart valve design

Device Testing

When a prosthetic valve design moves from phase 0 into phase 1 of the design process, a series of extensive testing regimens are initiated to ensure that the device meets the standards set forth by various international governing organizations. These testing methodologies are not only required for the successful market release of a new replacement cardiac valve, but they also provide insights into the design and development of the device and/or subsequent devices. For example, the testing results from a new replacement valve design can elicit information to the design team on how to alter the valve to treat an alternate pathology. The development and testing of transcatheter aortic valve replacements has led to the creation of prototype transcatheter mitral valve replacement devices.

Cardiac device testing can take many forms and often starts with basic static bench top testing without the use of native biological tissues such as silicone, nylon, sponge, or foam [126]. For example, mock silicone substrates approximating the anatomy of a human left ventricular out flow tract and aortic root can be created to investigate the deployed shape of a specific transcatheter aortic valve replacement frame. This is not only a more repeatable procedure due to a decrease in substrate variability, but it is also more cost-effective than obtaining live tissue or live animals to perform such initial basic testing. However, these techniques may not provide necessary insights into specific tissue interactions and/or biocompatibilities, which are primary concerns when developing valves to be placed within a human body.

In the case of replacement valves, all of the current therapies involve devices, delivery systems, and monitoring tools that are inserted into the body and exposed to a harsh biological environment. In some cases, this may be for only a short period of time (delivery systems/surgical tools), yet the prosthesis itself may remain in the patient for the rest of his/her life. Note that specific concerns regarding biocompatibility are discussed at length in Sect. 16.4.2 of this

chapter. In general, the potential for device rejection can be assessed with in vitro immunological responses to the device; a strong immunological response would be indicative of a possible problem relative to biocompatibility and thus a possible device rejection. However, today most replacement valves are constructed from well-studied materials with known levels of biocompatibility; as such, adverse reaction testing is predominantly assessed during chronic animal studies.

Another important factor to consider when designing a replacement valve is the combined effect that temperature and pressure may have on the device. Specifically, one should be aware that there are many polymers, metals, or compounds that change their elasticity properties when exposed to temperatures within the human body. This can be advantageous depending on how the device is designed. The informed engineer may choose to design the device, to be stiff when entering into the vein/artery, such as with a percutaneous delivery system, thus allowing for easier placement. The device would then become more malleable inside the body, as the temperature increases so as not to cause internal damage to the vasculature.

It is important to consider that before embarking upon the expensive animal testing protocols, which are required to prove the efficacy of a potential replacement valve technology, there is exceptional value in testing the device in reanimated beating heart models. Described at length in Chap. 15 , such an approach allows researchers to employ an isolated, living heart as a model to visualize what occurs inside the heart during device deployment and/or how the device may interact with the myocardium throughout all the phases of the cardiac cycle. Additionally, the reanimation of human donor hearts, deemed not viable for transplant, allows for the visualization of specific valve interaction with the varied endocardial anatomy of human hearts, both healthy hearts and those with indications of heart valve disease.

Once in vitro testing techniques have been properly utilized and the device design has been locked in, the development process moves into Phase 3, whereupon the device must be proven safe in appropriate preclinical testing. Generally this requires extensive testing in animal models (acute and/or chronic) before it can progress into a human clinical trial. The use of animals in valve development is discussed extensively in Chap. 14. Essentially, a well-written preclinical testing protocol defines that in order to predict the safety and performance of clinical use, a sufficient number of animals of the same species must be used (preferably the same gender and age). In addition, the animals should have both experimental and control valves implanted in them in all positions indicated by the IFU. The number of animals to be studied may be best determined based upon the risk analyses of the device and the required statistical significance of the experimental design. The duration of the experiment is typically specified in accordance to the parameter under investigation, and each animal must undergo a macroscopic and microscopic postmortem examination. Once the preclinical animal testing is performed using *Good Laboratory Practices*, a third party observer (outside auditor) typically will produce a report summarizing all data collected and making a recommendation regarding the clinical safety and performance of the device. To better understand the full extent of in vitro testing and preclinical testing, the reader is also referred to Chapters 12 and 14, respectively.

Clinical Testing and Regulatory Approval

Once a cardiac device (heart valve) has been proven safe and efficacious during rigorous animal testing, device developers will then embark upon human clinical trials before it can be properly market released. Current regulatory processes in the USA and European Union differ significantly in the requirements and guidelines laid out for clinical testing and market approval.

However, both regulatory committees share the same fundamental principles and apply frameworks designed to ensure the safe and effective release of medical devices into the market. This section will brie fl y highlight features of both approval processes, and additional details about the clinical trial process can be found in Chap. 17.

From a legal standpoint, human clinical testing of an unapproved cardiac device in the USA that poses a significant risk to the patient population cannot be initiated without preapproval from the Food and Drug Administration (FDA) in the form of an *Investigational Device Exemption* (IDE). The IDE is designed to provide the FDA with relevant data on device design and preclinical testing, as well as the intended study protocol. A device company must also apply for an IDE if they wish to expand the indication of an existing device. These clinical investigations may begin at an approved site 30 days after the FDA receives the IDE application, assuming that in-house *Institutional Review Board* approval has already been obtained and that the FDA has not notified the sponsor that the investigation may not begin [130]. To date, FDA approval is contingent on various factors and based upon the intentions of the device; the rigor associated with the approval process increases with the classification of the device. These device classifications are briefly defined as:

- *Class I devices* which pose the lowest risk to the patient, and include noninvasive devices such as surgical bandages and tongue depressors. These devices are placed under the general rules applied to all medical devices and nothing more. Controls include prohibitions against adulteration and misbranding, requirements on establishing registration and device listing, adverse event reporting, and *good manufacturing practices* [131].

- *Class II devices*, such as cardiac catheters, are deemed to pose a high enough risk that regulation through the general controls alone is not sufficient. The majority of class II devices require a premarket notification in the form of a 510(k) to provide data demonstrating that the described device is "of substantial equivalence" to an existing product with regard to its safety and effectiveness. Although a 510(k) can be substantiated through preclinical testing, approximately 10% of applications include clinical data [130].
- *Class III devices* which are used to support and sustain human life, such as implanted cardiac valves, and which also present a high risk of injury or fatality if the device fails. Almost all class III devices require *premarket approval* by the FDA, before they can be legally marketed, thus requiring clinical data demonstrating that the devices are safe and effective in the target population [130]. As such, all types of cardiac replacement valves fall exclusively into this category. Since the valve aids in sustaining human life and device failure could be fatal, the valve must be tested to ensure that it meets the testing required for class III devices.

Recently, development of the *Humanitarian Device Exemption* (HDE) has created a pathway for the accelerated market release of class III devices, an exemption which is intended for devices that address diseases or conditions that affect fewer than 4,000 patients a year in the USA. Nevertheless, approval of an HDE requires the sponsor to prove that the device is safe and effective and that all possible risks associated with it are outweighed by the foreseen benefits. Typically, such approval requires smaller clinical trials in fewer institutions, allowing smaller companies to develop class III devices beyond preclinical investigations.

The idiosyncrasies of clinical trial requirements, development, and completion are described in Chap. 17. Brie fl y in summation, gaining market approval in either the USA or the European Union can be a lengthy, expensive, and time-consuming endeavor. Before embarking on the development of a cardiac device, developing an understanding of these pathways and the intricacies of each regulatory body will help the designer complete the process in the most timely and cost-effective manner possible. To date, the differences between the US and the European Union regulatory bodies result in a large portion of pilot clinical trials and early device testing occurring outside of the USA. Thus the typical cardiac device is introduced into general clinical practice in the USA 1–3 years after its market release in the European Union [130].

Conclusions

Designing and testing of cardiac devices can be a long and arduous process. However, the benefits will hopefully outweigh the challenges. Numerous individuals and companies strive to design and market medical devices to ultimately extend and improve the lives of many individuals. Although the devices may be very different from one another, the key principles of device conception, design, testing, and approval are still in place and pertinent to the success of each device. When the design process is undertaken for a valve replacement or repair device, the creators must take many things into consideration including the implications of the device, how it is to be used, and who will be implementing and receiving the device. Once these issues have been addressed, then the valve platform must not only become manufacturable, but all such products must meet or exceed the specifications set by the device manufacturer. The fields of cardiac surgery and cardiology continue to rapidly develop and expand the cardiac device industry and, in turn, provide innovative and revolutionary valve replacement and repair technologies. Although many valve therapies are conceived from a need within the operating room or cardiac catheterization laboratory, their design and development will lead to future novel

procedures and techniques that continue to improve treatment for patients with valve pathologies. There is little doubt that these innovative improvements will continue to extend and enhance the overall quality of life for patients worldwide.

Ex-vivo Testing of Atrial Septal Tenting with Regards to Transseptal Punctures

Background

Transseptal punctures are required for a multitude of procedures including cardiac ablation, mitral valve repair, and left atrial appendage closure[1]. Currently transseptal punctures are a common procedure that is increasingly prevalent. Despite this prevalence, a thorough analysis of the biomechanical properties associated with this procedure has not been fully completed. An in depth understanding of the force required to displace the septum primum a distance may help to create computer models designed to streamline bench top testing for percutaneous cardiac devices.

In this study we utilized a pre-clinical test method which was described in chapter 3. The Visible Heart methodology [74] allowed us to visualize the amount of tenting the atrial septum encountered when a particular force was applied using a guiding sheath and dilator for ablation equipment. By correlating the force applied to the tip of the dilator to the distance of tenting, an initial look at the response of the tissue when exerted upon by transseptal equipment is being generated. Similarly, this data can be correlated to bench top testing to validate the data generated with that method (discussed in detail in chapter 8).

Methods

To measure the force placed on the septum primum, we needed to create a catheter with distal force sensing properties. The first issue in creating the catheter is that the anatomy of the heart, without going through the free wall of the right atrium, does not allow for a straight on approach to get to the septum. Even if one were to go through the free wall, slight modifications

in trajectory would need to be made to accurately reach and tent the atrial septum. Another primary issue is that with bench top models the anatomy can be distorted or reoriented and essentially creates a completely new environment for the tissue, which could potentially change or alter the outcomes. These two issues are the primary reasons that this experiment was performed with Visible Heart methodologies, allowing for direct visualization of the procedure, as well as a fully functioning and uncompromised cardiac anatomical specimen.

Catheter Development

A method for sensing was created by utilizing an existing sheath used for cardiac ablations. The sheath will allow for more controllable placement of the dilator tip onto the atrial septum. Since the sheath would potentially bend at a specified location along the system, the pressure sensor either must not be affected by the bending, or the bending must be compensated for in some fashion to account for its effect on the sensor. The design we opted for was the former, utilizing a fiber optic cable with gratings set at 1552nm from one another[132]. This is a Fiber Bragg grating (FBG) system (Micron Optics) that senses small changes in the length of the cable that can in turn be measured as strain.

In brief, the gratings are perturbations in the fiber optic cable that alter the refractive index of the fiber and ultimately allow for specific wavelengths of light to be passed through it[132]. By utilizing a DI401 interrogator (HBM, Darmstadt, Germany) we recorded the length of light which was able to pass through the gratings. When no strain was detected by the interrogator 1552nm was the baseline wavelength. If the fiber was bent or compressed, it altered the spacing between the gratings to where they would either increase or decrease and allow for a different wavelength of light to optimally pass through the cable. This change in wavelength could then be correlated to a force if properly embedded in a stable material.

To do this, we employed a FlexCath 12F Steerable Sheath (Medtronic Inc., Fridley, MN) and modified it by fitting it with a Fiber Bragg fiber optic cable with the gratings <1cm from the end of the cable. The fiberoptic wire was threaded down the center lumen of the dilator and the dilator polymer (PBAX) was heated to encapsulate the fiberoptic cable in the grating section (Fig. 6.7). This was done by initially heating up and fitting shrink tubing around the distal portion of the dilator simply to retain the shape of the dilator and subsequently heating the PBAX through the shrink tubing until it flowed and reformed around the FBG cable. The shrink tubing was removed and the result was a dilator with an embedded FBG cable, so that if strain was placed on the dilator the FBG would in turn be affected and result in a recordable change.

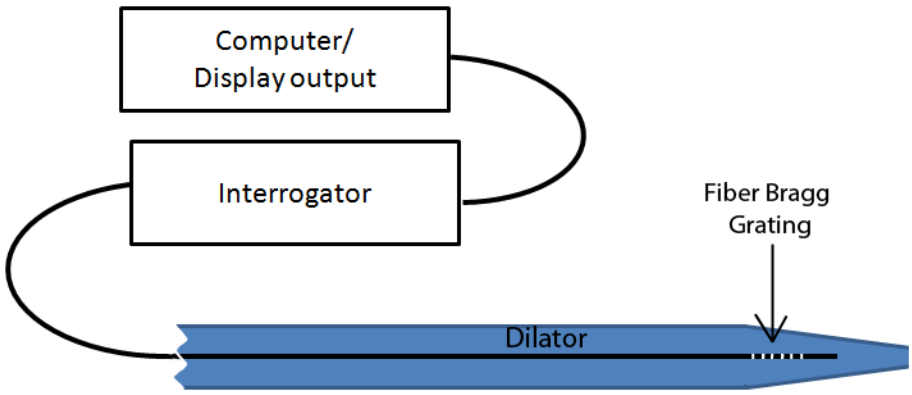

Figure 6.7: Fiber Bragg sensor setup within a dilator. The cable was attached to the fiber optic interrogator and the wavelength reading was output to a data recording system on a computer.

As mentioned before, the FBG can be calibrated to relate to a stress placed on the cable, or whatever medium it is embedded in. To create a calibration, the dilator was advanced through the steerable sheath and the distal half of the device placed in an environmentally controlled "hot box". The box was maintained between 98-100°F with a heater and circulating fan while the tip of the dilator was held stationary and a hand force gage (Chattilon, Largo, FL) placed strain onto the tip of the dilator. The change in wavelength was recorded by the interrogator as the maximal change. This was related to the force place on the tip of the dilator and a calibration curve was

created (Figure 6.8). The best fit line showed a relationship of 318.9gf to every 1nm change in wavelength with a 99% confidence interval of 15.0gf. In some cases bending at the tip was observed and noted. If bending was observed the data was excluded from the calibration.

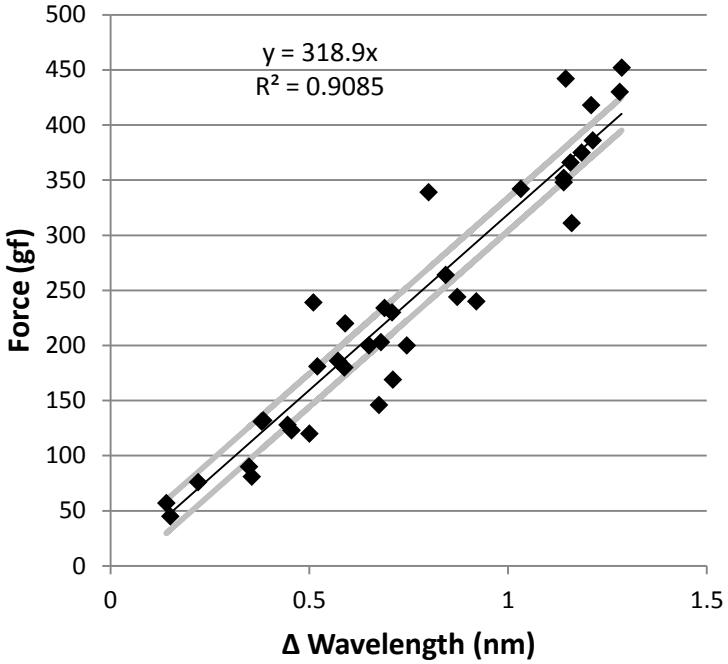

Figure 6.8: Calibration curve of the fiber bragg grating system embedded in the tip of the dilator. Makers are the discrete data points. Black line is the best fit curve with the equation shown in the figure. 99% confidence intervals are seen as the grey lines above and below the best fit line.

Visible Heart Setup and Tenting

Due to the use of swine as a pre-clinical model for transseptal punctures [133–135] and its similarity to human anatomy [136] this species was chosen for our testing purposes. A swine heart was reanimated using visible heart methodologies and is reported in brief here. The heart was arrested using a standard cardioplegia procedure wherein a cold solution of St. Thomas cardioplegia was injected directly into the aorta while the aorta was clamped distal to the injection point. The heart was subsequently cooled with ice until cessation of contraction was observed. The heart was excised and tubes were connected to the great vessels and it was attached

to the visible heart apparatus. This ultimately simulated a transplantation procedure and allowed for direct visualization of the anatomy through endoscopes place inside of the cardiac chambers.

As the heart warmed up it was defibrillated to regain normal sinus rhythm and began to beat using its native conduction system. Through a cannula placed into the inferior vena cava, the steerable sheath and dilator with the embedded FBG was advanced to the atrial septum. The fossa ovalis was located visually and the tip of the dilator was set to point directly at the septum primum, as that is the primary location for physician to tent and perform the transseptal puncture (Fig 6.9).

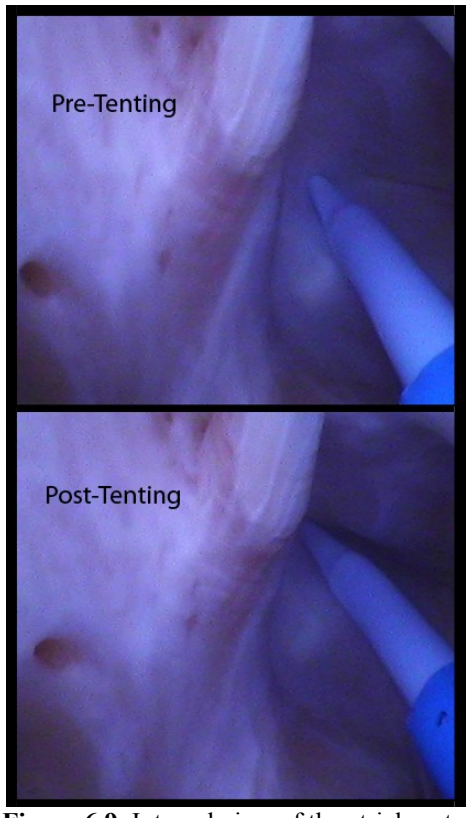

Figure 6.9: Internal view of the atrial septum as seen from the right atrium. These images depict a standard tenting procedure as would happen clinically. The pre- and post-tenting forces were subsequently recorded and analyzed below.

In the left atrium, a standard 7F steerable ablation catheter was placed near the atrial septum as a reference for size. As tenting occurred, the dimensions of the catheter tip allowed for a standardization of the measurements for each series of tenting that was performed.

With each tenting test, the baseline force was recorded with the computer software attached to the interrogator. The sheath with the dilator was placed onto or near the septum and the baseline level of tenting or atrial septal location was recorded with endoscopic images (Fig 6.10). The advancement of the sheath resulted in a shift in recorded wavelengths via the FBG. This was then correlated to the calibration created earlier to derive the force place on the septum to create the tenting.

From the video files, images were extracted and analyzed using ImageJ software[106]. The relative magnitude of tenting was measured and correlated to the recorded force placed on the septum (Fig 6.10).

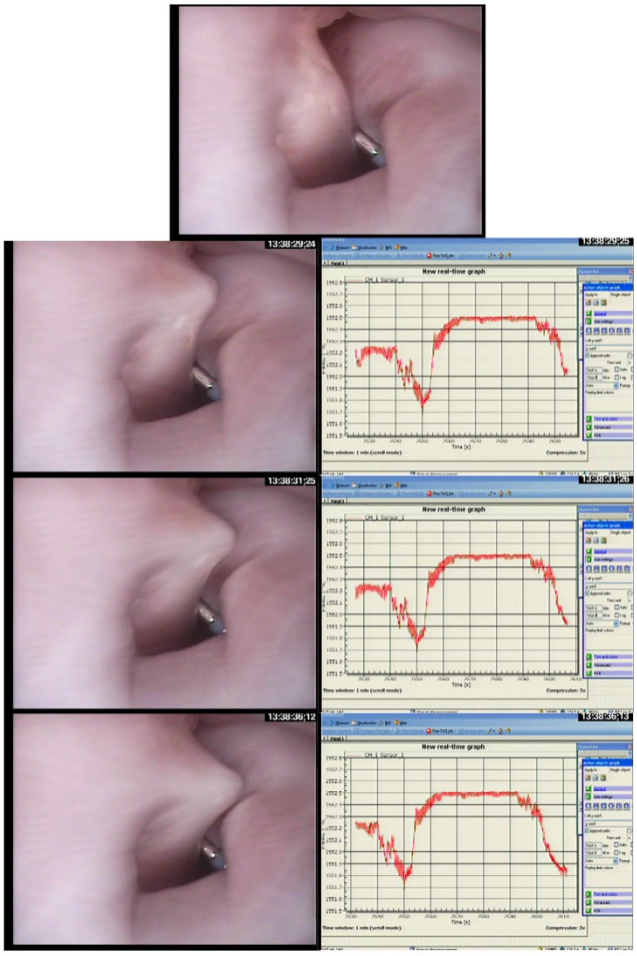

Figure 6.10: Stepwise progression of tenting the atrial septum. The top image depicts the left atrial anatomy prior to any tenting. The subsequent images show the increase in the tenting as well as a decrease in the wavelength recording in the graphs on the right. Note that this decrease in force correlates to an increase in the force placed on the septum.

Bench Top Testing

An experimental setup was developed and explained in detail in Ch. 8 of this thesis. Briefly, excised swine hearts were obtained and dissected to expose the atrial septum. A suction device was placed onto the septum but yet still allowed for tenting and puncturing of the tissue within the suction head. Using a mechanical force tester 44 swine hearts were analyzed for the amount of force required to tent the septum at 5 distinct locations. The average force required to tent the septum 8mm was found to be 109.5, 149.7, 141.3, 143.1 and 136.5gf for the 5 different locations.

Statistics

All data is reported as mean±SE unless stated otherwise and considered significant if $p<0.05$

Results

These data showed a fairly linear relationship between the amount of tenting and the force required to tent the septum that distance (Fig 6.11). The best fit linear curve suggests that about 18.9±3.3gf is required to displace the septum primum 1mm. This data seems to be in correlation to bench top data which was performed and discussed in Chapter 8 of this thesis. The data from the bench top testing suggested a relationship of 17.0±0.9gf/mm of tenting. A comparison was done between the two data sets and it found that no significant difference was seen between the bench and in-vitro testing ($p>0.5$).

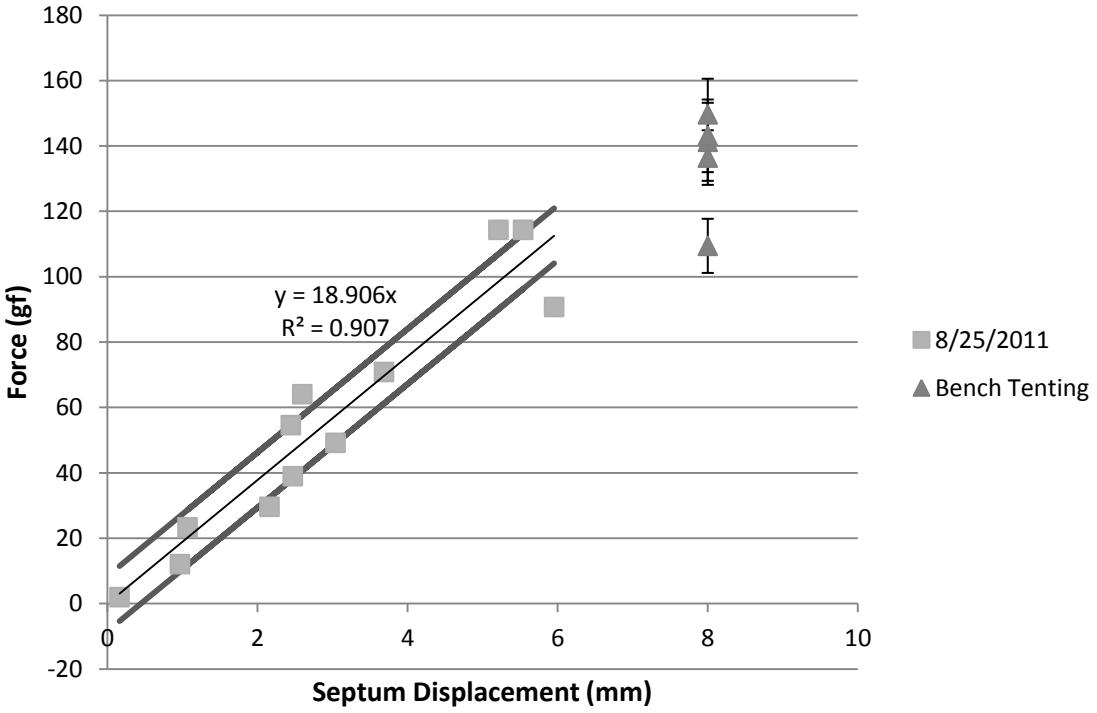

Figure 6.11: Plot of atrial septal displacement compared to the force required to tent that distance. The best fit line is shown as the thin black line and the 99% confidence interval for the line is represented by the dark grey lines.

Limitations

Although these data suggest a good correlation between the in vitro test method and the bench-top testing, more studies need to be completed to fully verify this trend. The bench top data is representative of individual tenting procedures (n=213) performed on different swine heart specimens (n=44) and the in vitro data is representative of n=4 tenting procedures (with multiple displacement vs. force measurements) performed on n=1 heart.

Also, the analysis of the still framed images assumes that the tenting of the atrial septum is perfectly perpendicular to the direction that the image was taken. Due to the non-geometrical shape of the heart this is difficult to obtain, but the authors feel that within this model there is enough accuracy and validity due to the nature of the whole heart preparation.

Discussion

This study allowed for an analysis of atrial septal tenting forces required during a transseptal puncture procedure. The analysis of the ex-vivo of the swine heart allowed for direct visualization of the functional anatomy and assisted in correctly identifying and reaching the fossa ovalis. The tenting was successfully performed and the records of the force measurements showed a linear correlation between tenting distance and the force applied to the tip of the dilator.

The data showed good correlation between the bench top data performed previously and the whole heart model. This implies that the bench top experimental setup may produce valid biomechanical properties compared to those that would be obtained in a whole heart prep and yet have less variability due to the constraints and controlled variables utilized by the procedure.

To the best of the authors' knowledge, this is the first reported look into the biomechanical properties of the fossa ovalis. The data here quantifies the interaction between a transseptal device and the septum primum; something that has been experienced by physicians for many years but never explicitly quantified. Although some may perceive this experiment as insignificant, we believe that it shows that deformation and tenting properties can be deduced from a fully functional whole heart prep under normal physiological parameters and that an experimental model such as this can help to add validity to bench top testing that is being performed.

Section IV: Holes in the Heart

Section Preface:

As shown in previous chapters, atrial septal defects (ASDs) can naturally occur in patients. If they are found, cardiologists will commonly close them through the use of atrial septal occluder devices for the fear that emboli or other substances may traverse the atrial septum and potentially cause a stroke or transient ischemic attack [137]. For these patients this can be an effective treatment to stop or reduce interatrial shunting. However in recent years another sort of defect has been becoming increasingly prevalent.

Iatrogenic atrial septal defects (IASDs) are a form of ASDs that occur as a result of a clinical procedure. The consequence of treating a particular condition on the left side of the heart results in a formation of a hole in the inter atrial septum. This hole size will vary from patient to patient based on many factors including the type of procedure and particular equipment used [105,138]. The interesting point is that the physicians are creating defects similar to those, that if found congenitally, they would consider closing. To add to this confusion, in many cases they do not want to close said defect for fear that they may have to re-do a procedure, which would lead to a more difficult second procedure. Once an occlusion device is implanted into the atrial septum, it acts as a barrier between the atrial because of the device material and endothelialization of the device. This added complexity in turn could potentially result in worse outcomes for the patient [139,140].

The upside of these considerations is that there have been a number of studies conducted to determine the clinical implications of IASDs, when they close, and associated patient outcomes

[1]. In many cases the results suggest that the holes close in a reasonable amount of time and minimal post-procedural complications are seen[138]. However, with the vast differences in catheter sizes and procedural types, the outcomes for an 8 Fr catheter ablation procedure will likely be different from that of a 24 Fr valvular repair device implantation. Very little work has been done to combine this data and determine the procedural and device related clinical impacts of these different types of procedures [138]. To supplement this work I will present a review of the literature pertaining to these defects along with an analysis of the data. But, first I will give an introduction to transseptal punctures, their potential complications and which procedures are at risk for producing such defects.

Finally in the last section of this thesis, I will present some work being prepared for publication regarding the biomechanical properties of the interatrial septum. Cardiac tissue properties of this sort are difficult to come by in the literature, and in many cases only pertain to the biomechanics of valvular tissue [141–143]. This leaves a large gap in the knowledge base surrounding the properties of the interatrial septum. Since we previously reported on the structure of the septum and fossa ovalis, it is only right to address the physical properties of these structures.

Chapter 7: Clinical Outcomes of Transseptal Punctures

Preface

As described previously understanding the anatomy is vitally important for understanding how cardiac devices will interact with the anatomy. Similarly, understanding the procedure utilizing said device is equally important. Here I will present a review of how to perform transseptal punctures, complications that may arise and finally a review and analysis of what has currently been reported in the literature regarding IASDs.

To put together this section I had to rely upon the information from the previous chapters and utilize direct visualization of the anatomy and device interactions. This provides pertinent information regarding the procedure and helps gain a better understanding of the anatomical response to such interventions.

Transseptal Punctures: How to and Clinical Complications

As mentioned previously transseptal punctures (TSP) have been utilized in clinical practice since the late 1950s. In that time little has changed in the procedure. The method for performing the TSP has been improved with better visualization methods such as intercardiac echo (ICE) instead of relying solely on fluoroscopy and pressure sensing [28]. Since its inception, the prevalence of the procedure has ebbed and flowed. Initially it was widely adopted before other methods for pressure sensing or cardiac function assessment, such as echocardiography became more prevalent [144]. In recent years the incidence of TSPs has been increasing, primarily due to an increase in left sided cardiac ablation therapies (Fig. 7.1).

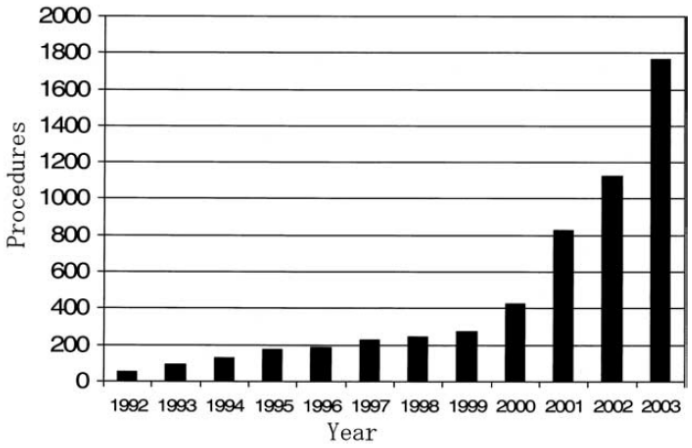

Figure 7.1: Number of transseptal punctures performed at select centers between 1992 and 2003 [145]. *Reprinted from Journal of the American College of Cardiology, Vol 47, De Ponti R., Cappato R., Curnis A., Della Bella P., Padeletti L., Raviele A., Santini M., and Salerno-Uriarte J. A, Trans-septal catheterization in the electrophysiology laboratory: data from a multicenter survey spanning 12 years, pp1037-42, ©2006, with permission from Elsevier and American College of Cardiology.*

The stepwise process has been detailed previously by Dr. Mark Earley [23], but here I will explain the steps with the help of internal endoscopic images taken in the visible heart apparatus. A human heart was reanimated and a transseptal procedure was performed to initially gain access to the left atrium (LA) and perform ablation experiments with another steerable sheath and ablation device.

Catheter Insertion

The transseptal delivery sheath is advanced, generally from the femoral vein, into the right atrium. The sheath includes an inner dilator with a blunt tip. The tip of the dilator protrudes from the sheath enough to allow for optimal localization of the flap valve of the fossa ovalis. With the sheath system fully in the right atrium, the physician will place the tip of the dilator into the superior vena cava (SVC) over a guidewire already placed into the SVC. The next step is to locate the fossa ovalis, this is done by pointing the dilator and sheath in a posteriomedial orientation and slowly dragging the tip of the dilator inferiorly until a characteristic “jump” is seen by the dilator into the right atrium. The dilator is pulled back further until a second "jump" is seen where the dilator falls off of the muscular septum and into the septum primum region of the fossa ovals (Fig. 7.2)[23]. Once the tip of the dilator is in this location, the physician can verify its location utilizing either pressure traces or ICE [35,139,146]. The precise location of the TSP location can be determined using ICE and will depend highly on the type of procedure as well as the patient specific anatomy.

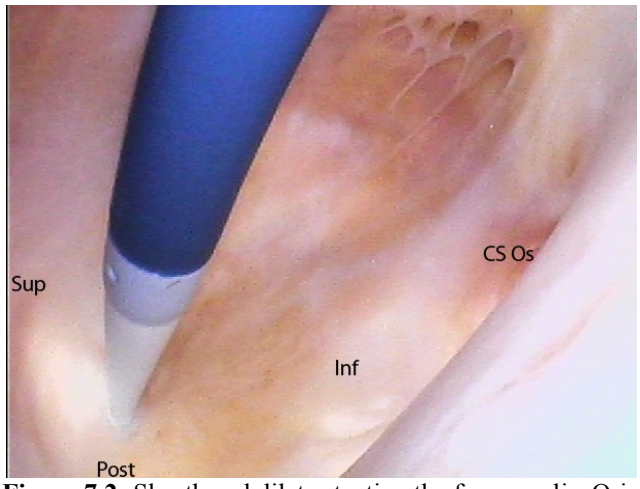

Figure 7.2: Sheath and dilator tenting the fossa ovalis. Orientation is described by superior (Sup), posterior (Post), and inferior (Inf) aspects of the fossa ovalis. Likewise location of the coronary sinus ostium (CS Os) is labeled as an anatomical landmark.

Tenting the Fossa Ovalis

From the left atrium a different picture is seen when the tenting is performed (Fig 7.3). When the optimal location has been obtained and visualized via tenting of the atrial septum, the transseptal needle is advanced and begins to perforate the septum. Following the needle perforation, the dilator is advanced and the needle is withdrawn once the dilator is verified to be within the septum so to reduce the risk of unintended perforation or pericardial tamponade.

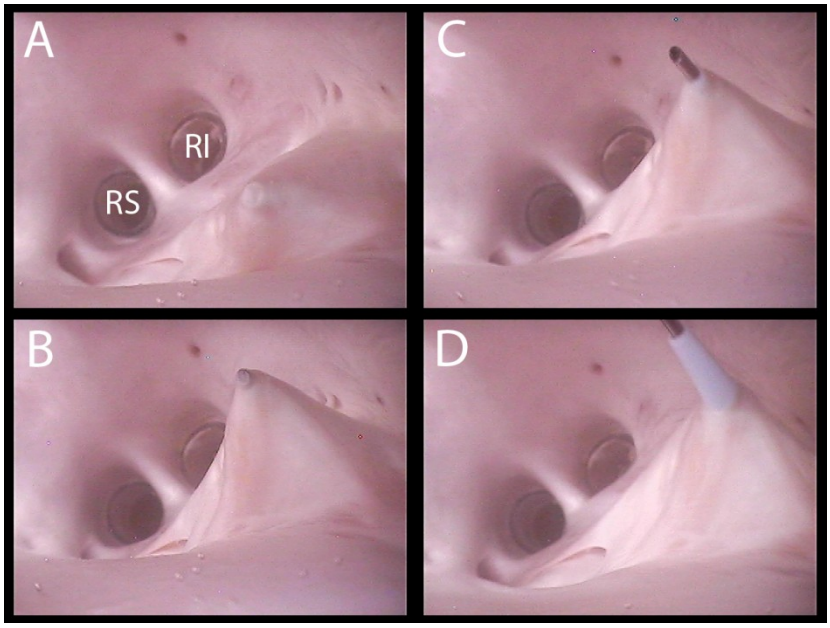

Figure 7.3: Puncturing of the septum primum with a Brockenbrough needle and transseptal sheath. The locations of the right inferior and superior veins (RI and RS respectively) are labeled for anatomical landmarks. The progression of tenting and ultimate puncturing is seen in the progression of images. A) Tenting of the fossa ovalis, B) advancement of the transseptal needle, C) perforation of the atrial septum with the needle and D) advancement of the dilator and transseptal sheath.

Catheter Advancement and Replacement

The transseptal sheath is then advanced with the dilator into the atrial septum to maintain LA access. Then a guidewire is advanced into the LA and positioned deep enough to assure TS access (Fig. 7.4). The sheath and dilator can then be retracted while leaving the guidewire in place. Another guiding sheath can be exchanged by utilizing the guidewire to follow along and

pass through the atrial septal wall (Fig 7.5). One thing to keep in mind when performing this procedure is that by passing a catheter through the atrial septum, it will create what is known as an iatrogenic atrial septal defect (Fig. 7.4D). For all intents and purposes, it is a remnant hole in the atrial septum as a result of the transseptal maneuver.

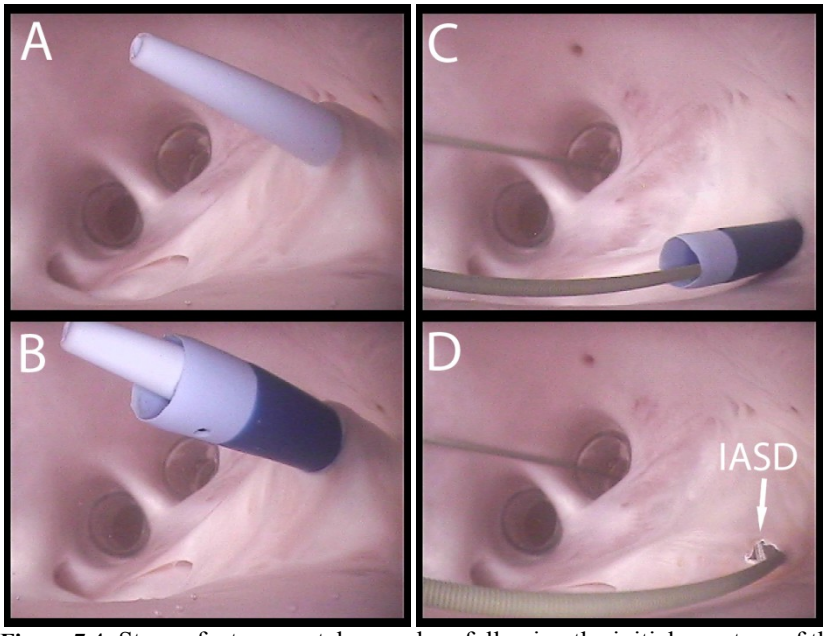

Figure 7.4: Steps of a transseptal procedure following the initial puncture of the septum as viewed from the LA. The goal for this portion of the procedure is to place a guidewire into the LA, remove the transseptal sheath and replace it with the therapy delivery sheath. These steps are illustrated in A) the needle is removed from the dilator, B) the sheath and guide wire are advanced into the LA, C) The dilator is removed while keeping the guidewire in the LA, and D) the transseptal sheath is removed with the guidewire still present in the LA. Notice that in the final frame, as a result of the TSP, an iatrogenic atrial septal defect (IASD) is clearly seen as a hole in the atrial septum.

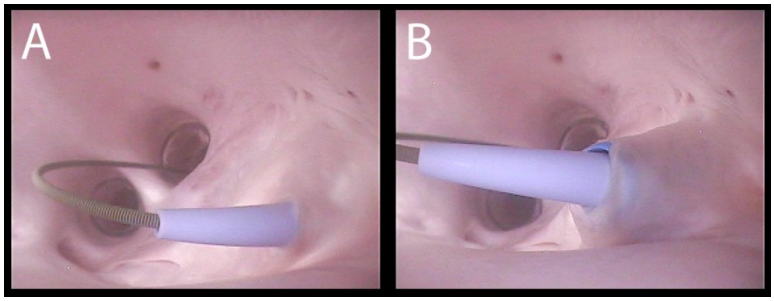

Figure 7.5: Another guiding sheath is placed over the wire and advanced into the atrial septum. As can be seen in A) the dilator passes through the atrial septum and B) the sheath of the transseptal system follows behind it to transition into the left atrium.

Complications of TSPs

No clinical procedure is without side effects. Generally the consequences are both positive and negative and hopefully there are more of the former to outweigh the latter. Transseptal punctures are not an exception from this rule. Obviously the procedure that the patient is undergoing will likely be of benefit for the patient and thus be one of the positive consequences. The negative consequences reported in the literature range anywhere from having to perform a second transseptal puncture to death secondary caused by aortic perforation. Generally this procedure has an overall complication rate between 0.8%-8.7%[11,145,147,148]. Not all complications are considered life threatening and many are reported as subsiding without persistence post procedure and it has been noted that there seems to be a decline in the incidence of complications as physicians become more experienced in the procedure [149].

The primary complications that are reported in the literature are atrial perforation, aortic perforation, stroke or embolic event, and transseptal equipment complications. Issues with the transseptal equipment were reported by B-Lundqvist et al. in 1986 where in 0.8% of the procedures the transseptal needle punctured through the sheath; the TSP was aborted in each case [148]. Such reports are not as prevalent in recent literature which may suggest improved catheter performance or better manufacturing practices.

Perforation is the most common complication that is reported, accounting for between 75% and 90% of the reported complications [148–150]. Perforation can occur in a couple of different scenarios. Following TSP the advancement of the sheath, generally in a superior and posterio-medial direction can be too far and perforate the roof of the left atrium (LA) or the free wall. Alternatively, the perforation can occur as a result of a misplacement of the transseptal sheath and needle. Puncturing too high on the septum will result in a trans-atrial puncture into the

pericardial space rather than the LA. The most important potential puncture site is the root of the aorta. This can occur due to either a non-traditional alignment of the aorta in respect to the atria (generally congenital or surgical malformation), or by not paying attention to or not using various markers to show where the aorta lies. Many institutes will utilize a pigtail catheter placed retrograde into the aorta as a marker for its location [35], or utilize intracardiac echo for visualization of the TSP equipment in relation to the various anatomical structures. All in all the perforation rate ranges anywhere from 0.5% to 4.3% depending upon the institution [145,147]. Aortic perforation was less frequent than other perforation events, likely due to the increased caution taken in regards to the aorta.

Issues relating to perforation generally involve blood being deposited in places it is not supposed to be. For instance, perforation of the atrial wall can lead to a pericardial effusion and potentially tamponade (Fig. 7.6). In instances of tamponade, the heart function will decrease significantly to a point where emergency procedures may be required[151]. When the aorta is punctured, according to physician advice at Transcatheter Cardiovascular Thearapies conference in 2012, the best practice is to leave the catheter in the aorta and call the surgeon immediately. Due to its pressure a patient can bleed out in a matter of minutes and there have been reported incidents of death secondary to aortic puncture [11,152].

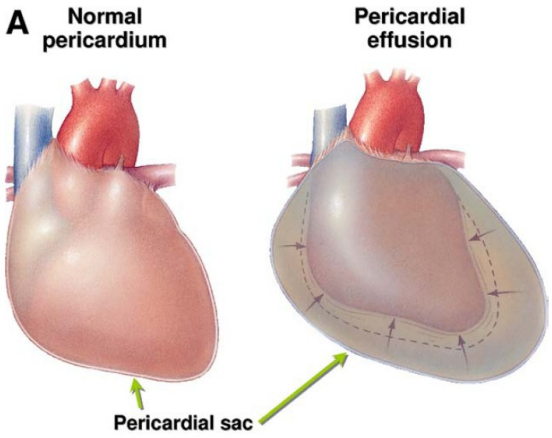

Figure 7.6: Normal pericardium compared to pericardial effusion. Pericardial effusion is illustrated here and clearly shows a fluid layer surrounding the ventricular portion of the heart. This is considered to be pericardial effusion and can lead to cardiac tamponade. The increase in the interpericardial pressure can begin to restrict the motion and function of the heart and lead to tamponade [151]. *Reprinted from Journal of American College of Cardiology, Vol 2, Holmes D. R., Nishimura R., Fountain R., and Turi Z. G, Iatrogenic pericardial effusion and tamponade in the percutaneous intracardiac intervention era, pp 705-17, © 2009, with permission from Elsevier and American College of Cardiology.*

Other notable complications reported include stroke or embolic complications. This distinction of complications is difficult to fully allocate responsibility to the TSP procedure itself, as it is possible that catheter manipulation or the mere presence in the LA would potentially cause the embolus to occur. Ultimately when it is reported in the literature, they relate it to the procedure as a whole, TSP and catheter manipulation together. Incidents of these events have been reported to occur 0.1% to 1.2% of the procedures [145,148–150,153].

The other most notable complication reported in the literature is iatrogenic atrial septal defects (IASDs). This is caused by the TSP as the sheath crosses the septum and a hole is left as a result. As can be expected, these will occur in every patient due to the nature of the defect. However, as will be discussed further in the next section, the rate at which these defects close varies depending upon the nature of the procedure and the patient population. In many patients, the hole closes within a day, maybe even within hours post procedurally[32,150,154].

Iatrogenic Atrial Septal Defect: Literature Review and Data Analysis

Stephen A. Howard
Melissa White
Paul A. Iaizzo

Introduction

Transseptal punctures (TSP) are currently utilized in a number of clinical procedures and there are new procedures on the horizon which may also utilize this approach. In all cases the procedure requires a formation of a hole between the left and right atria (LA and RA). As was already presented in Chapter 4, the defects created are little fenestrations in the fossa ovalis. Clinically these defects have been seen and the incidence and presence post procedurally have been reported.

When discussing issues pertaining to iatrogenic atrial septal defect (IASD) formation, there are a number of factors that can increase the likelihood of its formation. The size of the catheters crossing the septum, the time following the procedure, as well as procedural length have been cited as potential correlates to the presence of IASDs post-procedurally [1]. In this section I will discuss the literature and analyzed data from several studies to demonstrate what factors impact the formation of IASDs the most as seen clinically.

Methods

A literature search of PubMed revealed 18 publications pertaining to clinical studies of iatrogenic atrial septal defects (IASDs). Of these publications 17 were clinical studies and one presented an analysis of 10 of the studies that were included in the 17 reported here[1]. Of the clinical studies, six reported clinical outcomes in point ablation [30,150,155–158], six from valvuloplasty procedures[83,149,154,159–161], two from left atrial appendage occlusion

[32,162], one from cryo-balloon ablation[163], and two from Mitra Clip placement procedures[105,138].

The incidence of recorded IASDs, patient population size, procedural type, largest catheter size and recorded length (if available) were analyzed to determine relationships between these factors and the presence of IASDs. Since the data presented varied in detection technique, time interval, length, and procedural variations, the data was cumbersome due to its diversity. To simplify the data to a manageable level, each study was separated into its discrete observation time points and these points were treated as either specific times or considered to be immediate, early, intermediate or late follow-up, similar to the method utilized by Smith et al. [138]. However, the relationship to time became slightly ambiguous while utilizing the definition of time by Smith et al. which was: immediate 0-1month; early >1-3months; intermediate >3-9months; late >9months. Since there were a number of studies that by this definition had multiple early or immediate time points, to separate them out by virtue of clearer definitions, I set immediate as <1 month, early:1-4 months, intermediate: 4-9months, and late as >9months. If there was variability in the follow-up time (as seen with Casale et al. [161]), the average follow-up time was used to determine the time definition.

Data were analyzed using Minitab statistical software for the linear regression analysis. Otherwise Student T-test was use to compare two sets of data together. Significance was determined with a p-value <0.05.

Results

Due to inherent differences within the studies and the potential error that is not controllable including author bias, physician skill, population size, procedural technique, etc, all

studies are taken to be discrete data points for each of the reported follow-up times. This created a population of studies with single or multiple time points that report %IASDs within the population and the corresponding variables that describe those specific data. Although the larger studies may have finer resolution of the data, this analysis did not take into consideration the population size and thus may be limited within that respect. However, the largest reported study in this cohort was eliminated from the analysis based on the IASD detection technique[150]. As purported by McGinty et al., the studies by Fagundes et al., Ishikura et al. and Casale et al., may have underestimated the true incident of IASDs since each of these studies solely relied on transthoracic echocardiogram (TTE) for post-procedural imaging[1,150,154,161]. This lack of precision was reported on by Di Tullio et al. where they showed that within a cohort, transesophageal echocardiography showed a prevalence of 39% having PFOs. Within this same population, TTE only found 18% and transcranial doppler found 27% [85].Based on these observation these three studies were excluded from this cohort. One exception was made for this analysis wherein the Ishikura et al. study was included in the linear regression analysis since they reported average procedure time. Due to the limited number of other studies that also reported this value (n=5) it was determined that using this data set would potentially help to show the effect of procedure time on IASD formation.

Initial Regression Analysis

A linear regression analysis was performed with respect to the following variables:

Response: %ASDs

Predictors: Catheter size (Fr), time post-procedure (wks), procedure time (min), time indication (value 1-4 relating to immediate, early, intermediate or late time point).

The regression analysis of these variables produced the following:

Regression Analysis: % ASD versus Catheter size, weeks, ...

The regression equation is
% ASD = 54.0 - 0.67 Catheter size + 0.38 weeks - 19.4 time indication
+ 0.154 Procedure time (min)

18 cases used, 20 cases contain missing values

Predictor	Coef	SE Coef	T	P
Constant	53.98	62.13	0.87	0.401
Catheter size	-0.672	3.843	-0.17	0.864
Weeks	0.384	1.078	0.36	0.727
Time indication	-19.44	18.21	-1.07	0.305
Procedure time (min)	0.15425	0.07127	2.16	0.050

One important point to note is that due to the incomplete nature of the data, less than half of the data points were utilized, but this uses the unadulterated data (analysis of the rest of the data will be done in the next section). Since the associated p-values of catheter size and time (wks) post-procedure, these two variables were deemed un-related too %ASDs and were removed from the predictor variables. The analysis was run again and produced results of:

Regression Analysis: % ASD versus time indication, Procedure time (min)

The regression equation is
% ASD = 38.5 - 13.2 time indication + 0.149 Procedure time (min)

18 cases used, 20 cases contain missing values

Predictor	Coef	SE Coef	T	P
Constant	38.52	14.85	2.59	0.020
Time indication	-13.188	4.782	-2.76	0.015
Procedure time (min)	0.14912	0.06188	2.41	0.029

S = 21.6204 R-Sq = 46.8% R-Sq(adj) = 39.7%

Analysis of Variance

Source	DF	SS	MS	F	P
Regression	2	6162.0	3081.0	6.59	0.009
Residual Error	15	7011.6	467.4		
Total	17	13173.6			

Source	DF	Seq SS
Time indication	1	3447.6
Procedure time (min)	1	2714.4

Unusual Observations

Obs	time indication	% ASD	Fit	SE Fit	Residual	St Resid
11	1.00	87.00	35.02	9.34	51.98	2.67R

R denotes an observation with a large standardized residual.

After removing the two variables above from the analysis, it was evident that time indication and procedure time both significantly affected the outcome of IASD prevalence. As one would expect, the procedure time seemed to have a direct correlation to the prevalence and time indication was inversely correlated to the prevalence. Ultimately this suggests that the longer a procedure takes, the more likely the IASD is to be present post procedurally, and the more time post procedurally that it is the less likely the IASD will be present. When breaking up the studies into 0-8months time points and 9+ month time points, and reported procedure length, those procedures that required more than 1.5 hrs did not significantly differ from those requiring less time at the early time points, however, they did show statistical significance when looked at 9+months (Fig. 7.7).

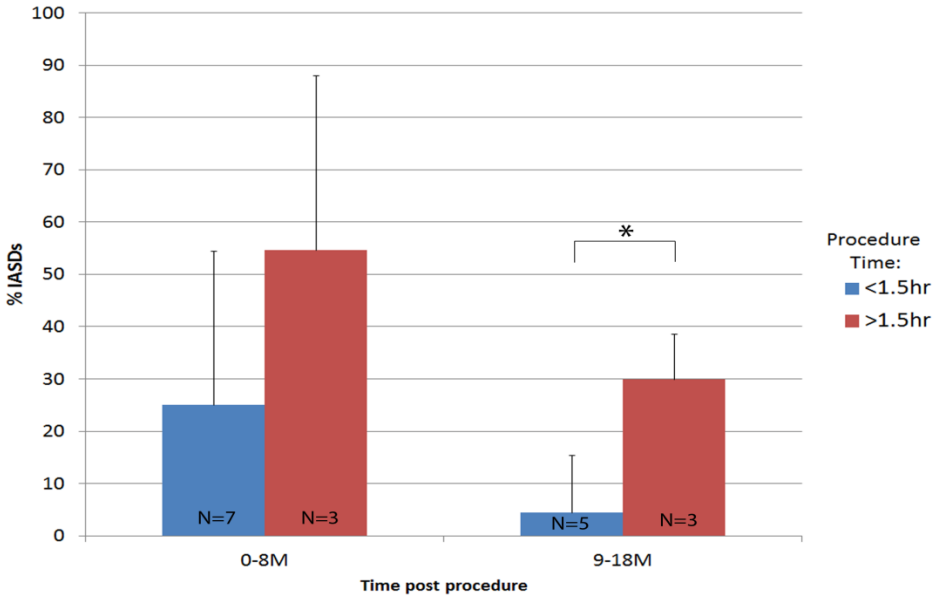

Figure 7.7: Analysis of procedure time with early and late outcomes of %IASDs reported in the literature from various studies.

A potential pitfall to the analysis as performed above is that only half of the data points were considered due to the incomplete nature of the procedural time data. However, since it involves all of the data points related to procedure time, we believe that it is a good model for that variable. To compensate for the lack of procedure time data, values were found in the literature for the various procedure types and the data were given to the data points that were incomplete with this regard. Missing data for the Mitraclip procedures received 231 minutes as a procedure time based on reports from previous Mitraclip studies from similar authors [164]. The point ablation procedures received 240 minutes because of the reports by Rillig et al. 2010 and Hammerstingl et al. 2006 (both of which reported time points included in this study)[155,158]. The mitral balloon valvuloplasty were given 51minutes due to the time reported by Ishikura et al. 1990 [154]. The remaining procedures all had reported procedure times.

Based on these changes to the linear regression model, the following results were obtained:

Regression Analysis: % ASD versus Catheter size, weeks, ...

The regression equation is
% ASD = 48.6 + 1.70 Catheter size + 0.118 weeks - 17.7 time indication
+ 0.0243 assumed procedure time

Predictor	Coef	SE Coef	T	P
Constant	48.57	20.12	2.41	0.022
Catheter size	1.696	1.003	1.69	0.100
Weeks	0.1182	0.5171	0.23	0.821
Time indication	-17.658	9.443	-1.87	0.070
Assumed procedure time	0.02431	0.04722	0.51	0.610

S = 25.4236 R-Sq = 39.2% R-Sq(adj) = 31.8%

Analysis of Variance

Source	DF	SS	MS	F	P
Regression	4	13760.6	3440.1	5.32	0.002
Residual Error	33	21329.8	646.4		
Total	37	35090.4			

Source	DF	Seq SS
Catheter size	1	2395.5
Weeks	1	9059.0
Time indication	1	2134.9
Assumed procedure time	1	171.2

Unusual Observations

Obs	Catheter size	% ASD	Fit	SE Fit	Residual	St Resid
10	9.0	48.00	-0.12	9.02	48.12	2.02R
30	14.0	19.00	12.14	17.75	6.86	0.38 X

R denotes an observation with a large standardized residual.
X denotes an observation whose X value gives it large leverage.

Once again, the weeks post procedure was not significantly correlated to the IASD response so it was removed from the analysis:

Regression Analysis: % ASD versus Catheter size, time indication, ...

The regression equation is
% ASD = 46.5 + 1.69 Catheter size - 15.7 time indication
+ 0.0227 assumed procedure time

Predictor	Coef	SE Coef	T	P
Constant	46.50	17.73	2.62	0.013
Catheter size	1.6864	0.9878	1.71	0.097
Time indication	-15.679	3.722	-4.21	0.000
Assumed procedure time	0.02268	0.04603	0.49	0.625

S = 25.0667 R-Sq = 39.1% R-Sq(adj) = 33.7%

Analysis of Variance

Source	DF	SS	MS	F	P
Regression	3	13726.8	4575.6	7.28	0.001
Residual Error	34	21363.6	628.3		
Total	37	35090.4			

In this analysis the assumed procedure time (involving the native and the added procedure times) showed no significant correlation to IASD prevalence, thus it was removed from the analysis. This effectively nulls the use of the data that was put in place of the absence of data. Then a linear regression using catheter size and the time indication was performed.

Regression Analysis: % ASD versus Catheter size, time indication

The regression equation is
% ASD = 49.3 + 1.72 Catheter size - 15.7 time indication

Predictor		Coef	SE Coef	T	P
Constant		49.26	16.64	2.96	0.005
Catheter size		1.7215	0.9745	1.77	0.086
Time indication	-15.697	3.681	-4.26	0.000	

S = 24.7941 R-Sq = 38.7% R-Sq(adj) = 35.2%

Analysis of Variance

Source	DF	SS	MS	F	P
Regression	2	13574.3	6787.1	11.04	0.000
Residual Error	35	21516.2	614.7		
Total	37	35090.4			

Source	DF	Seq SS

Catheter size 1 2395.5
Time indication 1 11178.8

When looking at this data, this regression model shows that based on these values a statistical model can be created and is highly correlated to both catheter size and the time indication ($p<0.001$). This suggests that these two variables are related to the prevalence of IASDs. Since this data utilizes the whole data set instead of the subset that gave a procedure time, this may be more accurate in regards to how the catheter size plays a role in the IASD formation.

By breaking the data up into the immediate, early, intermediate and late categories, the data becomes a bit more organized (Figs 7.8 and 7.9).

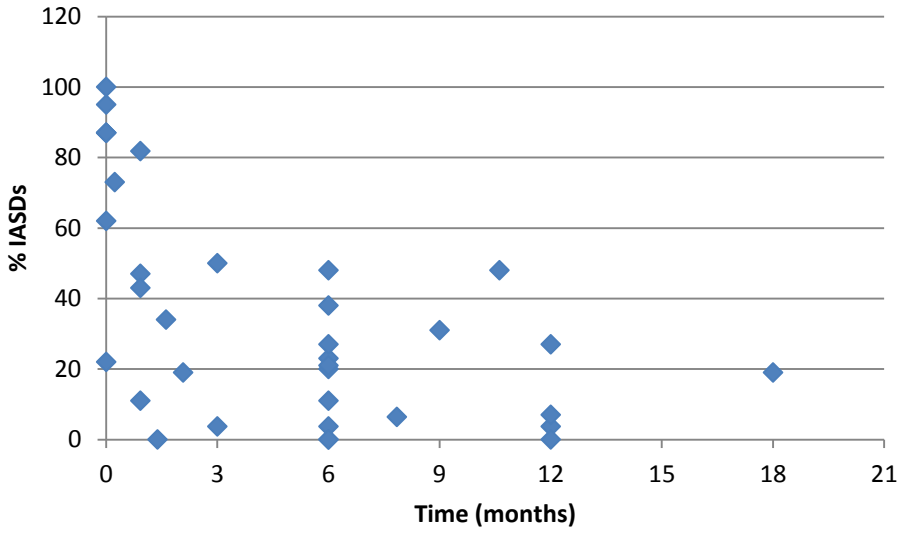

Figure 7.8: The prevalence of IASDs in the reported literature at various time points.

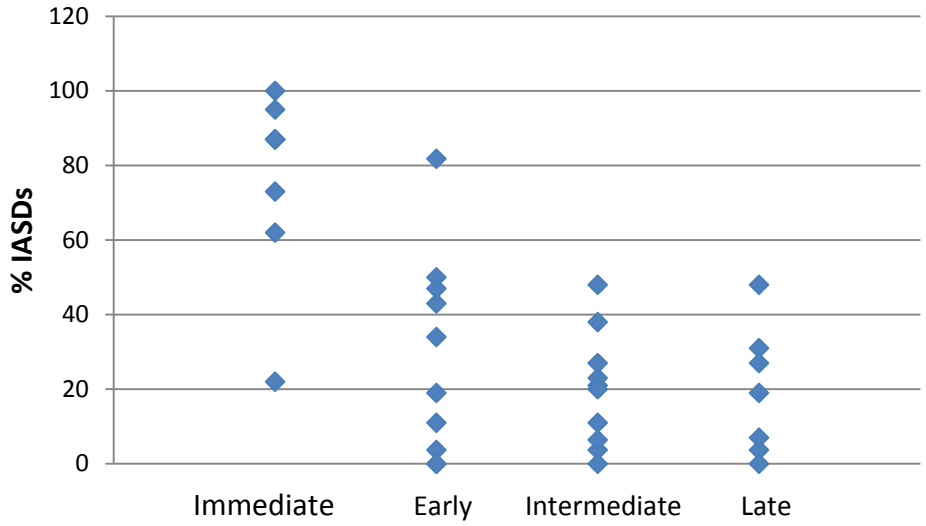

Figure 7.9: Analysis of immediate, early, intermediate and late time points post procedurally and there incidence of IASDS. After consolidating the data points from Figure B into relative time points following procedures the data becomes more coordinated. The time points relate to: immediate as <1 month, early:1-4 months, intermediate: 4-9months, and late as >9months as stated above.

To further break down the data for analysis we separated out the data into the different catheter sizes to see how they related to IASD formation (Figure 7.10).

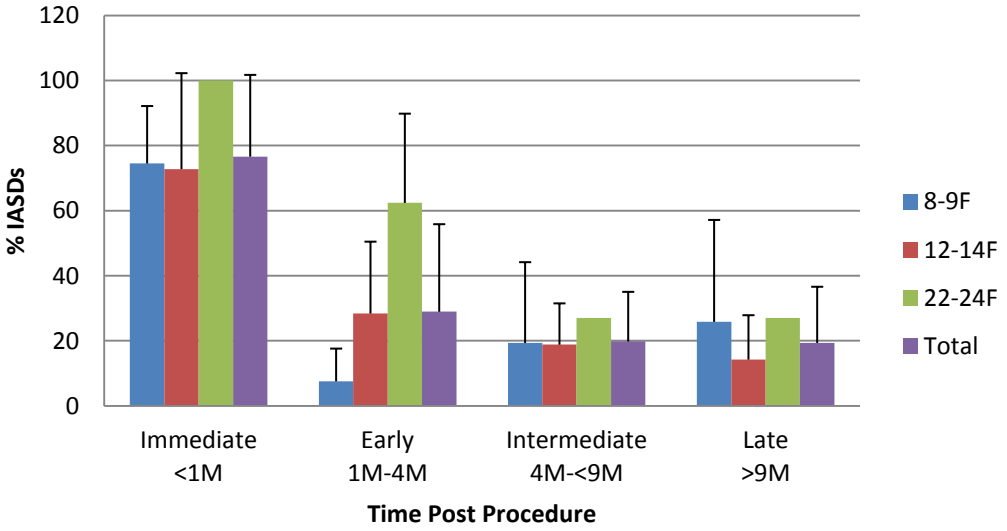

Figure 7.10: Breakdown of catheter size with the prevalence of IASDs at different points in time. Error bars show mean±SD, where they are absent n=1 so no SD could be calculated.

Discussion:

From this analysis of reported values in the literature, it suggests that the primary variables that will increase the prevalence of IASDs following a procedure are the time frame post procedure, catheter size, and procedural length. Although the latter was only found to be true from reported data of half of the literature reports, the results are consistent with initial premonitions. As the procedure length goes up, one would expect to see an increase in the IASDs due to more manipulations being performed in the fossa region thus increasing the propensity for the septum to rip and create a larger IASD. This is something that has been suggested in the literature [154] but yet in other studies no significant difference have been found [32,158].

Since it is fairly convincing that the data shows an indirect correlation between time post-procedure increase and prevalence of IASDs (which would be initially assumed because of healing) this point will not be discussed. The effect of catheter size seems to be one that may need more data or controlled experiments (such as those discussed in chapter 8) to fully understand the effect of catheter size on the IASD prevalence. The data seems to suggest that there is a correlation between catheter size and IASD prevalence, however it may be difficult to elucidate with the current data at hand with only a few studies with data for catheters larger than 20F [105,138,161].

Conclusion:

In recent literature there has been a more relaxed view given to the IASDs following TSP procedures. In one response to a clinical report of IASD outcomes [158] the authors state that the clinical outcomes from these types of procedures do not pose clinically significant consequences to the patient's health[165]. However most of this data is based on 8-14F catheters. Even with larger catheter sizes some suggest that IASDs from mitral valvuloplasty may not be that critical to

follow-up with or worry about post-procedurally[166]. With the limited number of procedures being reported on for larger sized catheters (>20F), there may still be more caution needed and a greater awareness of IASD prevalence for physicians, despite what has been stated.

There have already been initial reports of physicians implanting transcatheter valves into the mitral position via a transseptal approach [167]. If this becomes a more common place procedure, the incidence of IASDs may increase, especially with the positioning needed to accurately place such a device. Although septal occluders could be placed to diminish the IASDs effects, this will severely limit the availability of repeat TSP procedures [139], and depending upon the patient, this could be a major factor in whether or not to occlude the defect. Ultimately based on the current literature there seems to be a need for more studies assessing the outcomes of larger catheter sized devices and what needs to be understood when using such devices.

Chapter 8: Biomechanical Assessment of the Fossa Ovalis

Preface

Currently very little is known about the biomechanical properties of atrial septal tissue, particularly as they relate to transseptal punctures. Even though it is a common place procedure, it seems as though the tissue properties of the interatrial septum are severely under defined. To better understand these properties and try to ascertain these values we designed experiments to deduce the force required to performing tenting and puncturing of the fossa ovalis. To further this study, the tensile forces of the septum were also characterized to determine how a device may interact with the septum during a clinical procedure.

We utilized mechanical force testing techniques to obtain common tissue properties like peak stress, strain at failure and Young's modulus. However, to supplement these tests, a novel setup was designed and created to test the biomechanical properties of the septum as they relate specifically to transseptal punctures. As described in the previous section, a transseptal puncture is performed by initially tenting the fossa ovalis (FO) in the thin membranous region, the floor of the FO. Following the tenting the septum is punctured with a transseptal needle, followed by the rest of the transseptal sheath passing through the anatomy.

With this procedure in mind we created test methodologies to assess the amount of force required to cross the septum and the force required to tent the septum. From these experiments we were able to determine how these factors change with respect to different catheter sizes and locations within the septum. Due to the scarcity of human tissue, these tests were performed on swine hearts. However, to understand how this data relates to human tissue a subset of these tests

were also performed on fresh human hearts. This not only gives us data pertaining to how human tissue responds to this procedure, but creates a more translational model for these experiments.

Biomechanical Properties of the Fossa Ovalis as They Relate to Transseptal Punctures: A Translational Approach

Stephen A. Howard[1,2]
Stephen G. Quallich[1,2]
Mark A. Benscoter[4]
B. Cole Holmgren[1,2]
Christopher D. Rolfes[1,2]
Paul A. Iaizzo[1,2,3]

Departments of Biomedical Engineering[1], Surgery[2], and Integrated Physiology and Biology[3]
University of Minnesota, Minneapolis, MN

Medtronic Inc.[4]
Mounds View, MN

Transseptal puncture (TSP) is a commonly performed procedure that is conducted for the treatment of atrial fibrillation, percutaneous mitral valve repair, and left atrial appendage closure. The basic procedure has not changed in many years with the exception of the advances in medical imaging. However, one aspect that is beginning to change is the types of devices and procedures that use the septum as a crossing point to reach the left atrium (LA). This research is focusing on how differences in catheter size affect the puncture, what a transseptal indication means, and how well the swine model can be a predictive indicator for human. A broad range of devices from 4F to 18F were advanced through atrial septa of swine hearts and a subset were compared to human heart tests performed with a 10F catheter showing that it took more force to puncture through the septum of the human compared to swine. Likewise larger catheters took more force to get across causing more dilation of the tissue and in some instances tearing of the floor of the fossa ovalis (FO), which is the thinnest portion of the atrial septum. The analysis of the remnant holes showed that there was an exponential increase in the size of the iatrogenic atrial septal defect (IASD) that directly correlated with the increase in catheter size. Tensile testing and tearing forces were also assessed on the septum primum and showed that the tissue would rip at a lower exerted force in a superior to inferior direction compared to an anterior to posterior direction.

Ultimately this study begins to look at how these tissue properties impact the way that therapy is delivered into or through the atrial septum. By understanding how the fossa rips preferentially in one direction, this can give physicians the knowledge of what to expect when investigating an IASD, or understand a consequence of TSPs. If the physician deems it necessary to close said defect they will have greater insight into how the defect may behave or present itself. With the comparative data showing the differences between swine and human septa, a correlation between the species gives insight into the differences in tissue behavior.

Background:

Transseptal punctures (TSP) have been performed since the 1960s for clinical procedures[28]. The fossa ovalis in the atrial septum provides optimal location for access as the tissue is thin enough to facilitate tenting and puncturing and delivering percutaneous cardiac devices to the left side of the heart. Other routes (e.g. through the arterial vasculature or transmyocardially) may have alternative complications or be more difficult for the procedure and thus the transseptal approach is often preferred[23]. To perform a TSP, access to the right atrium is obtained through the venous system. Transseptal sheaths are advanced through the vasculature and into the right atrium. By watching for a characteristic "jump" of the dilator tip following retraction and dragging of the transseptal equipment inferiorly, the fossa ovalis (FO) is reached. After the fossa ovalis has been located, the tenting can be generally visualized through fluoroscopy and more commonly echocardiography[146,147]. A physician will tend to look for the most optimal portion of the septum to puncture based on the location. Location of the TSP will vary depending on the type of left atrial procedure that needs to be conducted. Additionally, more than one puncture may be conducted to advance different types of catheters in to the left atrium. Optimal placement of the puncture location is very important for the success of the procedure in a number of instances[168].

The complication rate for transseptal punctures has been cited as low as 0.74% of procedures intraoperatively[145]. The post-operative outcomes however are separate and have shown incidences of remnant interatrial shunts. McGinty et al. presented a review of literature showing prevalence of iatrogenic atrial septal defects to be as high a 87% post-procedurally and at an 18-month follow-up citing incidences as high as 15%[1]. Although they suggest that most of the holes were resolved over time and the iASDs were not associated with clinical issues such as

embolism, cyanosis or right heart failure, these could still be issues especially if one were to begin assessing potential new procedures involving TSPs with larger sheaths.

There are a number of procedures that require a TSP including left sided cardiac ablation, percutaneous mitral valve repair, mitral balloon valvulotomy, left atrial appendage closure and certain ventricular assist device placements [22,23,26,32,105,150,155,157,158,161,169]. These procedures along with some newer and future procedures, including left ventricular endocardial pacing and percutaneous valve implantation, could potentially bring about a greater prevalence of TSPs as well as potential complications to begin to consider[33,34,170]. As cardiology procedures have progressed, the range of sizes for transseptal devices have increased. The smallest transseptal device can be 4F ranging up to the largest reported of 22F[1,171]. This size range prompts a discussion regarding what is the FO capable of tolerating, although some of these have been addressed in previous publications [1,155,158,163]. A detailed study looking at the specific puncture forces, tenting forces along with tensile testing of the FO and the impact of the various sized catheters on the iASD formation is necessary to help understand clinical limits.

In addition to the puncture that is created in the fossa ovalis, manipulation of catheters and tools across the septum may result in the dilated tissue being stretched to its maximum and then result in a tear and elongate the hole, subsequently creating a larger iASD. An initial study into this was done by Saitoh et al. with a mitral valve clip procedure under echocardiography[105]. The holes identified were elongated and elliptical and not circular, suggesting that the simple puncture forces are not the only strains being placed on the septum, but rather some radial forces applied by the catheter could potentially cause tears in an axial direction. This study will provide insight into the biomechanical properties of the fossa ovalis in relation to TSPs. By looking at various device sizes, an idea of how the tissue responds to the

range of potential catheters that could be put through the septum will be studied. The utilization of swine hearts as a model TSP has been reported previously so we believe that it provides a good anatomical basis for study. By utilizing both ex-vivo swine and human hearts, multiple variables can be assessed and a relation to human anatomy can be created[133–135].

Finally the biomechanical characterization of the heart as a whole is currently underway. For instance, interest in tissue engineered heart valves has led to the study of valve properties to better mimic their behavior [141,143]. However, studies assessing the biomechanical properties of the fossa ovalis and methods to reduce damage during procedures to the best of our knowledge are nonexistent. Such information is useful for improving the understanding of the tear forces and biomechanical properties to attain a complete view of IASD creation. As technology continues to advance, computational modeling's role in device development and personalized medicine will likely become readily available and important. [172]

Methods:

Obtaining Tissue and Preparation

Swine hearts (n=48) were obtained fresh and were transported on ice and then dissected. The right and left atria were opened to expose the interatrial septum while keeping intact the tissue surrounding and supporting the FO. The hearts were warmed to 37°C using a circulating water bath. Images of the FO were taken pre and post puncture.

Human hearts (n=7) were received as a donation for research to the University of Minnesota from organ donors deemed not-viable for transplantation (Lifesource, St. Paul, MN). Medical histories were available (Table 8.1) for the patients and 3 had listed relevant cardiac conditions one with atrial fibrillation (AF), one with hypertension and one with an unspecified "heart problem." Exclusion criteria for testing included a lack of an intact atrial septum and no other abnormalities

that would disallow the suction device to be implemented. In all human hearts tested, the IVC was absent due to methods of heart excision and was thusly opened to expose the interatrial septum. These hearts were warmed with 37°C saline.

Table 8.1: Baseline characteristics of the human hearts tested.

N=	7
Male (%)	57.1
Age	58.4±5.7
Weight (kg)	86.0±30
Height (cm)	168.7±7.7
Heart Weight (g)	428±130
Fossa size	
Si (mm)	20.8±6.2
AP (mm)	15.7±6.2
Thickness (mm)	0.68±0.27

Catheter and fossa holder method

A suction device provided circumferential adhesion surrounding the FO (Fig 8.1) to hold the interatrial septum secure in a repeatable way. The suction head was mounted on a movable arm that was able to be fixed in a position to provide optimal maneuverability and placement of the septum normal to the puncture catheters. The devices used in the experiment had an internal diameter (ID) of 4, 8, 10, 12, 16 and 18 French according to their manufacture's specifications. Devices were composed of a dilator and sheath. Only the 4, 8, 10 and 12F devices were indicated for use through the atrial septum, where the remaining two devices are specified for alternative uses within the body, but allowed for testing of larger diameter sheaths. The specific measurements of the outer diameter (OD) as they relate to the catheter size are listed in table 8.2.

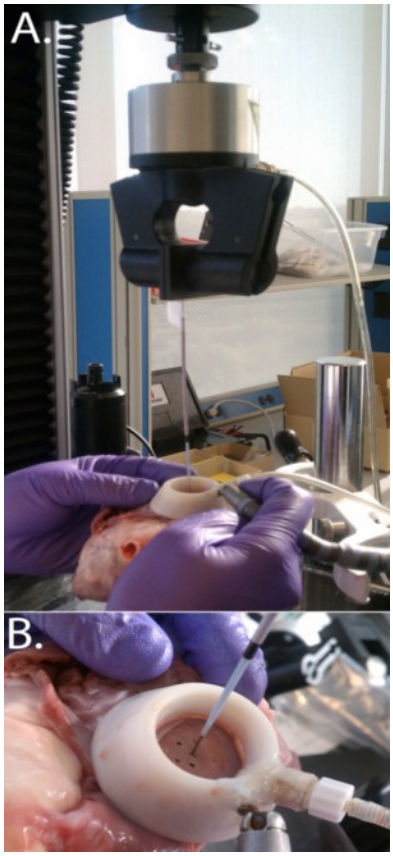

Figure 8.1: Radial adhering suction device for stabilization of the atrial septum for tissue puncturing. (A) Force testing machine with transseptal device attached and puncturing the atrial septum. (B) Close-up of the atrial septum and stabilization device for puncturing.

Table 8.2: Size and dimensions of the catheters utilized in this experiment

Manufacture Labeled Catheter Size	Dilator OD (mm)	Sheath OD (mm)
4F	1.8	2.2
8F	3.2	3.8
10F	3.6	4.1
12F	3.9	4.8
16F	5.3	6.5
18F	6.0	7.2

Catheters were trimmed to a length of 15cm and if curved, they were straightened to keep the structural integrity yet provide a linear direction of force normal to the fossa ovalis. The dilator and sheath were bonded together with UV cure adhesive (Loctite, Henkel, Düsseldorf, Germany) at the cut end of the catheter. The internal lumen of the dilator remained unobstructed

to allow for a Brockenbrough® transseptal needle, cut 18cm from the tip and straightened, to protrude from the dilator tip as it would in clinical practice. Alternative designs were used for the 4F, 16F and 18F devices, since they would not allow for proper protrusion of the needle tip beyond the dilator tip. The end of a Brockenbrough® needle was separated from the main shaft and adhered into the tips of each of the dilators of those catheters with a stiff metal rod through the dilator to provide mechanical support for the needle tip (Figure 8.2). The catheters were either clamped or inserted into a connector attached to a load cell for obtaining puncture forces.

Figure 8.2: Schematic of the transseptal devices for testing. The dilator was seated into the sheath and attached at the proximal end via adhesive. The center lumen was kept clear for a needle to be placed through it and protrude from the distal tip.

Tenting and puncture testing

A circumferential suction device was attached to the atrial septum of either swine or human hearts (Fig. 8.1) to allow for continuous and repeatable fixation of the FO. The suction device was locked into place with the FO in the center of the suction ring. The FO was placed perpendicular to the trajectory of the TS catheter.

The forces required to puncture and tent the fossa ovalis at various locations were obtained by using mechanical force testing systems (Instron, Norwood, MA and Chatillon TCD225, Largo, FL). The locations of tenting and puncturing were defined in relation to the superior, inferior, anterior, and posterior orientation (Fig. 8.3). The shortened catheters were affixed to the load cell so that their trajectory was normal to the floor of the fossa ovalis. Following the stabilization of the FO with the suction device, the catheters, without the needle protruding from the dilator, depressed the FO to a depth of 8mm for swine hearts and 12 mm for

human hearts at a rate of 254 mm/min and then retracted to the starting position. The difference in the protocol between human and swine is related to the differences in the tissue compliance between the swine and human tissue. Pilot studies suggested that the tissue was more easily depressed in the human versus the swine tissue (data not shown). The first tenting location was the center of the floor of the fossa ovalis, followed by the inferior, posterior, superior and anterior portion. This experiment provided the information regarding how much force is required to displace the septum of the swine and human, and to determine the variation between the two. Then the catheters were driven through the fossa ovalis with a Brockenbrough® (BRK, Medtronic, Fridley, MN) TS needle protruding from the dilator at a rate of 254 mm/min at various locations on the FO, beginning with the center followed by subsequent puncturing at alternate locations.

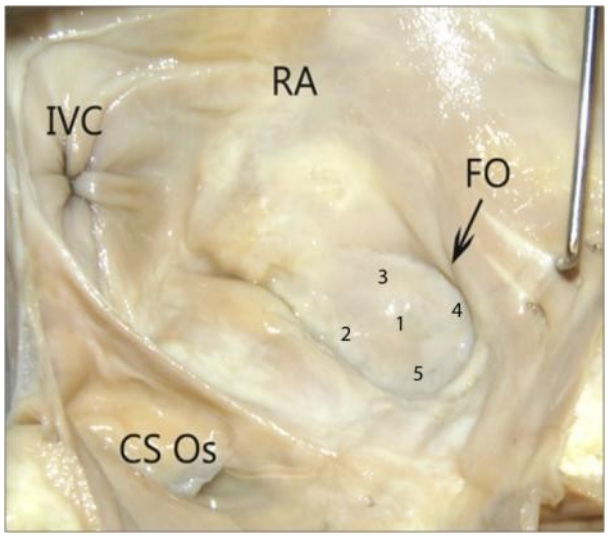

Figure 8.3: The location of the fossa ovalis (FO) in relation to other anatomy within the right atrium (RA) [inferior vena cava – IVC. Coronary sinus ostium – CS Os]. The numbers indicate various puncture locations (1) center, (2) inferior, (3) posterior, (4) superior, and (5) anterior.

An initial analysis of the force versus distance graph showed that the largest forces required for transseptal puncture were when the tip of the needle, tip of the dilator, dilation of the septum and the tip of the sheath were going through the septum (Fig 8.4). The force and distance

were recorded by the system for each of these events for the various puncture location. Following the punctures, the sizes of the remnant holes were recorded.

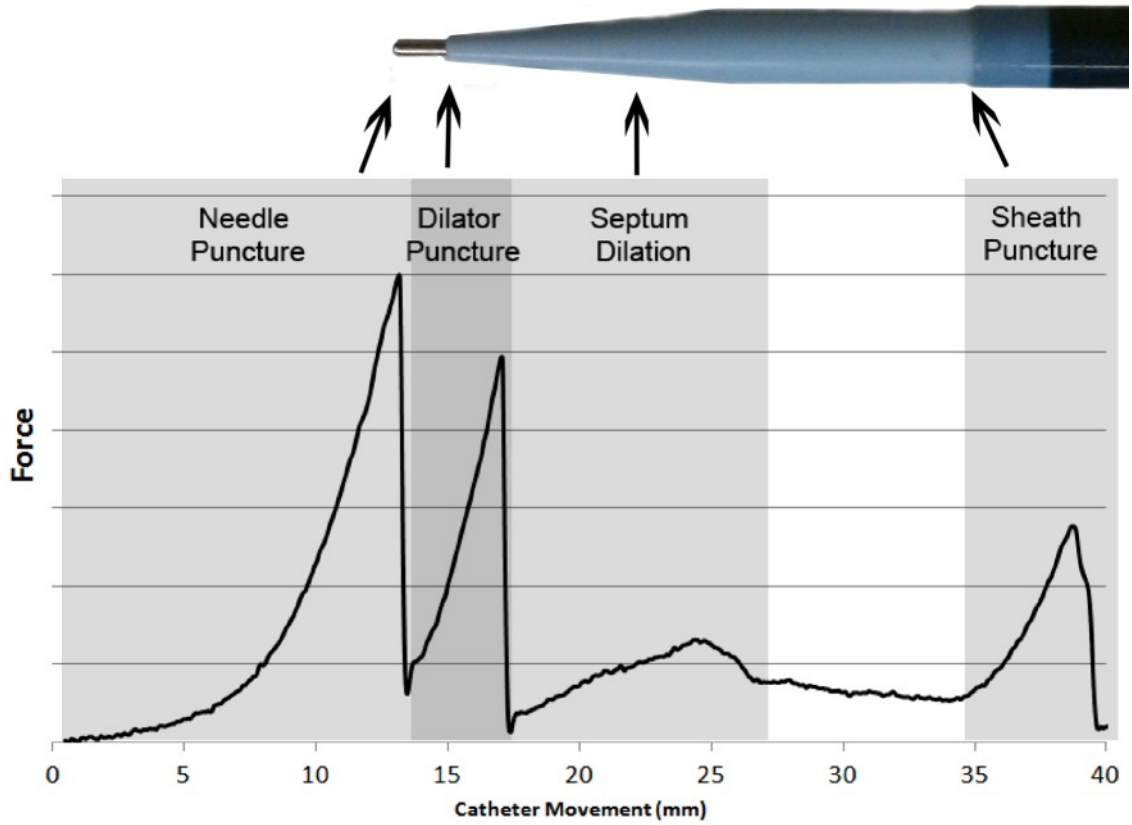

Figure 8.4: Characteristic force verses distance graph during FO puncturing. Note the distinctive peaks during each transition of the dilator and sheath; upon reaching a new layer the force increases due to the need for FO expansion.

Fossa Ripping Force Analysis

Yorkshire X swine hearts were obtained from the University of Minnesota Meat Sciences Laboratory and the Visible Heart Lab (n = 70 animals/samples). The hearts ranged from 400-650g in size. The entire atrial septum including approximately 5 mm of tissue surrounding the floor of the fossa ovalis (FO) was excised from the heart. Samples were randomized to size and direction groups and the inferior or posterior portion of the musculature surrounding the FO floor was cut off (Fig 8.5A). The FO was punctured with a transseptal Brockenbrough® needle and a 4, 12, or 18 F sheath was advanced through the septum. The sheath and dilator were maintained

in a perpendicular position relative to the floor of the FO via a custom fixture (Fig 8.5B). While the side of the FO opposite the cut side was anchored, the sheath was pulled away from the base causing it to rip through the FO at a rate of 100 mm/min with a mechanical force tester (Chatillon, Largo, FL). The atrial septa were ripped towards the cut section of the septum in either a superior or posterior direction. The average sheath ripping force was defined as the average force while the septum primum was ripping. To illustrate this, an example graph shows that during the 10-19 mm extension portion for this sample was defined as the average ripping force, while the peak sheath ripping force was the highest force recorded (Fig. 8.5C). FO dimensions, average and peak sheath ripping force were also recorded.

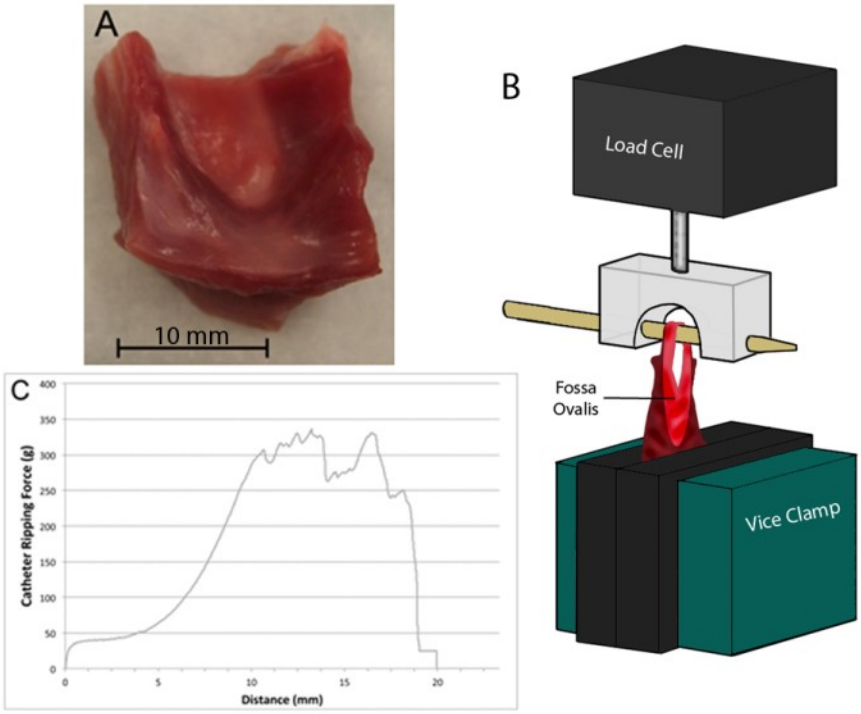

Figure 8.5: Fossa ripping test setup. The muscular tissue adjacent to the septum primum (posterior rim of the fossa ovalis for posterior pulls and the superior rim inferior pulls), was cut off to allow the sheath to fully disengage from the atrial septum without consequence from the muscular portion of the atrium surrounding the floor of the FO (A). The fossa ovalis was ripped by a catheter which was inserted through the floor of the fossa ovalis in the mechanical force tester (B). An example of the resultant force versus extension plot is shown in (C).

Tensile Testing

The atrial septa were harvested is the same way as described previously (n=16 animals, n = 41 samples). The FO was dissected into several (1-5) strips along either the superior/inferior or anterior/posterior direction. The strips were cut in a dog-bone shape and 2-0 silk sutures were tied to both ends (Fig. 8.6). The dog-bone shape resulted in a repeatable tissue break in the middle of the specimen. Any specimen which broke at a location other than the middle was considered faulty and discarded from the results. The samples were pulled at a rate of 100 mm/min until failure with a mechanical force tester. The dimensions of each sample were recorded along with the strain at failure, peak force and calculated Young's modulus.

Figure 8.6: Dog-bone shaped samples prepared for testing (A) and with 2-0 silk suture attached while mounted in the testing pull tester (B). The Young's modulus and peak tear force was calculated for each sample.

Statistical Analysis

All data groups were tested to find significance using Student's T-test for one to one comparison and ANOVA for comparing 3 or more groups. All data in this paper are represented as the mean±SE unless otherwise noted. Significance was determined with a p-value<0.05.

Results:

Tenting

The tenting experiments showed that although the average force require to tent the septum primum 8mm was greater in humans compared to swine (199±30gf vs. 135±5gf respectively, $p<0.001$, Fig. 8.7). By breaking down the data to assess the effect of location on the tenting force, only one difference was seen in the inferior portion of the FO where the human tenting was significantly higher (145g±65g, n=40, vs. 292g±213g, n=8; $p<0.01$). The remainder of the locations remained not significantly different from one another, although when all the data is combined, the swine requires significantly less force to tent the fossa regardless of the location (swine 138±5g n=180 vs. human 199±30g, n=23, $p<0.001$). In general the lowest tenting forces were seen in the center of the fossa, however the data was not significant ($p>0.05$).

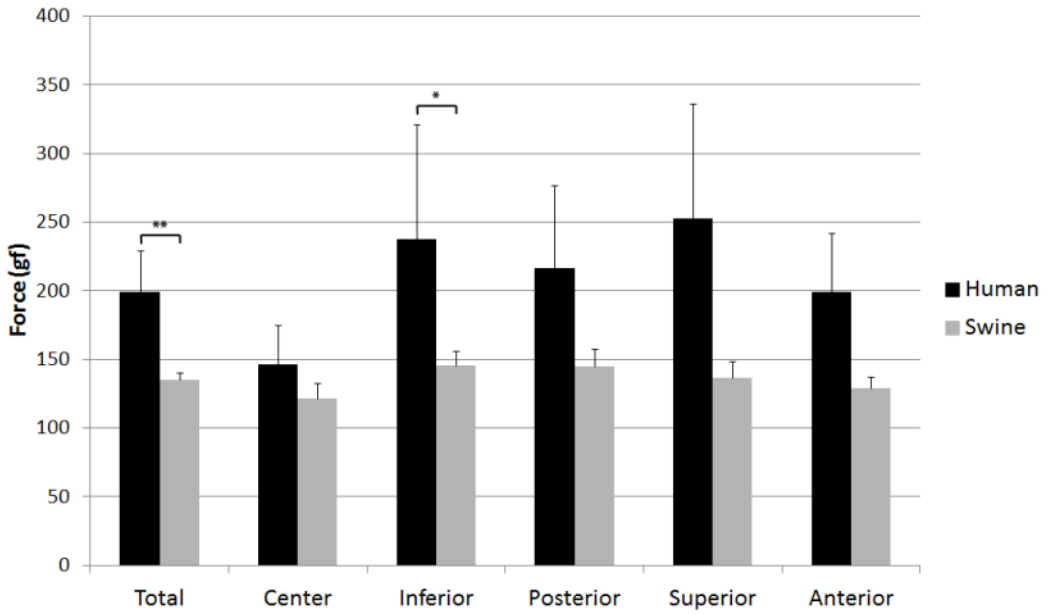

Figure 8.7: Force required to tent the fossa ovalis 8mm. Experiments were performed on excised human (n=8) and swine (n=40) hearts. Error bars depict SE. (*=$p<0.01$, **=$p<0.001$)

Puncture Force: Human vs. Swine

Because of the rarity of usable human heart specimens, the 8 hearts were punctured only with the 10F catheter for comparison to the swine hearts. The punctures resulted with a

characteristic force vs. distance plot where the force for the needle, tip of the dilator, and the sheath to pass across the septum were easily obtainable as peak forces (Fig. 8.4). The other force recorded was the maximum force seen during the dilation phase (eg. when the tapered portion of the dilator passed through the septum).

When comparing the 10F catheter between the swine and human data, the results showed a higher force required for each portion of the catheter (Fig 8.8). The greatest difference was seen between the peak force of the tip of the dilator for the human and swine tissue, with it requiring 240% of the force required for swine hearts. Significant differences were found when comparing the average force required to pass the various potions of the catheter through the septum for the tip of the dilator, dilation and the sheath ($p<0.01$ for each).

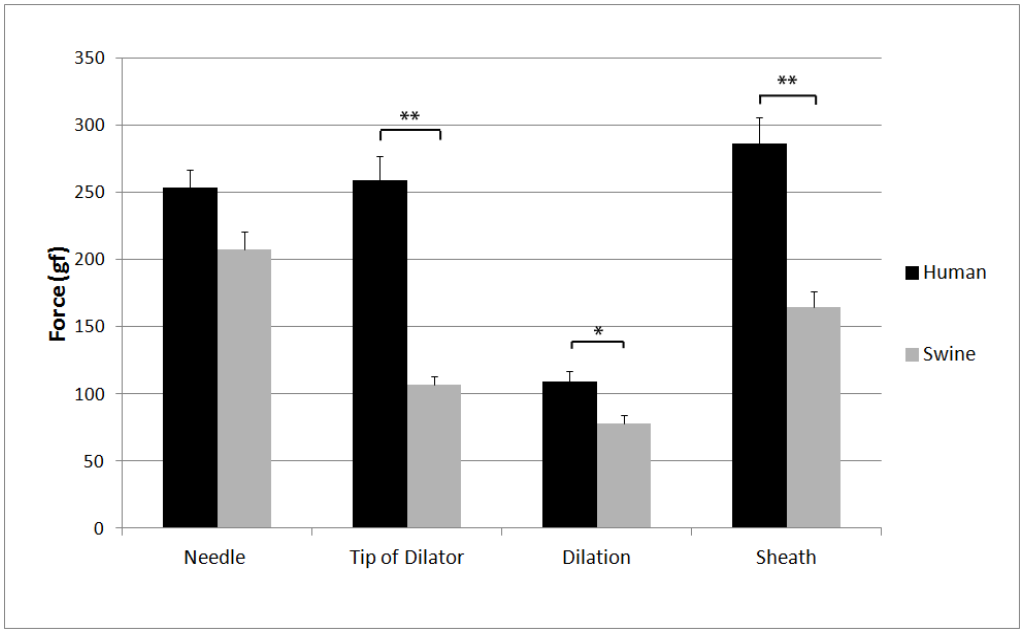

Figure 8.8: Average peak force required to pass various portions of a 10F sheath through the septum primum in human and swine hearts. Significant differences were found between the two species when comparing the tip of the dilator, dilation and sheath forces (*=$p<0.01$, **=$p<0.001$). Error bars represent SE.

While assessing the distribution of the peak protrusion force for each portion of the TSP catheter, it was found that there is a larger range of values within the human tissue data compared

to the swine tissue. Looking at the plots of the distribution of force required to pass the various portions of the sheath through the septum showed a larger distribution between the human data as compared to the swine data (Fig 8.9). Although this trend was seen for the tip of the dilator and sheath, the range for the needle puncturing produced a plot with similar distributions for both the swine and human data.

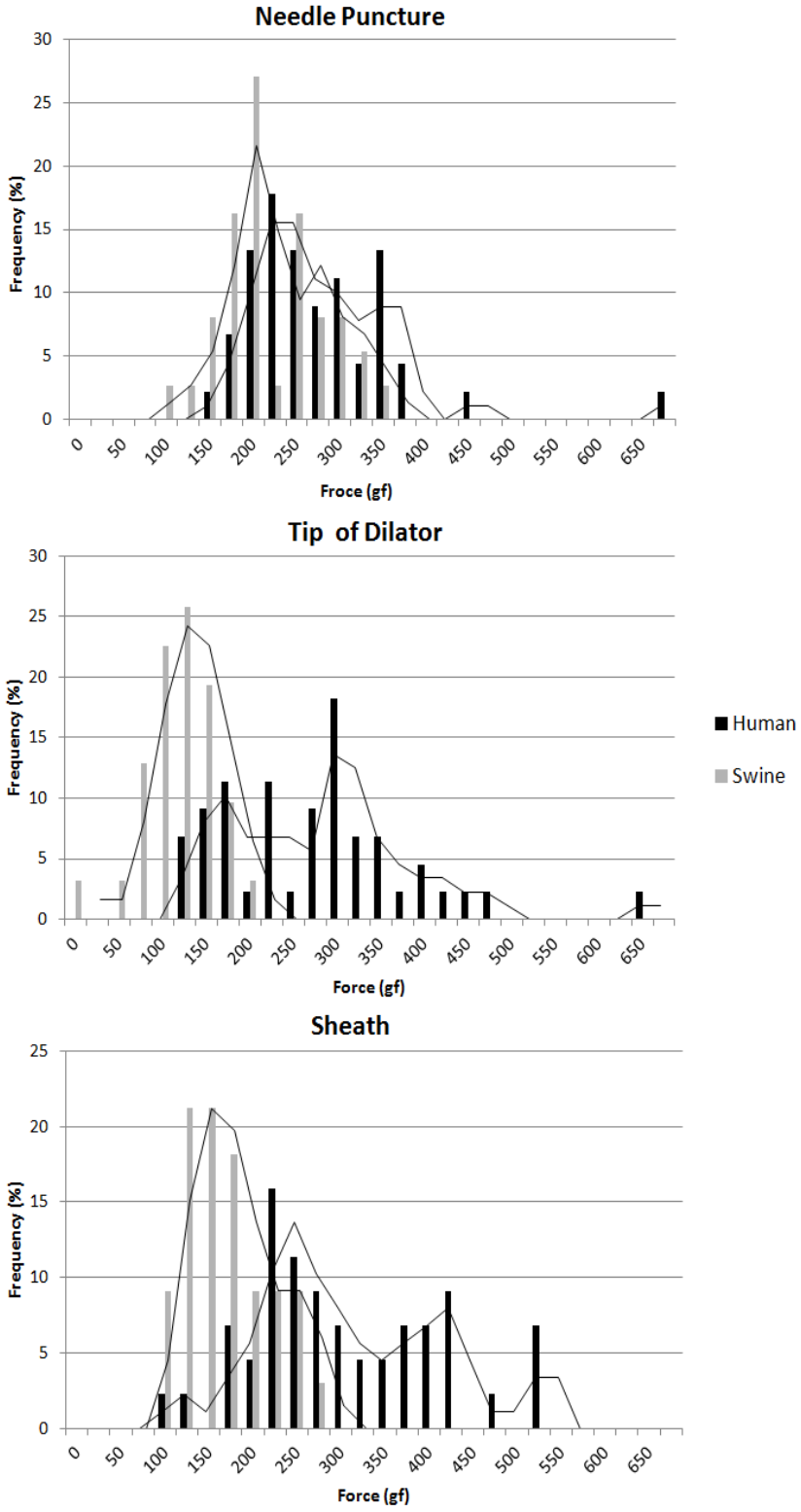

Figure 8.9: Distribution of peak forces required to traverse the septum with various portions of a sheath.

Puncture Force: Sheath Size Comparison

The variability in the needle puncture alone resulted in an average puncture force of 201±75gf (±SD) when considering the 176 punctures that were performed with the Brockenbrough needle. To account for this variation between the differences in tissue performance, the subsequent portions of the sheath were normalized to the needle puncture force. This will help determine the relationship between sheath size and resultant force required to traverse the septum. The results showed that there was a direct correlation between catheter size and force required to pass through the septum. On average the needle puncture required greater force than both the tip of the dilator and the dilation force. ANOVAs were performed for each of the sheath sections and found that there was significant differences within each group with p-values<0.001 (Fig 8.10). The other notable trend seen was that the dilation force was significantly less for each of the sheath sizes compared to both the tip of the dilator and the sheath ($p<0.02$ in all instances).

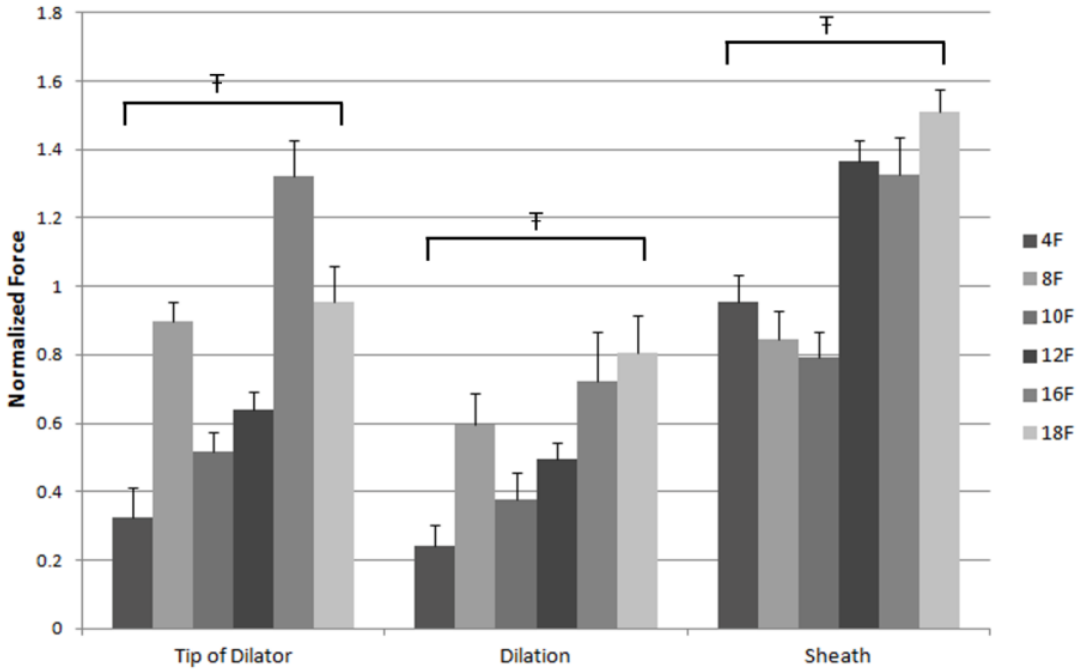

Figure 8.10: Relative force required to traverse the atrial septum with the various portions of a transseptal sheath of difference sizes. (Ŧ=p<0.001 based on ANOVA of all catheter sizes for the measurement)

Following the punctures, images were taken of the resultant holes formed in the atrial septum. The minimum and maximum lengths were found and plotted in relation to the OD of the sheath. There was a direct correlation between the hole size and the sheath size as one would imagine. The data seemed to show an exponential increase in the hole size with the increase corresponding to the increase in cross-sectional area (Fig 8.11).

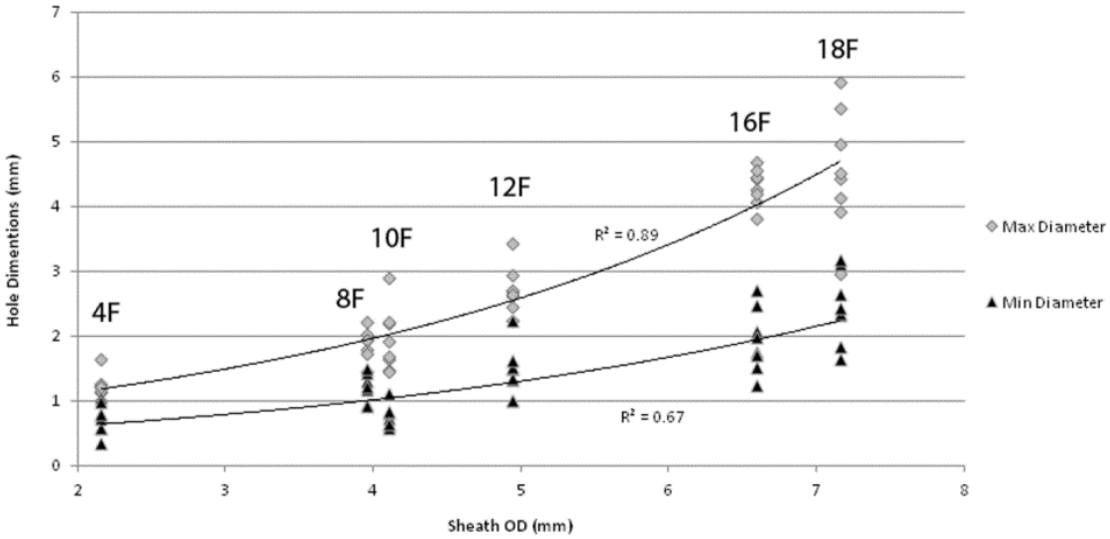

Figure 8.11: Minimum and maximum diameter of iatrogenic atrial septal defect following simulated transseptal punctures with various sized catheters.

Another aspect of transseptal crossing of devices relates to the differences in size between the different parts of the catheter (ie. the increase in the diameter going from the dilator to the sheath). Intuitively the increase in the transition gap will require more force to move across the septum (Fig 8.12). Increasing the diameter discrepancy between the subsequent portions of the TSP sheath requires an increase in force. The data shows that there is a bit of a plateau of force with the increase in the area difference.

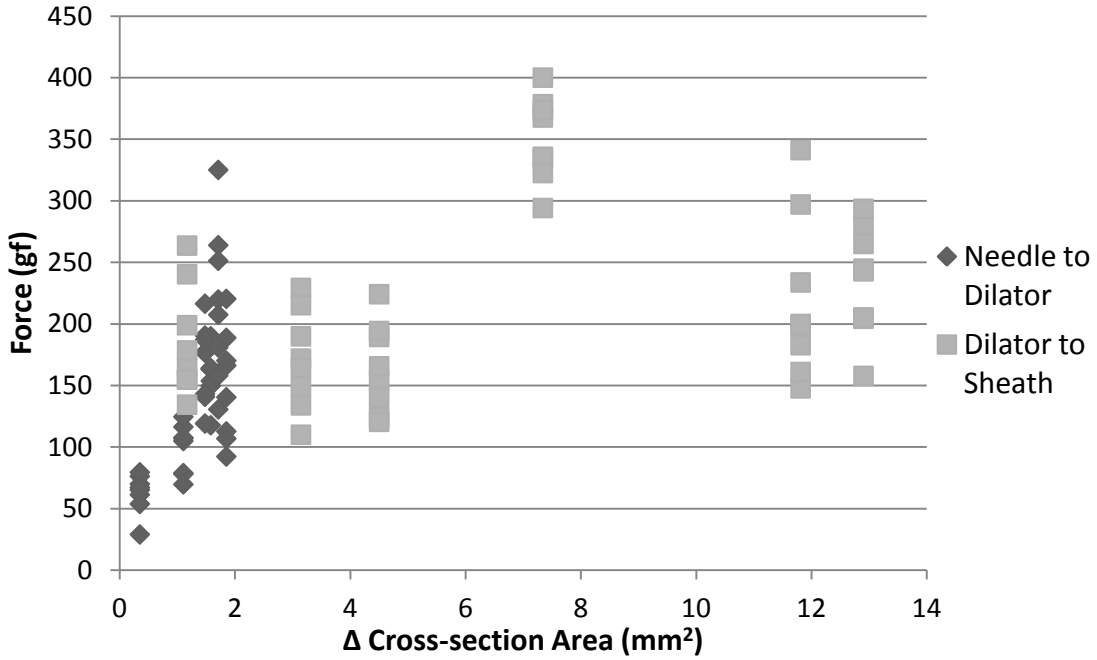

Figure 8.12: Force required to transition from one portion of the TSP sheath to the other. An increase in the cross-sectional area of the relative portions of the catheter requires more force to pass the catheter through the septum.

Septal Ripping Force

The summary of the septum ripping with different sheath sizes is presented in Table 8.3. The direction of FO ripping had a significant impact on average and peak tearing force ($p<0.05$). Superior-inferior (SI) rips only required an average of the mean tearing force of 301±26 gf, while anterior-posterior (AP) rips required a 363±41 gf (Table 8.4). Also, a larger force was required to rip the septum with larger sized sheaths (Fig. 8.13). The average of the mean sheath tearing force was 258±20, 362±25, and 555±56 g for 4, 12, and 18 F sheaths respectively; there was a significant difference between the sheath size and the sheath tearing force between the 18 F and 12/5 F groups ($p<0.001$). Heart weight, animal weight, FO thickness, width (anterior to posterior), and width (superior to inferior) did not statistically differ between any of the groups ($p > 0.05$).

Table 8.3: Summary of fossa ovalis dimensions and sheath tearing forces by sheath size

	4 F	12 F	18 F	p-value
Thickness (mm)	1.1±0.1	1.2±0.1	1.1±0.1	0.727
SI Width (mm)	16.5±1.1	14.3±0.7	15.7±1.2	0.241
AP Width (mm)	10.7±0.9	7.7±0.6	9.2±0.7	0.005
Average Tearing Force (gf)	258±20	301±26	555±56	p<0.001
Peak Tearing Force (gf)	344±26	417±37	704±72	p<0.001
Heart Weight (g)	487±10	464±13	451±10	0.563
N=	15	20	15	

*Values are reported as mean±SE.

Table 8.4: Directional differences in septal tearing forces with a 12F sheath across the septum

	SI	AP	p-value
Thickness (mm)	1.2±0.1	1.1±0.1	0.717
SI Width (mm)	14.3±0.7	14.8±1.1	0.569
AP Width (mm)	7.7±0.6	7.9±0.7	0.480
Average Tearing Force (gf)	301±26	424±41	0.012
Peak Tearing Force (gf)	417±37	551±60	0.033
Heart Weight (g)	464±13	452±18	0.844
N=	20	20	

*Values are reported as mean±SE.

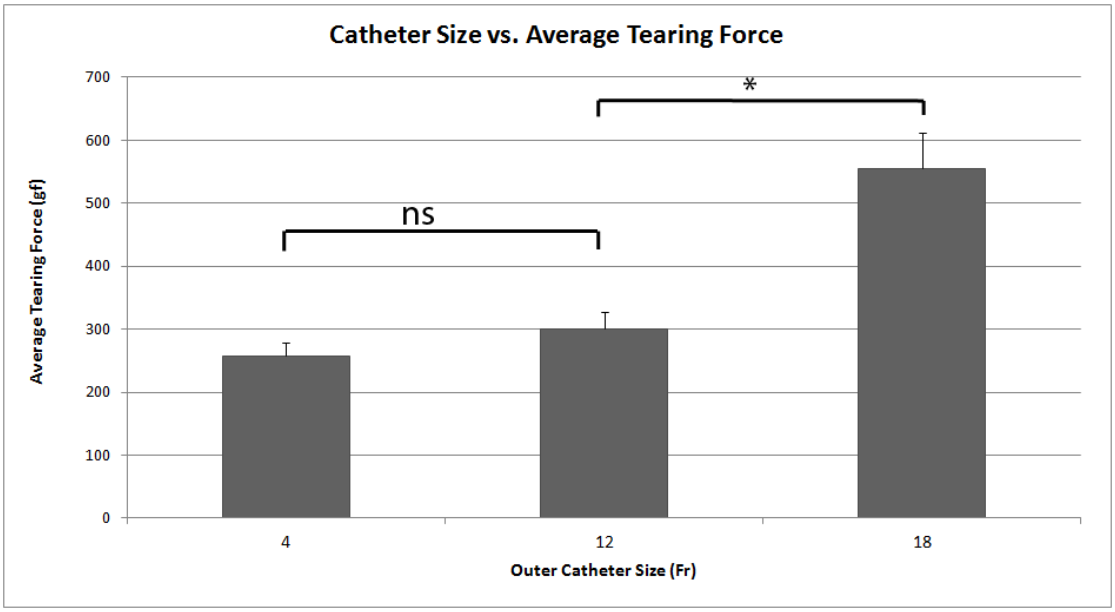

Figure 8.13: The tearing forces of the fossa ovalis increased with the usage of a larger diameter sheath but did not significantly differ between the 4F and 12F sheaths (p>0.05). Error bars depict mean±SE. *p-value<0.001

Tensile Testing

The data showed no statistical differences in the normalized peak force with the SI pull tests having a higher average force (136±11 gf/mm^2) than AP pulls (116±10 gf/mm^2). However, the strain at failure was found to be significantly higher for SI pulls (90±7%) than for AP pulls (55±7%) ($p<0.01$). The Young's modulus was consistent along both axes with an average value of 32±3 kPa. Heart weight, FO thickness and FO dimensions were not statistically different between the two groups ($p>0.05$).

Table 8.5: Summary of tensile testing stress, strain, and Young's Modulus

	SI	**AP**	**p-value**
Normalized Peak Force (gf/mm^2)	136±11	116±10	0.178
Strain at Failure (%)	90±7	55±7	0.002
Young's Modulus (kPa)	32±2	32±3	0.864
Number	22	19	

Discussion:

To start a transseptal puncture, tenting of the septum is required. When training in a new fellow or performing experimental protocols swine may be utilized. When this model is used, it is helpful to know that the force required may be less than those seen in humans (121±11gf vs. 146±26gf, $p<0.001$). With the exception of potentially trying to tent the muscular septum, the location at which you choose to puncture does not seem to matter as far as the amount of force required to produce tenting that may be visible under ultrasound guidance. When analyzing how devices punctured the septum, it was interesting to note that on average the needle tented the septum 9.3±.3mm in humans and 9.8±.14mm in swine ($p=0.2$) prior to perforating the septum. This means that in an average heart, which can range from approximately 30mm to 50mm in diameter[46,72,173], the needle will strain the FO approximately 25% of the distance into the LA before perforating and entering into the LA. Keep in mind that this does not even take into

consideration the fact that as the physician advances the device, there is a slightly lateral but also superior trajectory on the needle and TSP device. This could potentially be the cause for some of the incidents of LA perforation or tamponade [150].

As can be expected, when working with cardiac tissue we found a bit of variability between the test samples, but this variability seemed to be similar between the swine and human tissue groups where the standard deviation was 33% of the mean for the human punctures, and 37% for swine. These values correlated to 75gf in the swine hearts and 90gf in the human hearts when assessing the Brockenbrough needle puncture force alone. Since the needle style was never changed, this variation is most likely due to the variation in the anatomy, biomechanical properties, the experimental setup or any combination of the three. In general, greater force was required to pass a larger sheath through the septum compared to a smaller sheath.

Another predictor of the force needed to traverse the septum was the difference in the diameter between the various steps (i.e., between the needle diameter and the tip of the dilator diameter). The larger the step, the more force needed to pass through the FO. As one would expect a larger catheter resulted in larger forces required to go across the septum; similarly, as catheter size increases so does the remnant hole that was created. This remnant hole size seemed to increase exponentially in relation to the catheter diameter and upon further analysis seemed to increase linearly with the increase in the sheath cross-sectional area. This is a point that device manufacturers must be aware of and take into consideration when assessing current or novel devices that are utilized via a transseptal approach. Studies show that the IASDs do close in patients over time, but there will be still a certain amount of time until all of them close, up to a year in some cases (most likely depending upon catheter size, procedure type and operator)[1].

When investigating the puncture forces more closely, it makes sense that the needle puncture force is higher than the other portions since its matter of perforation vs dilation. The act of stretching the tissue seems to require less force, especially in the case of the dilator tip and the dilation portion. However, this is not necessarily the case for human tissue. The dilator tip required more than twice the force required for the swine tissue. This suggests there are distinctive differences between the two species models, which could potentially relate to the tissue structure or composition. Another source of variability could come from the inconsistency of disease state and cardiac morphology within the donated human hearts. However, these hearts will be more representative of what could be encountered clinically.

With advances in medical technology moving as rapidly as they currently are more potential therapies requiring transseptal punctures are being created and thus are making these data more important to consider. As medical device development progresses, the overwhelming theme is smaller, better, faster. However catheter sizes in the realm of TSPs are getting both larger and smaller due to the clinical need and current technological limitations, with endocardial pacing leads being placed through a 4 F sheath and Mitra Clip being placed through a 22F catheter. Transcatheter mitral valves may be another potential device that could be delivered via TSP and if you look at the current transcatheter aortic valves, their delivery catheter size range from 18 to 24F[174]. Needless to say, such mitral valve delivery catheters would probably be similar in size if not larger due to the difference in mitral and aortic valve areas. If this technology were to come about, a good understanding of how the septum will react to the TSP with such a large catheter must be considered especially since current valvar therapies are being delivered via a TSP with such devices like the Mitra Clip [105,138].

When looking at the biomechanical properties of the atrial septum there was a significant difference between directions while ripping the septum primum with a 12 F sheath; ripping in the SI direction required a lower force that rips in the AP direction. In order to allow for higher power tests of the 4 and 18 F sheaths, only rips in the SI direction were performed. While navigating catheters to the PVs during an ablation procedure, extensive sheath manipulation is often used which may initiate FO tearing. Furthermore, during other procedures that utilize transseptal punctures, substantial catheter torquing may be required to reach the appropriate anatomy. Larger sheath catheters required large forces to initiate tearing of the thin portion of the FO. This suggests that although procedures are trending toward larger sheath usage, the incidence of FO tearing may be less. Even though this experimental paradigm showed this to be true in situ, other factors may play a role in tear initiation. If the pertinent anatomy is relatively far from the FO, initiation of tearing may appear easier because catheter torquing will amplify this force at the FO. Further studies will need to be conducted looking at FO tearing in order to fully characterize damages sustained to the FO during procedures.

The tensile testing of the tissue in the SI and AP orientation had no statistically significant differences in either the average normalized peak break force or the Young's Modulus, but there was a significant difference in the maximal strain at tissue rupture. This along with the sheath ripping force differences in the SI and AP direction seem to indicate that there could be a particular alignment of tissue or fiber orientation that could potentially account for these differences. When the sheath is being pulled through the floor of the FO in a SI orientation, it is breaking through the tissue fibers oriented perpendicularly to the direction of pull. We would predict from the ripping data that the SI direction would be stronger than the AP direction, but this is not supported by the data, rather that the SI is more malleable and able to undergo higher strain than the AP orientation. This also suggests that directionality of the rips in the FO is an

important factor to consider. A review of the literature showed that there are currently no histological studies of the FO for any species and we suggest that this may be an important avenue of research to pursue in order to understand the underlying micro-anatomy and what clinical implications it may have on the structure. Understanding the structural composition of the FO is the topic of ongoing research[84].

Limitations:

The limitation of human heart availability is expected, so a physiological analog of swine hearts was instead used to approximate human properties while still giving insight into true human cardiac puncture, tenting and tensile properties. Swine hearts provided a method to test multiple catheter types while still being able to be related to human anatomy and tissue properties. Although it may not be an exact analog as can seen by the data, however it does give some insight into how the different catheter sizes interact with one another and a relative comparison between species.

The suction method employed tries to approximate the structure or at least the rigidity of the atrial septum while the heart is pressurized with blood in the body. A true mimicking of physiological conditions imposes other issues related to force application on the catheter to puncture the atrial septum while accurately recording the displacement and the load. Having a consistent and repeatable suction device to hold the septum allows for a more controlled study in respect to load and displacement. Along with the consistency, the rate at which the tissue was pulled or punctured was kept consistent as a way to reduce the variables in the experimental setup.

These tests were performed primarily with catheters used for work across the septum. This does not mean that they are designated as transseptal tools in their instructions for use, although most are. However, the sizes do allow for an analysis to discuss what the implications

are for using larger catheters on the septum. Likewise since different catheters were utilized, the material properties may be different and some devices may be more or less hydrophilic which could lead to a change in the forces required to perform a transseptal puncture.

Thesis Summary

Through my experience in the Visible Heart® laboratory, I have learned much more than what was presented in this thesis, including a detailed knowledge of overall cardiac anatomy and physiology. With the expertise I gained, I was fortunate enough to assist teaching sessions at American Association for Heart Failure Nurses Conference and was a teaching assistant in the Advanced Cardiac Anatomy and Physiology Course for 5 years. On top of that I was privileged with the opportunity to pass on my knowledge to hundreds of individuals that visited that laboratory and beyond (e.g, at the State Fair and to 6th grade biology students. In each of these opportunities I also illustrate to all the importance of fully understanding cardiac anatomy and how this critically relates to biomedical engineering.

I also have had the privilege of working with numerous other graduate, medical, and undergraduate students on a number of projects including pericardial drug delivery, cryo-ablation in the Visible Heart apparatus, cellular modeling and pacing induced ventricular dyssynchrony (the latter two resulted in co-authorship for published work and the former two are in progress for publication) [81,175]. I would like to note that to date, during my graduate work, I have been able to publish or be a co-author on 7 papers, 3 book chapters: I have several papers still in progress to be published. Furthermore, I also must mention that one of the most important skills that I learned from my time in the lab was the ability to discuss my work in a way that is fully comprehendible by any type of audience. In other words, I feel that once someone has such a critical knowledge base on their particular topic that they can explain it to either middle school students or physicians it confirms true knowledge of the projects implications, performance and limitations.

As related to the research presented in this thesis, the described novel imaging, modeling and testing of the atrial septum, has brought light to many new and important findings. For instance, the dual orifice mitral valve was a congenital defect that elicited little or no clinical manifestations in that particular patient and was considered to be in a completely healthy heart. The interest to those working on mitral repair devices was that this congenital valvular bridge resembles the resultant anatomy following leaflet fusion procedures via an Alfieri stitch or a Mitra Clip implantation. This may suggest that these particular anatomies may be amenable to normal cardiac function. In another case report described in this thesis, no defects were identified until after a clinical cardiac intervention was performed. The visualization of these IASDs in the reanimated human heart illustrates the potential impacts of TSPs for atrial fibrillation procedures or any other procedure requiring atrial septal crossing. These defects were seen 2 months after the procedure and according to the literature could potentially stay patent for up to a year or more [30]. As discussed in this thesis, the catheters typically used for such ablation procedures are often 1/3 the diameters of current catheters used for the delivery of mitral repair devices. These findings should heed caution for designers and physicians to fully understand the implications of placing such a large defect into the atrial septum. Nevertheless, in either scenario, our laboratory's unique abilities to visualize functional anatomies allowed us to uniquely investigate the physiological and morphological manifestation of each.

As discussed in my thesis, it is important to create clear representations of the large range of human anatomies that may exist in populations of patient for whom the therapies are intended. From these representations one must fully understand if medical therapies will be appropriate, easy to deliver, or even result in other undesired complications to adequately provide such treatments. In this sense, the development of detailed 3D models of a variety of human hearts will add unique and required levels of knowledge and thus will be highly useful. The images and

models that I created and described here help us to define detailed anatomies. It should also be noted, that with the limitations of specimen quality and quantity only a small database has been created to date. Nevertheless, the models that have been created suggested that the size shapes and PFO overlap areas that were characterized in 3D were well correlates with the physical distance measurements in actual heart specimens. This begins to confirm the notion that the 3D models are adequate surrogates for these types of measurements. Further, the generated 3D models also provided us with a more accurate depiction of the PFO overlap areas, since these features are typically not easily definable geometric structures on the actual physical specimens. It was also described within that chapter that further work needs to be continued to expand the overall numbers and qualities of these models. However, once a greater array of these models has been created, the next steps will be to utilize such models for a computational design system and/or for the modeling of device interactions and future developments. For example, today some of these initial models have been found to be very useful for investigating the PFO anatomy as it relates to the insertion of PFO closure devices into varied human heart anatomies by using a virtual reality simulator (Medical Device Center, University of Minnesota) and as bench top testing platforms for delivery sheaths or other cardiac catheters posed at treating conditions in the LA or LV.

In this thesis I performed novel experimental studies to determine the puncture, tenting and tearing forces of the human atrial septum, so to provide novel insight into how these unique and anatomically important cardiac tissue functions. The data presented here showed that it requires more force to traverse the septum with a larger catheter and that the resultant hole is directly associated with the cross-sectional area of the employed catheter. This is not to say that the catheter size is the only factor associated with IASD formation as suggested by the analysis of the literature. The procedure time and potentially the number of catheter manipulations may lead

to a larger defect size to be formed. Further, there is a notable difference between the tissue ripping and strain properties in the AP and SI directions. The clinical importance of these findings is that the manipulation of catheters in an SI direction may result in a larger defect compared to manipulations made in the AP direction due to the lower forces required to rip the septum with a catheter in place. Thus, I have strongly suggested here that these data should be well understood by all engineers engaged with designing the next versions of transseptally delivered medical therapies. The continuation of this work would be fruitful to determine how these data compare to human specimens since the ability to translate this data to a human model will verify or alter these findings as they relate to percutaneous cardiac interventions.

Furthermore, these biomechanical properties are useful and provide evidence surrounding IASD formation during a clinical percutaneous cardiac procedure via a transseptal approach. However, they also have added value in relation to computer modeling and simulations of new or existing technologies or therapies. More specifically, the utilization of these models in Virtual Reality is a recent application that includes the potential for computer simulated device placement or transseptal crossing without the use of animal or bench top models. One of the noted limitations of this work is that these biomechanical measurements are performed *ex-vivo,* in a non-clinical setting. Likewise, the majority of these measurements were made on tissues from fresh swine hearts, though they were compared to a small sample of very difficult to obtain human samples. Nevertheless, I believe that these values are novel and still relevant and provide a sufficient starting point to initiate further translational studies to compare these findings to data from more human specimens.

In conclusion, it should also be noted that in the field of cardiology, the employment of transseptal punctures and atrial septal defect closures is neither new nor novel. They have been

and will likely be performed for many years to come. However, with the expansion of the use of transseptal punctures for a variety of newly developing technologies (e.g., transcatheter mitral valve repairs/replacements), the data presented here should be used for questioning the consequences of deploying larger diameter catheters trans-septally and to fully understand the consequences of such procedures.

References

[1] McGinty P. M., Smith T. W., and Rogers J. H., 2011, "Transseptal left heart catheterization and the incidence of persistent iatrogenic atrial septal defects.," Journal of interventional cardiology, **24**(3), pp. 254–63.

[2] Carroll J. D., 2008, "PFO anatomy: 3D characterization and device performance.," Catheterization and cardiovascular interventions : official journal of the Society for Cardiac Angiography & Interventions, **71**(2), pp. 229–30.

[3] Tanaka J., Izumo M., Fukuoka Y., Saitoh T., Harada K., Harada K., Gurudevan S. V, Tolstrup K., Siegel R. J., and Shiota T., 2013, "Comparison of two-dimensional versus real-time three-dimensional transesophageal echocardiography for evaluation of patent foramen ovale morphology.," The American journal of cardiology, **111**(7), pp. 1052–6.

[4] Kato R., Lickfett L., Meininger G., Dickfeld T., Wu R., Juang G., Angkeow P., LaCorte J., Bluemke D., Berger R., Halperin H. R., and Calkins H., 2003, "Pulmonary vein anatomy in patients undergoing catheter ablation of atrial fibrillation: lessons learned by use of magnetic resonance imaging.," Circulation, **107**(15), pp. 2004–10.

[5] Iaizzo P. A., 2013, "Atlas of Human Cardiac Anatomy" [Online]. Available: www.vhlab.umn.edu/atlas.

[6] Widmaier E. P., Raff H., and Strang K. T., eds., 2004, Vander, Sherman & Luciano's Human Physiology, McGraw-Hill, New York.

[7] Kutty S., Sengupta P. P., and Khandheria B. K., 2012, "Patent foramen ovale: the known and the to be known.," Journal of the American College of Cardiology, **59**(19), pp. 1665–71.

[8] Martins J. D. F., and Anderson R. H., 2008, "The anatomy of interatrial communications – what does the interventionist need to know?," Cardiology in the Young, **10**(05), pp. 464–473.

[9] Sweeney L. J., and Rosenquist GC, 1979, “The normal anatomy of the atrial septum in the human heart.,” The American heart journal, **98**(2), pp. 194–199.

[10] Ferreira S. M., Ho S. Y., and Anderson R. H., 1992, “Morphological study of defects of the atrial septum within the oval fossa: implications for transcatheter closure of left-to-right shunt.,” British heart journal, **67**(4), pp. 316–20.

[11] Roelke M., Smith a J., and Palacios I. F., 1994, “The technique and safety of transseptal left heart catheterization: the Massachusetts General Hospital experience with 1,279 procedures.,” Catheterization and cardiovascular diagnosis, **32**(4), pp. 332–9.

[12] Netter F. H., 2011, Atlas of Human Anatomy 5th Ed., Saunders, Philadephia, PA.

[13] Runge M. S., Stouffer G. A., and Patterson C., eds., 2004, Netter’s Cardiology 2nd Ed., Elsevier, Philadephia, PA.

[14] Howard S. A., Quill J. L., Eggen M. D., Swingen C. M., and Iaizzo P. A., 2013, “Novel imaging of atrial septal defects in isolated human hearts.,” Journal of cardiovascular translational research, **6**(2), pp. 218–20.

[15] Lloyd-Jones D., Adams R., Brown T. M., Carnethon M., Dai S., De Simone G., Ferguson T. B., Ford E., Furie K., Gillespie C., Go A., Greenlund K., Haase N., Hailpern S., Ho P. M., Howard V., Kissela B., Kittner S., Lackland D., Lisabeth L., Marelli A., McDermott M. M., Meigs J., Mozaffarian D., Mussolino M., Nichol G., Roger V. L., Rosamond W., Sacco R., Sorlie P., Stafford R., Thom T., Wasserthiel-Smoller S., Wong N. D., and Wylie-Rosett J., 2010, “Heart disease and stroke statistics--2010 update: a report from the American Heart Association.,” Circulation, **121**(7), pp. e46–e215.

[16] Hagen P. T., Scholz D. G., and Edwards W. D., 1984, “Incidence and size of patent foramen ovale during the first 10 decades of life: an autopsy study of 965 normal hearts.,” Mayo Clinic proceedings. Mayo Clinic, **59**(1), pp. 17–20.

[17] Feldt R. H., Avasthey P., Yoshimasu F., Kurland L. T., and Titus J. L., 1971, “Incidence of Congenital Heart Disease In Children Born to Residents of Olmsted County, Minnesota, 1950-1969,” Mayo Clinic proceedings. Mayo Clinic, **46**, pp. 794–9.

[18] Vis J. C., Engelen K. Van, Bouma B. J., Bilardo C., Blom N. A., and Mulder B. J. M., 2010, “Cardiovascular Disorders among Persons with Down Syndrome,” International Review of Research in Mental Retardation-Volume 39, Elsevier Inc., pp. 165–194.

[19] Thanigaraj S., Zajarias A., Valika A., Lasala J., and Pérez J. E., 2006, “Caught in the act: serial, real time images of a thrombus traversing from the right to left atrium across a patent foramen ovale.,” European Journal of Echocardiography, **7**(2), pp. 179–81.

[20] Soliman O. I. I., Geleijnse M. L., Meijboom F. J., Nemes A., Kamp O., Nihoyannopoulos P., Masani N., Feinstein S. B., and Ten Cate F. J., 2007, “The use of contrast echocardiography for the detection of cardiac shunts.,” European journal of echocardiography, **8**(3), pp. S2–12.

[21] Purvis J. A., Morgan D. R., and Hughes S. M., 2011, “Prevalence of patent foramen ovale in a consecutive cohort of 261 patients undergoing routine ‘coronary’ 64-multi-detector cardiac computed tomography.,” The Ulster medical journal, **80**(2), pp. 72–5.

[22] Cope C., 1963, “Newer Techniques of Transseptal Left-Heart Catheterization,” Circulation, **27**(4), pp. 758–761.

[23] Earley M. J., 2008, “How to perform a transseptal puncture,” Heart, **95**(1), pp. 85–92.

[24] Venables A. W., 1970, “Balloon atrial septostomy in complete transposition of great arteries in infancy,” British heart journal, **32**, pp. 61–65.

[25] Sandoval J., Gaspar J., Pulido T., Bautista E., Martínez-Guerra M. L., Zeballos M., Palomar A., and Gómez A., 1998, “Graded balloon dilation atrial septostomy in severe primary pulmonary hypertension,” Journal of the American College of Cardiology, **32**(2), pp. 297–304.

[26] Sur J. P., Pagani F. D., and Moscucci M., 2009, “Percutaneous closure of an iatrogenic atrial septal defect.,” Catheterization and cardiovascular interventions, **73**, pp. 267–71.

[27] El-Said H. G., Bexold L., Grifka R. G., Pignatelli R. H., McMahon C. J., Schutte D. A., Smith E. O., and Mullins C. E., 2001, “Sizing of Atrial Septal Defects,” Tex Heart Inst J, **28**, pp. 177–182.

[28] Braunwald E., Brockenbrough E. C., Frahm C. J., and Ross J., 1961, “Left Atrial and Left Ventricular Pressures in Subjects without Cardiovascular Disease: Observations in Eighteen Patients Studied by Transseptal Left Heart Catheterization,” Circulation, **24**, pp. 267–269.

[29] Leclercq F., Hager F. X., Macia J. C., Mariottini C. J., Pasquié J. L., and Grolleau R., 1999, “Left ventricular lead insertion using a modified transseptal catheterization technique: A totally endocardial approach for permanent biventricular pacing in end-stage heart failure.,” Pacing and clinical electrophysiology : PACE, **22**(11), pp. 1570–5.

[30] Rillig A., Meyerfeldt U., Birkemeyer R., Treusch F., Kunze M., and Jung W., 2008, “Persistent iatrogenic atrial septal defect after pulmonary vein isolation : incidence and clinical implications.,” Journal of interventional cardiac electrophysiology, **22**(3), pp. 177–81.

[31] Yeo K. K., Rogers J., and Low R., 2013, “Atlas of Percutaneous Edge-to-Edge Mitral Valve Repair,” pp. 113–129.

[32] Omran H., Hardung D., Schmidt H., Hammerstingl C., and Lüderitz B., 2003, “Mechanical occlusion of the left atrial appendage.,” Journal of cardiovascular electrophysiology, **14**(9 Suppl), pp. S56–9.

[33] Bordachar P., Grenz N., Jais P., Ritter P., Leclercq C., Morgan J. M., Gras D., and Yang P., 2012, "Left ventricular endocardial or triventricular pacing to optimize cardiac resynchronization therapy in a chronic canine model of ischemic heart failure.," American journal of physiology. Heart and circulatory physiology, **303**(2), pp. H207–15.

[34] Van Gelder B. M., Houthuizen P., and Bracke F. a, 2011, "Transseptal left ventricular endocardial pacing: preliminary experience from a femoral approach with subclavian pull-through.," Europace, **13**(10), pp. 1454–8.

[35] Babaliaros V. C., Green J. T., Lerakis S., Lloyd M., and Block P. C., 2008, "Emerging applications for transseptal left heart catheterization old techniques for new procedures.," Journal of the American College of Cardiology, **51**(22), pp. 2116–22.

[36] Raval A. N., Karmarkar P. V, Guttman M. a, Ozturk C., Desilva R., Aviles R. J., Wright V. J., Schenke W. H., Atalar E., McVeigh E. R., and Lederman R. J., 2006, "Real-time MRI guided atrial septal puncture and balloon septostomy in swine.," Catheterization and cardiovascular interventions, **67**(4), pp. 637–43.

[37] Sandoval J., Gaspar J., Pulido T., Bautista E., Martínez-Guerra M. L., Zeballos M., Palomar A., and Gómez A., 1998, "Graded balloon dilation atrial septostomy in severe primary pulmonary hypertension," Journal of the American College of Cardiology, **32**(2), pp. 297–304.

[38] Rothman a, Sklansky M. S., Lucas V. W., Kashani I. a, Shaughnessy R. D., Channick R. N., Auger W. R., Fedullo P. F., Smith C. M., Kriett J. M., and Jamieson S. W., 1999, "Atrial septostomy as a bridge to lung transplantation in patients with severe pulmonary hypertension.," The American journal of cardiology, **84**(6), pp. 682–6.

[39] Gott V. L., 2005, "Lillehei, Lewis, and Wangensteen: the right mix for giant achievements in cardiac surgery.," The Annals of thoracic surgery, **79**(6), pp. S2210–3.

[40] Lillehei C. W., Cohen M., Warden H. E., Read R. C., Aust J. B., Dewall R. A., and Varco R. L., 1955, "Direct vision intracardiac surgical correction of the tetralogy of Fallot, pentalogy of Fallot, and pulmonary atresia defects; report of first ten cases.," Annals of surgery, **142**(3), pp. 418–42.

[41] Albers E., Janssen D., Ammons D., and Doyle T., 2012, "Percutaneous closure of secundum atrial septal defects," Progress in Pediatric Cardiology, **33**(2), pp. 115–123.

[42] Ganau A., Devereux R. B., Roman M. J., de Simone G., Pickering T. G., Saba P. S., Vargiu P., Simongini I., and Laragh J. H., 1992, "Patterns of left ventricular hypertrophy and geometric remodeling in essential hypertension.," Journal of the American College of Cardiology, **19**(7), pp. 1550–8.

[43] Cohn J. N., Ferrari R., and Sharpe N., 2000, "Cardiac remodeling—concepts and clinical implications: a consensus paper from an international forum on cardiac remodeling," Journal of the American College of Cardiology, **35**(3), pp. 569–582.

[44] Pfeffer M. A., and Braunwald E., 1990, “Ventricular remodeling after myocardial infarction. Experimental observations and clinical implications,” Circulation, **81**(4), pp. 1161–1172.

[45] Thambo J.-B., Bordachar P., Garrigue S., Lafitte S., Sanders P., Reuter S., Girardot R., Crepin D., Reant P., Roudaut R., Jaïs P., Haïssaguerre M., Clementy J., and Jimenez M., 2004, “Detrimental ventricular remodeling in patients with congenital complete heart block and chronic right ventricular apical pacing.,” Circulation, **110**(25), pp. 3766–72.

[46] Reant P., Lafitte S., Jaïs P., Serri K., Weerasooriya R., Hocini M., Pillois X., Clementy J., Haïssaguerre M., and Roudaut R., 2005, “Reverse remodeling of the left cardiac chambers after catheter ablation after 1 year in a series of patients with isolated atrial fibrillation.,” Circulation, **112**(19), pp. 2896–903.

[47] Go A. S., Hylek E. M., Phillips K. A., Henault L. E., Selby J. V, and Singer D. E., 2001, “Prevalence of Diagnosed Atrial Fibrillation in Adults,” JAMA, **285**(18), pp. 2370–2375.

[48] Wijffels M. C. E. F., Kirchhof C. J. H. J., Dorland R., and Allessie M. A., 1995, “Atrial Fibrillation Begets Atrial Fibrillation : A Study in Awake Chronically Instrumented Goats,” Circulation, **92**(7), pp. 1954–1968.

[49] Rostock T., Steven D., Lutomsky B., Servatius H., Drewitz I., Klemm H., Müllerleile K., Ventura R., Meinertz T., and Willems S., 2008, “Atrial fibrillation begets atrial fibrillation in the pulmonary veins on the impact of atrial fibrillation on the electrophysiological properties of the pulmonary veins in humans.,” Journal of the American College of Cardiology, **51**(22), pp. 2153–60.

[50] Fuster V., Rydén L. E., Cannom D. S., Crijns H. J., Curtis A. B., Ellenbogen K. A., Halperin J. L., Le Heuzey J.-Y., Kay G. N., Lowe J. E., Olsson S. B., Prystowsky E. N., Tamargo J. L., Wann S., Smith S. C., Jacobs A. K., Adams C. D., Anderson J. L., Antman E. M., Hunt S. A., Nishimura R., Ornato J. P., Page R. L., Riegel B., Priori S. G., Blanc J.-J., Budaj A., Camm A. J., Dean V., Deckers J. W., Despres C., Dickstein K., Lekakis J., McGregor K., Metra M., Morais J., Osterspey A., and Zamorano J. L., 2006, “ACC/AHA/ESC 2006 Guidelines for the Management of Patients with Atrial Fibrillation: a report of the American College of Cardiology/American Heart Association Task Force on Practice Guidelines and the European Society of Cardiology Committee for Practice ,” Circulation, **114**(7), pp. e257–354.

[51] Feinberg W. M., Blackshear J. L., Laupacis A., Kronmal R., and Hart R. G., 1995, “Prevalence, age distribution, and gender of patients with atrial fibrillation: analysis and implications,” Archives of internal medicine, **155**(5), pp. 469–473.

[52] Hamer M. E., Blumenthal J. A., McCarthy E. A., Phillips B. G., and Pritchett E. L. C., 1994, “Quality-of-life assessment in patients with paroxysmal atrial fibrillation or paroxysmal supraventricular tachycardia,” The American journal of cardiology, **74**(8), pp. 826–829.

[53] Perret-Guillaume C., Briancon S., Wahl D., Guillemin F., and Empereur F., 2010, "Quality of Life in elderly inpatients with atrial fibrillation as compared with controlled subjects," The journal of nutrition, health & aging, **14**(2), pp. 161–166.

[54] Dąbrowski R., Smolis-Bąk E., Kowalik I., Kazimierska B., Wójcicka M., and Szwed H., 2010, "Quality of life and depression in patients with different patterns of atrial fibrillation.," Kardiologia polska, **68**(10), p. 1133.

[55] Park H., Hildreth A., Thomson R., and O'Connell J., 2007, "Non-valvular atrial fibrillation and cognitive decline: a longitudinal cohort study," Age and ageing, **36**(2), pp. 157–163.

[56] Puccio D., Novo G., Baiamonte V., Nuccio A., Fazio G., Corrado E., Coppola G., Muratori I., Vernuccio L., and Novo S., 2009, "Atrial fibrillation and mild cognitive impairment: what correlation?," Minerva cardioangiologica, **57**(2), pp. 143–150.

[57] Jozwiak A., Guzik P., Mathew A., Wykretowicz A., and Wysocki H., 2006, "Association of atrial fibrillation and focal neurologic deficits with impaired cognitive function in hospitalized patients≥ 65 years of age," The American journal of cardiology, **98**(9), pp. 1238–1241.

[58] Rastas S., Verkkoniemi A., Polvikoski T., Juva K., Niinistö L., Mattila K., Länsimies E., Pirttilä T., and Sulkava R., 2007, "Atrial fibrillation, stroke, and cognition a longitudinal population-based study of people aged 85 and older," Stroke, **38**(5), pp. 1454–1460.

[59] Beukema W. P., Elvan A., Sie H. T., Misier A. R. R., and Wellens H. J. J., 2005, "Successful radiofrequency ablation in patients with previous atrial fibrillation results in a significant decrease in left atrial size," Circulation, **112**(14), pp. 2089–2095.

[60] Leung D. Y., Chi C., Allman C., Boyd A., Ng A. C., Kadappu K. K., Leung M., and Thomas L., 2010, "Prognostic implications of left atrial volume index in patients in sinus rhythm," The American journal of cardiology, **105**(11), pp. 1635–1639.

[61] Abecasis J., Dourado R., Ferreira A., Saraiva C., Cavaco D., Santos K. R., Morgado F. B., Adragão P., and Silva A., 2009, "Left atrial volume calculated by multi-detector computed tomography may predict successful pulmonary vein isolation in catheter ablation of atrial fibrillation," Europace, **11**(10), pp. 1289–1294.

[62] Sunderland N., Maruthappu M., and Nagendran M., 2011, "What size of left atrium significantly impairs the success of maze surgery for atrial fibrillation?," Interactive CardioVascular and Thoracic Surgery, **13**(3), pp. 332–338.

[63] Marchese P., Bursi F., Delle Donne G., Malavasi V., Casali E., Barbieri A., Melandri F., and Modena M. G., 2011, "Indexed left atrial volume predicts the recurrence of non-valvular atrial fibrillation after successful cardioversion," European Journal of Echocardiography, **12**(3), pp. 214–221.

[64] Lee Y.-S., Hyun D. W., Jung B. C., Cho Y. K., Lee S. H., Shin D. G., Park H. S., Han S. W., and Kim Y. N., 2010, "Left atrial volume index as a predictor for occurrence of atrial fibrillation after ablation of typical atrial flutter," Journal of cardiology, **56**(3), pp. 348–353.

[65] Ayirala S., Kumar S., O'Sullivan D. M., and Silverman D. I., 2011, "Echocardiographic predictors of left atrial appendage thrombus formation," Journal of the American Society of Echocardiography, **24**(5), pp. 499–505.

[66] Beinart R., Heist E. K., Newell J. B., Holmvang G., Ruskin J. N., and Mansour M., 2011, "Left atrial appendage dimensions predict the risk of stroke/TIA in patients with atrial fibrillation," Journal of Cardiovascular Electrophysiology, **22**(1), pp. 10–15.

[67] Haissaguerre M., Jaïs P., Shah D. C., Takahashi A., Hocini M., Quiniou G., Garrigue S., Le Mouroux A., Le Métayer P., and Clémenty J., 1998, "Spontaneous initiation of atrial fibrillation by ectopic beats originating in the pulmonary veins," New England Journal of Medicine, **339**(10), pp. 659–666.

[68] Wittkampf F. H. M., Vonken E.-J., Derksen R., Loh P., Velthuis B., Wever E. F. D., Boersma L. V. A., Rensing B. J., and Cramer M.-J., 2003, "Pulmonary vein ostium geometry analysis by magnetic resonance angiography," Circulation, **107**(1), pp. 21–23.

[69] Beinart R., Abbara S., Blum A., Ferencik M., Heist K., Ruskin J., and Mansour M., 2011, "Left atrial wall thickness variability measured by CT scans in patients undergoing pulmonary vein isolation," Journal of cardiovascular electrophysiology, **22**(11), pp. 1232–1236.

[70] Anderson S. E., Hill A. J., and Iaizzo P. A., 2009, "Microanatomy of human left ventricular coronary veins," The Anatomical Record, **292**(1), pp. 23–28.

[71] Lester S. J., Ryan E. W., Schiller N. B., and Foster E., 1999, "Best method in clinical practice and in research studies to determine left atrial size," The American journal of cardiology, **84**(7), pp. 829–832.

[72] Nikitin N. P., Witte K. K. A., Thackray S. D. R., Goodge L. J., Clark A. L., and Cleland J. G. F., 2003, "Effect of Age and Sex on Left Atrial Morphology and Function," Eur J Echocardiography, **4**(1), pp. 36–42.

[73] Thomas L., Levett K., Boyd A., Leung D. Y. C., Schiller N. B., and Ross D. L., 2002, "Compensatory changes in atrial volumes with normal aging: is atrial enlargement inevitable?," Journal of the American College of Cardiology, **40**(9), pp. 1630–5.

[74] Hill A. J., Laske T. G., Coles J. A., Sigg D. C., Skadsberg N. D., Vincent S. A., Soule C. L., Gallagher W. J., and Iaizzo P. A., 2005, "In vitro studies of human hearts.," The Annals of thoracic surgery, **79**(1), pp. 168–77.

[75] Chinchoy E., Soule C. L., Houlton a J., Gallagher W. J., Hjelle M. a, Laske T. G., Morissette J., and Iaizzo P. a, 2000, "Isolated four-chamber working swine heart model.," The Annals of thoracic surgery, **70**(5), pp. 1607–14.

[76] Porter W. T., 1889, "A new method for the study of the isolated mammalian heart.," American Journal of Physiology, **1**(4), pp. 511–518.

[77] Blice J. P., 2003, "Imaging of Ocular and Adexal Trauma," Ophthalmic Care of the Combat Casualty, D.E. Lounsbury, R.F. Bellamy, and R. Zajtchuk, eds., Office of The Surgeon General at TMM Publications Borden Institute, Bethesda, Maryland, pp. 61–76.

[78] Gelfand A., 2011, "Dogs , Doses and Devices: The FDA's Ambitious Plans for Computational Modeling," Biomedical Computation Review, **Fall**, pp. 20–26.

[79] Feldt R. H., Avasthey P., Yoshimasu F., Kurland L. T., and Titus J. L., 1971, "Incidence of Congenital Heart Disease In Children Born to Residents of Olmsted County, Minnesota, 1950-1969," Mayo Clinic proceedings. Mayo Clinic, **46**(12), pp. 794–799.

[80] Nakamura F. F., Hauck A. J., and Nadas A. S., 1964, "Atrial Septal Defect in infants," Pediatrics, **34**, pp. 101–106.

[81] Eggen M. D., Bateman M. G., Rolfes C. D., Howard S. A., Swingen C. M., and Iaizzo P. A., 2010, "MRI assessment of pacing induced ventricular dyssynchrony in an isolated human heart.," Journal of magnetic resonance imaging, **31**(2), pp. 466–9.

[82] Eggen M. D., Swingen C. M., Matta P., Bateman M. G., Rolfes C. D., Quill J., Richardson E. S., Howard S. A., and Iaizzo P. A., 2009, "Design of a Novel Perfusion System to Perform MR Imaging of an Isolated Beating Heart," Journal of Medical Devices, **3**(June), p. 27536.

[83] Yoshida K., Yoshikawa J., Akasaka T., Yamaura Y., Shakudo M., Hozumi T., and Fukaya T., 1989, "Assessment of left-to-right atrial shunting after percutaneous mitral valvuloplasty by transesophageal color Doppler flow-mapping," Circulation, **80**(6), pp. 1521–1526.

[84] Hara H., Virmani R., Ladich E., Mackey-Bojack S., Titus J., Reisman M., Gray W., Nakamura M., Mooney M., Poulose A., and Schwartz R. S., 2005, "Patent foramen ovale: current pathology, pathophysiology, and clinical status.," Journal of the American College of Cardiology, **46**(9), pp. 1768–76.

[85] Di Tullio M., Sacco R. L., Venketasubramanian N., Sherman D., Mohr J. P., and Homma S., 1993, "Comparison of diagnostic techniques for the detection of a patent foramen ovale in stroke patients," Stroke, **24**(7), pp. 1020–1024.

[86] Koppen H., Palm-Meinders I. H., and Ferrari M. D., 2012, "Right-to-left shunts and micro-embolization in migraine.," Current opinion in neurology, **25**(3), pp. 263–8.

[87] Handke M., Harloff A., Olschewski M., Hetzel A., and Geibel A., 2007, "Patent foramen ovale and cryptogenic stroke in older patients.," The New England journal of medicine, **357**(22), pp. 2262–8.

[88] Lechat P., Mas J., Lascault G., Loron P., Theard M., Klimczac M., Drobinski G., Thomas D., and Grosgogeat Y., 1988, "Prevalence of patent foramen ovale in patients with stroke," New England Journal of Medicine, **318**(18), pp. 1148–52.

[89] Volman M., Mojadidi M. K., Gevorgyan R., Kaing A., Agrawal H., and Tobis J., 2012, "Incidence of patent foramen ovale and migraine headache in adults with congenital heart disease with no known cardiac shunts.," Catheterization and cardiovascular interventions, **000**(May).

[90] Thaler D. E., Di Angelantonio E., Di Tullio M. R., Donovan J. S., Griffith J., Homma S., Jaigobin C., Mas J.-L., Mattle H. P., Michel P., Mono M.-L., Nedeltchev K., Papetti F., Ruthazer R., Serena J., Weimar C., Elkind M. S. V, and Kent D. M., 2012, "The Risk of Paradoxical Embolism (RoPE) Study: initial description of the completed database.," International journal of stroke : official journal of the International Stroke Society, pp. 1–8.

[91] Furlan A. J., Reisman M., Massaro J., Mauri L., Adams H., Albers G. W., Felberg R., Herrmann H., Kar S., Landzberg M., Raizner A., and Wechsler L., 2012, "Closure or medical therapy for cryptogenic stroke with patent foramen ovale.," The New England journal of medicine, **366**(11), pp. 991–9.

[92] Homma S., and Sacco R. L., 2005, "Patent foramen ovale and stroke.," Circulation, **112**(7), pp. 1063–72.

[93] Thaler D. E., and Wahl A., 2012, "Critique of closure or medical therapy for cryptogenic stroke with patent foramen ovale: the hole truth?," Stroke; a journal of cerebral circulation, **43**(11), pp. 3147–9.

[94] Furlan A. J., 2013, "Letter by Furlan regarding 'critique of closure or medical therapy for cryptogenic stroke with patent foramen ovale: the hole truth?'.," Stroke; a journal of cerebral circulation, **44**(2), p. e9.

[95] Thaler D. E., and Wahl a., 2013, "Response to Letter Regarding Article, 'Critique of Closure or Medical Therapy for Cryptogenic Stroke With Patent Foramen Ovale: The Hole Truth?'," Stroke, **44**(2), pp. e10–e10.

[96] Kenny D., Turner M., and Martin R., 2008, "When to close a patent foramen ovale.," Archives of disease in childhood, **93**(3), pp. 255–9.

[97] Ruiz C. E., Kipshidze N., Chiam P. T. L., and Gogorishvili I., 2008, "Feasibility of patent foramen ovale closure with no-device left behind: first-in-man percutaneous suture closure.," Catheterization and cardiovascular interventions : official journal of the Society for Cardiac Angiography & Interventions, **71**(7), pp. 921–6.

[98] Zimmermann W. J., Heinisch C., Majunke N., Staubach S., Russell S., Wunderlich N., and Sievert H., 2010, "Patent foramen ovale closure with the SeptRx device initial experience with the first 'In-Tunnel' device.," JACC, **3**(9), pp. 963–7.

[99] Majunke N., Baranowski A., Zimmermann W., Heinisch C., Wilson N., Robertson G., Wunderlich N., and Sievert H., 2009, "A suture not always the ideal solution: problems encountered in developing a suture-based PFO closure technique.," Catheterization and cardiovascular interventions, **73**(3), pp. 376–82.

[100] Goel S. S., Tuzcu E. M., Shishehbor M. H., de Oliveira E. I., Borek P. P., Krasuski R. a, Rodriguez L. L., and Kapadia S. R., 2009, "Morphology of the patent foramen ovale in asymptomatic versus symptomatic (stroke or transient ischemic attack) patients.," The American journal of cardiology, **103**(1), pp. 124–9.

[101] McKenzie J. a, Edwards W. D., and Hagler D. J., 2009, "Anatomy of the patent foramen ovale for the interventionalist.," Catheterization and cardiovascular interventions : official journal of the Society for Cardiac Angiography & Interventions, **73**(6), pp. 821–6.

[102] Spence M. S., Khan A. a, and Mullen M. J., 2008, "Balloon assessment of patent foramen ovale morphology and the modification of tunnels using a balloon detunnelisation technique.," Catheterization and cardiovascular interventions : official journal of the Society for Cardiac Angiography & Interventions, **71**(2), pp. 222–8.

[103] Akhondi A., Gevorgyan R., Tseng C.-H., Slavin L., Dao C., Liebeskind D. S., and Tobis J. M., 2010, "The association of patent foramen ovale morphology and stroke size in patients with paradoxical embolism.," Circulation. Cardiovascular interventions, **3**(5), pp. 506–10.

[104] Rana B. S., Shapiro L. M., McCarthy K. P., and Ho S. Y., 2010, "Three-dimensional imaging of the atrial septum and patent foramen ovale anatomy: defining the morphological phenotypes of patent foramen ovale.," European journal of echocardiography, **11**(10), pp. i19–25.

[105] Saitoh T., Izumo M., Furugen A., Tanaka J., Miyata-Fukuoka Y., Gurudevan S. V, Tolstrup K., Siegel R. J., Kar S., and Shiota T., 2012, "Echocardiographic evaluation of iatrogenic atrial septal defect after catheter-based mitral valve clip insertion.," The American journal of cardiology, **109**(12), pp. 1787–91.

[106] Schneider C. a, Rasband W. S., and Eliceiri K. W., 2012, "NIH Image to ImageJ: 25 years of image analysis," Nature Methods, **9**(7), pp. 671–675.

[107] Marshall A. C., and Lock J. E., 2000, "Structural and compliant anatomy of the patent foramen ovale in patients undergoing transcatheter closure.," American heart journal, **140**(2), pp. 303–7.

[108] Tsang W., Bateman M. G., Weinert L., Pellegrini G., Mor-avi V., Sugeng L., Yeung H., Patel A. R., Hill A. J., Iaizzo P. A., and Lang R. M., 2012, "Accuracy of aortic annular measurements obtained from three-dimensional echocardiography , CT and MRI : human in vitro and in vivo studies," Heart, **98**(2), pp. 1146–1153.

[109] Di Biase L., Santangeli P., Anselmino M., Mohanty P., Salvetti I., Gili S., Horton R., Sanchez J. E., Bai R., Mohanty S., Pump A., Cereceda Brantes M., Gallinghouse G. J., Burkhardt J. D., Cesarani F., Scaglione M., Natale A., and Gaita F., 2012, "Does the left atrial appendage morphology correlate with the risk of stroke in patients with atrial fibrillation? Results from a multicenter study.," Journal of the American College of Cardiology, **60**(6), pp. 531–8.

[110] Miyazaki S., Shah A. J., Nault I., Wright M., Jadidi A. S., Forclaz A., Liu X., Linton N., Xhaët O., Rivard L., Derval N., Sacher F., Hocini M., Jaïs P., and Haïssaguerre M., 2011, "Impact of patent foramen ovale on left atrial linear lesions in the context of atrial fibrillation ablation.," Journal of cardiovascular electrophysiology, **22**(8), pp. 846–50.

[111] Gelfand A., 2011, "Dogs , Doses and Devices: The FDA's Ambitious Plans for Computational Modeling," Biomedical Computation Review, **Fall**, pp. 20–26.

[112] Crofts A., 2012, "World Medical Market Forecasts 2017," World Medical Market Forecasts 2017, p. 1 [Online]. Available: http://www.espicom.com/world-medical-market-forecasts.

[113] "Google Patents" [Online]. Available: www.google.com/patents. [Accessed: 26-Jul-2012].

[114] "USPTO" [Online]. Available: http://www.uspto.gov. [Accessed: 26-Jul-2012].

[115] Bothe W., Kvitting J.-P. E., Swanson J. C., Hartnett S., Ingels N. B., and Miller D. C., 2010, "Effects of different annuloplasty rings on anterior mitral leaflet dimensions.," The Journal of thoracic and cardiovascular surgery, **139**(5), pp. 1114–22.

[116] Inoue K., Owaki T., Nakamura T., Kitamura F., and Miyamoto N., 1984, "Clinical application of transvenous mitral commissurotomy by a new balloon catheter.," The Journal of thoracic and cardiovascular surgery, **87**(3), pp. 394–402.

[117] ISO 5840:2005, Cardiovascular implants, Cardiac Valve protheses, ISBN 1–57020–237–0.

[118] Williams D. F., 1987, Definitions in biomaterials: proceedings of a consensus conference of the European Society for Biomaterials, Chester, England, March 3-5, 1986, Elsevier Science Ltd.

[119] Ratner B., Hoffman A. S., Schoen F. I., and Lemons J. E., 2004, "Biomaterials science: an introduction to materials in medicine," San Diego, California, pp. 162–164.

[120] Schoen F. J., Goodenough S. H., Ionescu M. I., and Braunwald N. S., 1984, "Implications of late morphology of Braunwald-Cutter mitral heart valve prostheses.," The Journal of thoracic and cardiovascular surgery, **88**(2), p. 208.

[121] Schoen F. J., and Levy R. J., 2005, “Calcification of tissue heart valve substitutes: progress toward understanding and prevention,” The Annals of Thoracic Surgery, **79**(3), pp. 1072–1080.

[122] Chin H. P., Harrison E. C., Blankenhorn D. H., and Moacanin J., 1971, “Lipids in silicone rubber valve prostheses after human implantation,” Circulation, **43**(5S1), pp. I–51.

[123] Johansen P., 2004, “Mechanical heart valve cavitation,” Expert review of medical devices, **1**(1), pp. 95–104.

[124] Mykén P. S. U., and Bech-Hansen O., 2009, “A 20-year experience of 1712 patients with the Biocor porcine bioprosthesis,” The Journal of thoracic and cardiovascular surgery, **137**(1), pp. 76–81.

[125] Ulrich K. T., and Eppinger S. D., 1995, Product design and development, McGraw-Hill New York.

[126] Zenios S., Makower J., and Yock P., 2010, Biodesign: the process of innovating medical technologies, Cambridge University Press.

[127] “European Patent Office” [Online]. Available: http://www.epo.org. [Accessed: 26-Jul-2012].

[128] “EPO Patent Search” [Online]. Available: https://data.epo.org/publication-server/?lg=en . [Accessed: 26-Jul-2012].

[129] “Free Patents Online” [Online]. Available: http://www.freepatentsonline.com. [Accessed: 26-Jul-2012].

[130] Kaplan A. V, Baim D. S., Smith J. J., Feigal D. A., Simons M., Jefferys D., Fogarty T. J., Kuntz R. E., and Leon M. B., 2004, “Medical Device Development From Prototype to Regulatory Approval,” Circulation, **109**(25), pp. 3068–3072.

[131] Chai J. Y., 2000, “Medical device regulation in the United States and the European Union: a comparative study,” Food & Drug LJ, **55**, p. 57.

[132] Hill K. O., and Meltz G., 1997, “Fiber Bragg grating technology fundamentals and overview,” Journal of Lightwave Technology, **15**(8), pp. 1263–1276.

[133] Thiagalingam A., D’Avila A., Foley L., Fox M., Rothe C., Miller D., Malchano Z., Ruskin J. N., and Reddy V. Y., 2008, “Full-color direct visualization of the atrial septum to guide transseptal puncture.,” Journal of cardiovascular electrophysiology, **19**(12), pp. 1310–5.

[134] Elagha A. A., Kim A. H., Kocaturk O., and Lederman R. J., 2007, “Blunt atrial transseptal puncture using excimer laser in swine.,” Catheterization and Cardiovascular Interventions, **70**(4), pp. 585–90.

[135] Dondelinger R. F., Ghysels M. P., Brisbois D., Donkers E., Snaps F. R., Saunders J., and Deviere J., 1998, "Experimental radiology Original article Relevant radiological anatomy of the pig as a training model in interventional radiology," Experimental Radiology, **8**(7), pp. 1254–1273.

[136] Hill A. J., and Iaizzo P. A., 2009, "Comparative Cardiac Anatomy," Handbook of Cardiac Anatomy, Physiology, and Devices, P.A. Iaizzo, ed., Humana Press, Totowa, NJ, pp. 87–108.

[137] Tobis J., and Shenoda M., 2012, "Percutaneous treatment of patent foramen ovale and atrial septal defects.," Journal of the American College of Cardiology, **60**(18), pp. 1722–32.

[138] Smith T., McGinty P., Bommer W., Low R. I., Lim S., Fail P., and Rogers J. H., 2012, "Prevalence and echocardiographic features of iatrogenic atrial septal defect after catheter-based mitral valve repair with the MitraClip system.," Catheterization and cardiovascular interventions, **80**(4), pp. 678–85.

[139] Santangeli P., Di Biase L., Burkhardt J. D., Horton R., Sanchez J., Bailey S., Zagrodzky J. D., Lakkireddy D., Bai R., Mohanty P., Beheiry S., Hongo R., and Natale A., 2011, "Transseptal access and atrial fibrillation ablation guided by intracardiac echocardiography in patients with atrial septal closure devices.," Heart Rhythm, **8**(11), pp. 1669–75.

[140] Tzeis S., Andrikopoulos G., Deisenhofer I., Ho S. Y., and Theodorakis G., 2010, "Transseptal catheterization: considerations and caveats.," Pacing and clinical electrophysiology : PACE, **33**(2), pp. 231–42.

[141] Stella J., and Sacks M., 2007, "On the biaxial mechanical properties of the layers of the aortic valve leaflet.," Journal of biomechanical engineering, **129**(5), pp. 757–66.

[142] Ritchie J., Jimenez J., He Z., Sacks M. S., and Yoganathan A. P., 2006, "The material properties of the native porcine mitral valve chordae tendineae: an in vitro investigation.," Journal of biomechanics, **39**(6), pp. 1129–35.

[143] Sacks M. S., Schoen F. J., and Mayer J. E., 2009, "Bioengineering challenges for heart valve tissue engineering.," Annual review of biomedical engineering, **11**, pp. 289–313.

[144] Ross J., 2008, "Transseptal left heart catheterization a 50-year odyssey.," Journal of the American College of Cardiology, **51**(22), pp. 2107–15.

[145] De Ponti R., Cappato R., Curnis A., Della Bella P., Padeletti L., Raviele A., Santini M., and Salerno-Uriarte J. a, 2006, "Trans-septal catheterization in the electrophysiology laboratory: data from a multicenter survey spanning 12 years.," Journal of the American College of Cardiology, **47**(5), pp. 1037–42.

[146] Daoud E. G., 2005, "Transseptal catheterization.," Heart Rhythm, **2**(2), pp. 212–4.

[147] Hahn K., Gal R., Sarnoski J., Kubota J., Schmidt D. H., and Bajwa T. K., 1995, "Transesophageal echocardiographically guided atrial transseptal catheterization in patients with normal-sized atria: incidence of complications.," Clinical cardiology, **18**(4), pp. 217–20.

[148] B-Lundqvist C., Olsson S. B., and Varnauskas E., 1986, "Transseptal left heart catheterization: a review of 278 studies.," Clinical cardiology, **9**(1), pp. 21–6.

[149] Liu T.-J., Lai H.-C., Lee W.-L., Wang K.-Y., Wu T.-J., Huang J.-L., Hsueh C.-W., and Ting C.-T., 2006, "Immediate and late outcomes of patients undergoing transseptal left-sided heart catheterization for symptomatic valvular and arrhythmic diseases.," American heart journal, **151**(1), pp. 235–41.

[150] Fagundes R. L., Mantica M., De Luca L., Forleo G., Pappalardo A., Avella A., Fraticelli A., Dello Russo A., Casella M., Pelargonio G., and Tondo C., 2007, "Safety of single transseptal puncture for ablation of atrial fibrillation: retrospective study from a large cohort of patients.," Journal of cardiovascular electrophysiology, **18**(12), pp. 1277–81.

[151] Holmes D. R., Nishimura R., Fountain R., and Turi Z. G., 2009, "Iatrogenic pericardial effusion and tamponade in the percutaneous intracardiac intervention era.," JACC. Cardiovascular interventions, **2**(8), pp. 705–17.

[152] Peckham G. B., Chrysohou a, Aldridge H. E., and Wigle E. D., 1964, "Combined Percutaneous Retrograde Aortic and Transseptal Left Heart Catheterization.," British heart journal, **26**(1), pp. 460–8.

[153] Roelke M., Smith a J., and Palacios I. F., 1994, "The technique and safety of transseptal left heart catheterization: the Massachusetts General Hospital experience with 1,279 procedures.," Catheterization and cardiovascular diagnosis, **32**(4), pp. 332–9.

[154] Ishikura F., Nagata S., Yasuda S., Yamashita N., and Miyatake K., 1990, "Residual atrial septal perforation after percutaneous transvenous mitral commissurotomy with Inoue balloon catheter.," American heart journal, **120**(4), pp. 873–8.

[155] Hammerstingl C., Lickfett L., Jeong K.-M., Troatz C., Wedekind J.-A., Tiemann K., Lüderitz B., and Lewalter T., 2006, "Persistence of iatrogenic atrial septal defect after pulmonary vein isolation--an underestimated risk?," American heart journal, **152**(2), pp. 362.e1–5.

[156] Obel O., Mansour M., Picard M., Ruskin J., and Keane D., 2004, "Persistence of septal defects after transeptal puncture for pulmonary vein isolation procedures.," Pacing and clinical electrophysiology : PACE, **27**(10), pp. 1411–4.

[157] Fitchet A., Turkie W., and Fitzpatrick A. P., 1998, "Transeptal approach to ablation of left-sided arrhythmias does not lead to persisting interatrial shunt: a transesophageal echocardiographic study.," PACE, **21**(Pt. 1), pp. 2070–2.

[158] Rillig A., Meyerfeldt U., Kunze M., Birkemeyer R., Miljak T., Jäckle S., Hajredini B., Treusch F., and Jung W., 2010, "Persistent iatrogenic atrial septal defect after a single-puncture, double-transseptal approach for pulmonary vein isolation using a remote robotic navigation system: results from a prospective study.," Europace, **12**(3), pp. 331–6.

[159] Cequier a., Bonan R., Serra a., Dyrda I., Crepeau J., Dethy M., and Waters D., 1990, "Left-to-right atrial shunting after percutaneous mitral valvuloplasty. Incidence and long-term hemodynamic follow-up," Circulation, **81**(4), pp. 1190–1197.

[160] Kronzon I., Tunick P. a, Goldfarb A., Freedberg R. S., Chinitz L., Slater J., Schwinger M. E., Gindea A. J., Glassman E., and Daniel W. G., 1990, "Echocardiographic and hemodynamic characteristics of atrial septal defects created by percutaneous valvuloplasty.," Journal of the American Society of Echocardiography, **3**(1), pp. 64–71.

[161] Casale P., Block P. C., O'Shea J. P., and Palacios I. F., 1990, "Atrial septal defect after percutaneous mitral balloon valvuloplasty: Immediate results and follow-up," Journal of the American College of Cardiology, **15**(6), pp. 1300–1304.

[162] Singh S. M., Douglas P. S., and Reddy V. Y., 2011, "The incidence and long-term clinical outcome of iatrogenic atrial septal defects secondary to transseptal catheterization with a 12F transseptal sheath.," Circulation. Arrhythmia and electrophysiology, **4**(2), pp. 166–71.

[163] Chan N.-Y., Choy C.-C., Lau C.-L., Lo Y.-K., Chu P.-S., Yuen H.-C., Mok N.-S., Tsui P.-T., and Lau S.-T., 2011, "Persistent iatrogenic atrial septal defect after pulmonary vein isolation by cryoballoon: an under-recognized complication.," Europace, **13**(10), pp. 1406–10.

[164] Feldman T., Kar S., Rinaldi M., Fail P., Hermiller J., Smalling R., Whitlow P. L., Gray W., Low R., Herrmann H. C., Lim S., Foster E., and Glower D., 2009, "Percutaneous mitral repair with the MitraClip system: safety and midterm durability in the initial EVEREST (Endovascular Valve Edge-to-Edge REpair Study) cohort.," Journal of the American College of Cardiology, **54**(8), pp. 686–94.

[165] Sommer P., and Hindricks G., 2010, "Iatrogenic atrial septal defect after catheter ablation of atrial fibrillation: do we have to worry?," Europace, **12**(3), pp. 301–2.

[166] Korkmaz S., Demirkan B., Guray Y., Yilmaz M. B., and Sasmaz H., 2011, "Long-Term Follow-Up of Iatrogenic Atrial Septal Defect after percutaneous mitral balloon valvuloplasty," Tex Heart Inst J, **38**(5), pp. 523–528.

[167] Himbert D., Brochet E., Radu C., Iung B., Messika-Zeitoun D., Enguerrand D., Bougoin W., Nataf P., and Vahanian A., 2011, "Transseptal implantation of a transcatheter heart valve in a mitral annuloplasty ring to treat mitral repair failure.," Circulation. Cardiovascular interventions, **4**(4), pp. 396–8.

[168] Kautzner J., and Peichl P., 2010, "You get what you inspect, not what you expect: can we make the transseptal puncture safer?," Europace :, **12**(10), pp. 1353–5.

[169] Sy R. W., Klein G. J., Leong-Sit P., Gula L. J., Yee R., Krahn A. D., and Skanes A. C., 2011, "Troubleshooting difficult transseptal catheterization.," Journal of cardiovascular electrophysiology, **22**(6), pp. 723–7.

[170] Himbert D., Brochet E., Radu C., Iung B., Messika-Zeitoun D., Enguerrand D., Bougoin W., Nataf P., and Vahanian A., 2011, "Transseptal implantation of a transcatheter heart valve in a mitral annuloplasty ring to treat mitral repair failure.," Circulation. Cardiovascular interventions, **4**(4), pp. 396–8.

[171] Van Gelder B. M., Houthuizen P., and Bracke F. a, 2011, "Transseptal left ventricular endocardial pacing: preliminary experience from a femoral approach with subclavian pull-through.," Europace : European pacing, arrhythmias, and cardiac electrophysiology : journal of the working groups on cardiac pacing, arrhythmias, and cardiac cellular electrophysiology of the European Society of Cardiology, **13**(10), pp. 1454–8.

[172] Nordsletten D. a, Niederer S. a, Nash M. P., Hunter P. J., and Smith N. P., 2011, "Coupling multi-physics models to cardiac mechanics.," Progress in biophysics and molecular biology, **104**(1-3), pp. 77–88.

[173] Aurigemma G. P., Gottdiener J. S., Arnold A. M., Chinali M., Hill J. C., and Kitzman D., 2009, "Left atrial volume and geometry in healthy aging: The Cardiovascular Health Study.," Circ Cardiovasc Imaging, **2**, pp. 282–9.

[174] Eltchaninoff H., Prat A., Gilard M., Leguerrier A., Blanchard D., Fournial G., Iung B., Donzeau-Gouge P., Tribouilloy C., Debrux J.-L., Pavie A., and Gueret P., 2011, "Transcatheter aortic valve implantation: early results of the FRANCE (FRench Aortic National CoreValve and Edwards) registry.," European heart journal, **32**(2), pp. 191–7.

[175] Castle B. T., Howard S. A., and Odde D. J., 2011, "Assessment of Transport Mechanisms Underlying the Bicoid Morphogen Gradient," Cellular Molecular Bioengineering, **4**(1), pp. 116–121.

Appendix A:

Anatomical and Functional Assessment of a Human Heart Exhibiting a Double Orifice Mitral Valve

Michael G. Bateman, PhD
Stephen A. Howard, BA
Lesa Nord, BS
Alexander Hill, PhD
Robert Anderson, MD, FCRPath
Paul A. Iaizzo, PhD

University of Minnesota, Minneapolis, MN 55455

Address reprint requests and correspondence to:

Paul Iaizzo, PhD
Department of Surgery
University of Minnesota
Mayo Mail Code 107
420 Delaware Street SE
Minneapolis, MN 55455
Phone: 612-624-7912
Fax: 612-624-2002
Email: iaizz001@umn.edu

Keywords: mitral, edge-to-edge, congenital, Visible Heart®

Background: First described by Greenfield in 1876, the double orifice mitral valve (DOMV) is considered a rare congenital cardiac malformation that usually presents as a symptom of an overriding developmental disease. In a very few isolated cases the abnormality presents as an isolated incident in asymptomatic adults. We present here the imaging and analysis of a heart recovered from a 45 year-old male with no clinically diagnosed cardiac conditions presenting with a naturally occurring bridge between the aortic (anterior) and mural (posterior) leaflets.

Methods: Using Visible Heart methodologies the heart was reanimated and stabilized before recording hemodynamics and imaging the mitral valve from above and below. The specimen was then formalin fixed at a pressure of 50 ± 5 mmHg before being imaged and finally dissected to investigate the double orifice valve.

Results: Pre-recovery echocardiographic and hemodynamic data showed trivial mitral valve regurgitation and no evidence of any left ventricular (LV) anomalies often associated with DOMVs. The reanimated heart performed comparably to pre-recovery data; HR 82bpm, LV pressures 95/12 mmHg and LV contraction 629.6mmHg/s, no evidence of valve disfunction. A complete cardiac pathological work up indicated no abnormalities associated with common developmental diseases.

Discussion: The data reported here indicates that the presence of a DOMV has had a negligible effect on the cardiac health of the patient. This may have interesting clinical implications regarding the perception of edge to edge repairs of patients with moderate to severe mitral regurgitation. Nevertheless one must consider that the patient described grew into adulthood with the DOMV, rather than having the feature surgically induced later in life, and hence adapted appropriately to the valve abnormality.

Background

The left atrioventricular valve, or mitral valve as it is commonly known, normally presents with two leaflets; the aortic (anterior) and mural (posterior) leaflets. Each leaflet is hinged from the mitral annulus, and restrained by two papillary muscle complexes with their tendinous cords. In a healthy valve the two leaflets are separated along their full lengths of coaptation so that during diastole, a single orifice is formed between the left atrium (LA) and left ventricle (LV)[1]. Carpentier described the mitral valve as consisting of two opposing leaflets— a posterior leaflet with three scallops, an anterior leaflet with one scallop[2]. The regions of each leaflet were described alphanumerically to differentiate the predominant features of the valve (Figure 1). We present here a human specimen with a naturally occurring bridge between the aortic and mural leaflets at the midpoint of the valve, considered the A2-P2 region, thus creating a double orifice within the native valve.

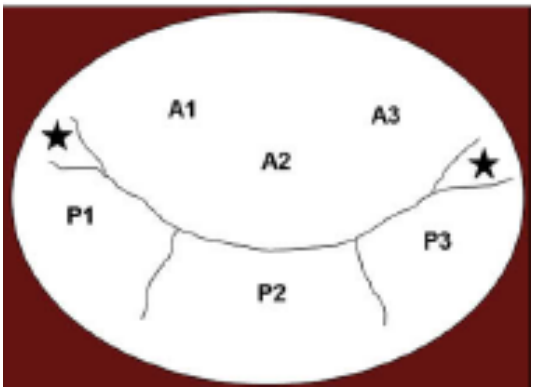

Figure 1: Carpentier's nomenclature of the mitral valve is diagrammed. The anterior leaflet has one scallop and is divided into three regions (A1-A3). The posterior leaflet is divided into three scallops, each with its own region (P1-P3).

Greenfield was the first to describe a double orifice mitral valve (DOMV) in 1876[3]. Since then approximately 200 cases of this congenital malformation have been reported[4]. Initially, instances were discovered during post-mortem examinations or in explanted hearts during transplant procedures. However the development and increased use of cardiac ultrasound examinations in the late 20th century has led to more clinical reports of the phenomenon. Yet the occurrence of a DOMV is still rare with Wojcik et al. finding only nine cases in ultrasound exams from close to 80,000 patients referred to hospital for cardiac examinations between 1993 and 2006[4].

It is considered that the bridge is caused by abnormal development of the mitral valve from the primary fold and the primitive left ventricle during the delamination process[5, 6]. The phenomenon has been further classified by Trowitzsch et al. defining three distinct types: complete bridge, incomplete bridge and a hole[7]. The DOMV commonly presents in conjunction with other congenital defects[4, 8-14] and can occasionally coexist with more complex cardiac malformations

such as tetralogy of Fallot or Shone syndrome[15, 16]. The defect can be corrected surgically in instances where the abnormality presents as an isolated condition and is detected early, such as in the pediatric patient[17]. In adults, isolated cases have been reported in patients admitted for chest pain, shortness of breath, or heart murmurs[18-25] and are occasionally reported as asymptomatic in younger adults[23, 25]. Patients with a DOMV over 40 years old often present with additional symptoms such as severe valvular dysfunctions, pulmonary hypertension and/or cardiomegaly[18-20, 24]. At the time of writing the authors found only two reported cases of DOMV in elderly asymptomatic patients: one 42 year old described by Lee et al.[21] and the other a 75 year old reported by Kim et al.[22].

Methods

Upon receiving the heart from LifeSource (Organ Procurement Organization, St. Paul, MN), the specimen was visually inspected and weighed before being prepared for reanimation using Visible Heart methodologies[26]. Briefly, with the heart still arrested, the great vessels of the heart were cannulated and the heart was perfused and re-warmed with a modified Krebs Heinseleight buffer. The heart was then defibrillated and allowed to function autonomously in sinus rhythm while intra atrial and ventricular hemodynamic data were recorded. With the heart beating in a four chamber working mode the valve was simultaneously imaged using both a 4mm and a 6mm diameter endoscope (Olympus Corporation, Tokyo, Japan), which were advanced into the LA via the right superior pulmonary vein, and the LV via an apical incision[27]. Once the data and video footage had been recorded the specimen was removed from the apparatus and perfusion fixed in 10% buffered formalin by attaching the cannulated great vessels to a pressure head of approximately 50 mmHg as described by Anderson et al.[28]. This technique, first utilized by Thomas et al. and adapted by Kilner et al., fixes the heart in an approximation of the end-diastolic state (Figure 5)[29, 30]. The heart was then imaged with the endoscopes to obtain fixed internal footage[31].

Subsequently, the formalin fixed heart was suspended in agar gel and imaged using MR imaging described by Eggen et al.[32] Cardiac MR imaging was performed using a 3D, T1-weighted, gradient-echo scan sequence in a 3 Tesla scanner (Trio; Siemens Medical Systems, US), to create high resolution short- and long-axis image stacks of the fixed specimen.

To determine the presence of any overriding pathological conditions the heart was then removed from the agar gel and dissected as follows:

1. Both atria were removed to expose the cardiac skeleton. The apex was then carefully removed allowing visualization of the sub-valvular apparatus of the mitral valve.
2. An incision was then made up the free wall of the left ventricle avoiding the subvalvular apparatus.
3. The papillary muscles were then dissected off the walls of the left ventricle.
4. Subsequently, the tissue surrounding the annulus was dissected away to isolate the valve and subvalvular apparatus.

Patient Information

A 45 year-old male, BMI 30.4, was hospitalized with severe thoracic trauma and a large intracranial hemorrhage. Once stabilized in the hospital the patient maintained an average BP and HR of 130/68 mmHg and 105 bpm respectively. Phenylephrine administration was required to treat hypovolemic shock and maintain adequate blood pressures.

Before organ recovery heart tones were found to be normal and systemic perfusion was adequate. An echocardiographic evaluation of cardiovascular function was performed and concluded that cardiac rhythm was regular and ventricular wall motion appeared normal. The LV ejection fraction was estimated at 65%, LV wall thickness was reported as 8mm with dimensions of all other cardiac chambers being described as normal. No stenosis of any valve or regurgitation of the semi lunar valves was reported. However, trivial mitral valve and mild tricuspid valve regurgitations were noted.

The individual had no known past medical history of cardiac problems.

Results

Images and data from reanimated heart

The heart (446g wet weight upon arrival) was attached to the Visible Heart® apparatus for imaging and analysis (Figure 2), and functional images of the DOMV, (Figure 3),were reported

by Howard et al.[33]. Once the heart was beating autonomously, video footage, echocardiographic footage and hemodynamic data were recorded. Approximately 60 min post defibrillation the heart rate was recorded as 82bpm, the LV wall thickness (taken at the papillary level from a long axis echocardiographic shot) was measured as13.5mm, and the baseline pressures across the mitral valve were noted(Figure 4). To determine the relative performance of the heart the hemodynamic data was compared to previously reanimated human hearts (Table 1).

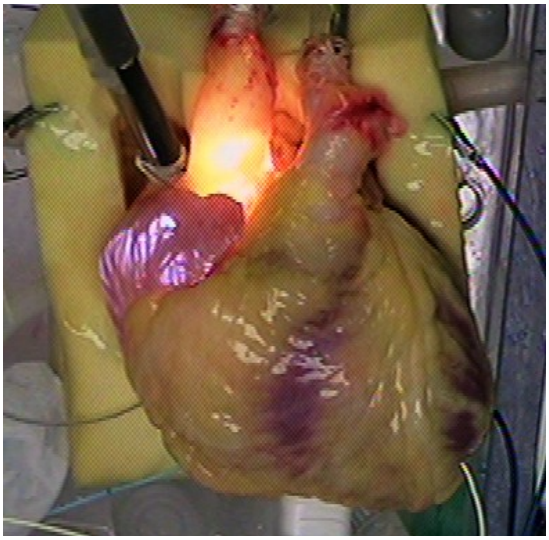

Figure 2: Still shot of the reanimated heart on the apparatus from an approximation of the anterior posterior aspect. Light from the endoscopes can be seen in the right atrium and the ascending aorta. Video footage of the functioning valve can be found in the supplementary data.

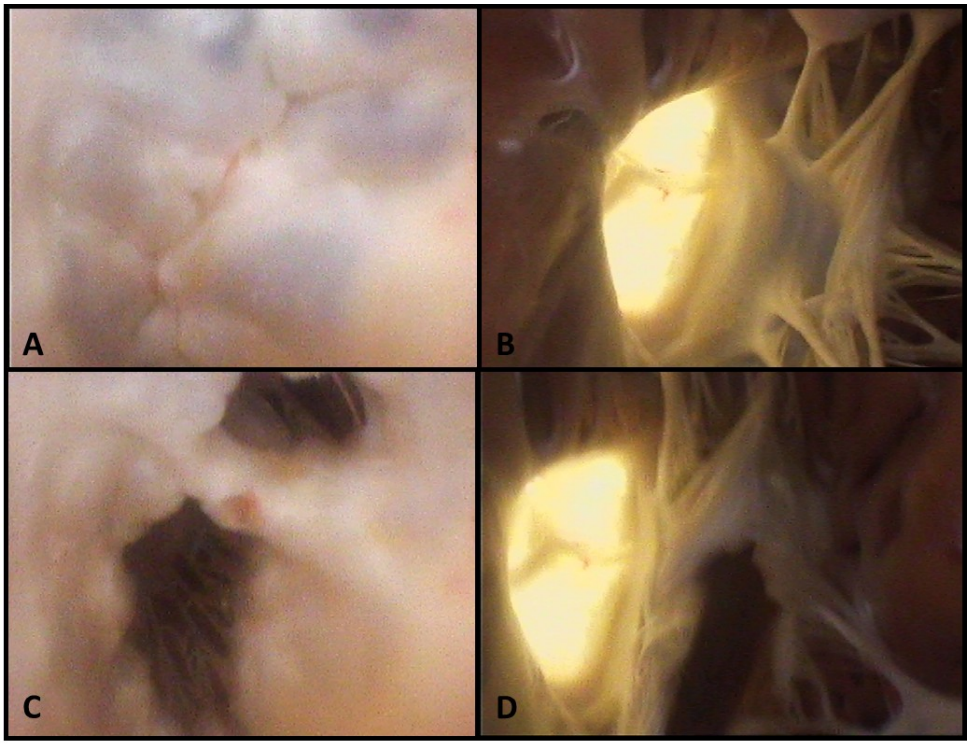

Figure 3: Shown here is a series of four screenshots of a human mitral valve in both systole (A&B) and diastole (C&D) from the left atrium (A&C) and the left ventricle (B&D). These images clearly show the fibrous connection between the mural (postero-inferior) and aortic (antero-superior) leaflets in the central (second) region[33].

	HR [bpm]	LVSP [mmHg]	LVEDP [mmHg]	+dLVP/dt [mmHg/s]	-dLVP/dt [mmHg/s]
Previously Reanimated Human Hearts (N=11)	90 ± 16	43 ± 20	15 ± 6	383 ± 160	-334 ± 157
DOMV	82	95	13	630	-513

Table 1. Hemodynamic data when compared to previously reanimated hearts[26]. Data represented as mean ± SD

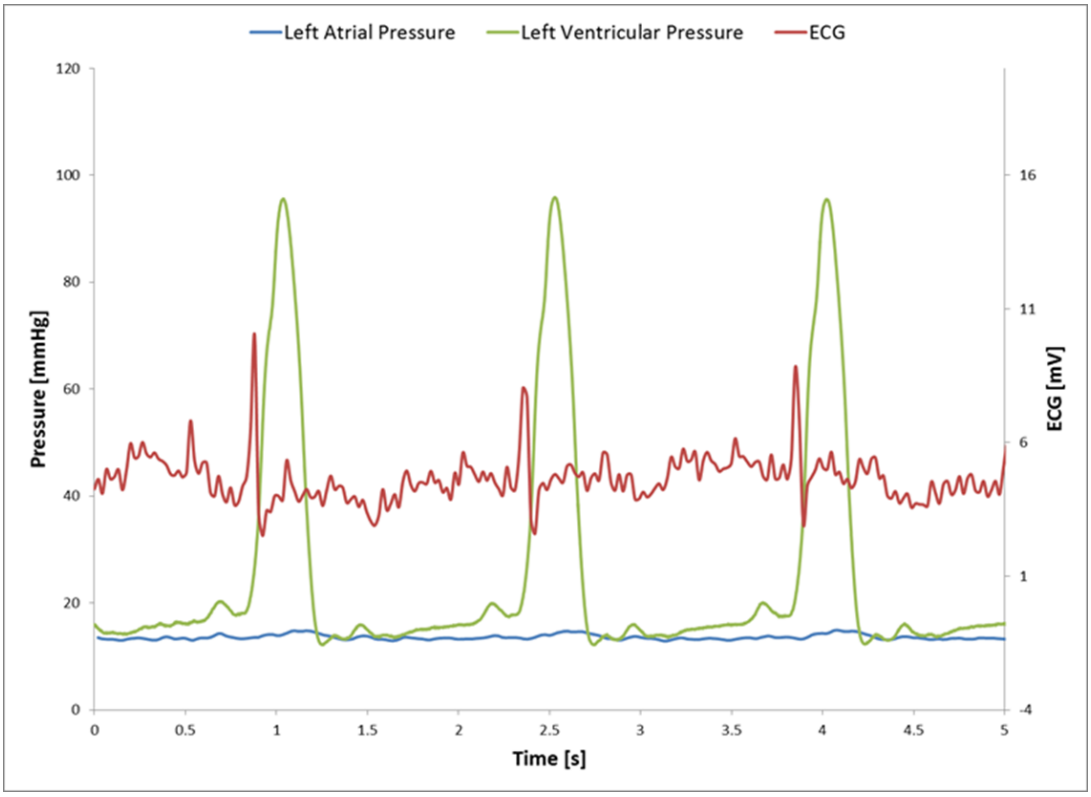

Figure 4:
Electrical and hemodynamic cardiac function during reanimation. Left ventricular pressure (green) and left atrial pressure (blue) scaled to the left y-axis in mmHg, ECG (red) scaled to the right y axis in mV.
Pressures across the valve: End Diastolic – LV 13mmHg, LA 15mmHg
Systolic – LV 95mmHg, LA 12mmHg

Pathological inspection of the valve

A full pathology report can be seen in appendix A.1. The mitral valve was found to exhibit slight calcifications on the ventricular side of the aortic leaflet and negligible calcifications on the ventricular side of the mural leaflet. The aortic leaflet displayed no visible clefts whereas the mural leaflet possessed two large clefts near the fibrous connection thus presenting three distinct scallops: one toward the superior commissure and one larger cleft toward the inferior commissure. The sub-valvular apparatus was observed to be made up of two distinct papillary complexes and showed no obvious anatomical abnormalities. The fibrous connection of the mitral valve observed here could best be defined as an incomplete bridge situated toward the superior commissure of the valve. This formation resulted in a smaller superior (anterolateral) orifice and a larger inferior (posteromedial) orifice (Figure 5).

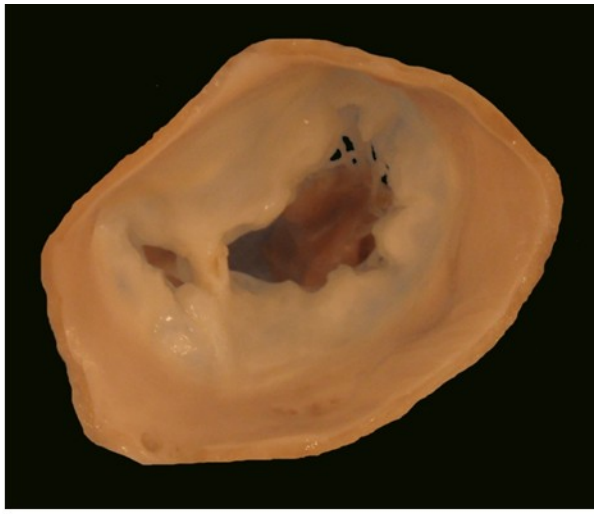

Figure 5: Images of the dissected mitral valve showing:
a) the subvalvular apparatus of the valve and
b) the valve from the left atrium highlighting the fibrous connection between the valve leaflets.

Discussion

DOMVs are a rare congenital abnormality that usually present with other coexisting congenital malformations[4]. The majority of isolated cases are reported in patients presenting with other cardiac or circulatory symptoms and clinical reports of a DOMV in a patient over the age of 40 years old are considered extremely rare. However, it should be noted that typically patients with asymptomatic DOMVs exhibit no cardiac functional abnormalities and thus rarely undergo the appropriate examinations to diagnose such an abnormality.

The post-mortem examination of a heart recovered from a 45 year old male, whose cause of death and previous medical history showed no evidence of a congenital malformation, presents a unique case. The DOMV or fibrous bridge was not recognized until the heart was reanimated within our laboratory. The condition of the heart during preparation gave no indication of cardiomegaly or any other sign of left sided hypertrophy or dilation often associated with dysfunctional mitral valves. The echocardiographic exam performed prior to organ recovery made no mention of any valve stenosis and only noted a trivial mitral regurgitation. Once reanimated the heart performed well when compared to other specimens reanimated with the same procedure (Table 1).

To further confirm this hypothesis, a pathological work up of the heart was performed, concentrating on the anatomical health of the valves, the left ventricle and determining the presence of any other congenital abnormalities. Our findings indicated that the specimen was in good health and apart from the DOMV exhibited no cardiac abnormalities. There was a reported increase in LV wall thickness; however this swelling can be attributed to cellular edema caused by a difference in the oncotic levels of the modified Krebs Henseleight buffer and the intracellular fluids. Additionally, information from echocardiographic exams (both pre-recovery and during reanimation) appear to confirm this finding and suggests that this altered anatomy was the result of tissue fluid retention during the reanimation process and not due to any pre-existing cardiovascular conditions. It should also be noted that the pathology examination was partially hindered by the edemic musculature making the diagnosis of subtle cardiac abnormalities more challenging.

Although one must consider that the patient described here grew into adulthood with a DOMV and did not have the feature surgically induced later in life, the imaging and analysis presented here may have interesting clinical implications regarding the perception of edge to edge repairs of patients with moderate to severe mitral regurgitation. For example, the Alfieri stitch is currently used as a technique to surgically repair mitral leaflet prolapse[34] and concerns have been raised regarding the function of the surgically created dual orifice valve in comparison to a typical single orifice valve. Yet, Quill et al. showed in a number of in-vitro swine studies that this type of procedure did not cause mitral stenosis in otherwise healthy valves[35]. These data, compared with the analysis presented here, support the use of the Alfieri stitch to treat certain etiologies of mitral regurgitation.

Conclusions

The footage and data of a rarely reported congenital malformation of the mitral valve presented in this paper indicates that, in this isolated instance, the presence of a double orifice mitral valve has had a negligible effect on the cardiac health of the patient. The 45 year old individual presented with a healthy and anatomically unremarkable heart indicating that the fibrous connection between the opposing mitral leaflets did not affect the hemodynamic performance of the valve.

References

1. Bateman MG, Quill JL, Hill AJ, Iaizzo PA. The clinical anatomy and pathology of the human atrioventricular valves: Implications for repair or replacement. *J Cardiovasc Transl Res*. 2013;6:155-165

2. Carpentier A. Cardiac valve surgery--the"french correction". *J Thorac Cardiovasc Surg*. 1983:323-337

3. Greenfield WS. Double mitral valve. *Transactions of the Pathological Society of London*. 1876;27:128-129

4. Wojcik A, Klisiewicz A, Szymanski P, Rozanski J, Hoffman P. Double-orifice mitral valve - echocardiographic findings. *Kardiologia polska*. 2011;69:139-143

5. Elfenbein B, Paplanus SH. Duplication of the mitral and tricuspid valves. *Archives of pathology*. 1968;85:675-680

6. Erdemli O, Ayik I, Karadeniz U, Yamak B, Birincioglu CL, Caglar K. A double-orifice atrioventricular valve case: Intraoperative transesophageal echocardiography in diagnosis and treatment. *Anesthesia and analgesia*. 2003;97:650-653

7. Trowitzsch E, Bano-Rodrigo A, Burger BM, Colan SD, Sanders SP. Two-dimensional echocardiographic findings in double orifice mitral valve. *J Am Coll Cardiol*. 1985;6:383-387

8. Zalzstein E, Hamilton R, Zucker N, Levitas A, Gross GJ. Presentation, natural history, and outcome in children and adolescents with double orifice mitral valve. *Am J Cardiol*. 2004;93:1067-1069

9. Westendorp IC, de Bruin-Bon HA, Hrudova J. Double orifice mitral valve; a coincidental finding. *Eur J Echocardiogr*. 2006;7:463-464

10. Sharma S, Loya YS, Daxini BV. Coarctation of aorta with unusual association of diverticulum of the left ventricle and double orifice mitral valve. *Int J Cardiol*. 1991;30:113-115

11. Seguela PE, Dulac Y, Acar P. Double-orifice mitral valve assessed by two- and three-dimensional echocardiography in a newborn. *Archives of cardiovascular diseases*. 2011;104:361-362

12. Deng X, Li X, Li J, Zhou X, Hu J, Yang Y. A rare case of gerbode defect associated with double orifice mitral valve. *The Thoracic and cardiovascular surgeon*. 2010;58:372-374

13. van Buuren F, Faber L, Bogunovic N. Double orifice mitral valve with normal function: An echocardiography and mri study of a rare finding. *Eur Heart J*. 2011;32:137

14. Goicolea FJ, Laraudogoitia E, Bethencourt A, Medina A, Hernandez E, Coello I. [double mitral orifice associated with a bicuspid aortic valve detected using bidimensional echocardiography]. *Rev Esp Cardiol*. 1989;42:65-67

15. Sasaoka T, Ohguri H, Makita Y, Kurokawa S, Izumi T. Double-orifice mitral valve in an elderly patient with tetralogy of fallot. *Japanese heart journal*. 1996;37:503-507

16. Linka AZ, Fatio R, Jost CA. Images in cardiology: Double orifice mitral valve. *Heart*. 2000;84:244

17. Yurdakul Y, Bilgic A, Saylam A, Sarioglu T, Kosker S, Aytac A. Congenital double-orifice mitral valve. Report of a case with valve replacement. *Japanese heart journal*. 1980;21:545-550

18. Congiu S, Josa M, Freixa X, Azqueta M, Mestres C, Mulet J. Mitral insufficiency with a double-orifice mitral valve in an adult patient. *J Thorac Cardiovasc Surg*. 2007;134:250-251

19. Heyse AM, Vanhercke D, Nimmegeers J, Missault L, Claeys R, Hollanders G, Versee L. Mitral insufficiency with congenital double-orifice mitral valve in an elderly patient. *Eur J Echocardiogr*. 2003;4:334-335

20. Kron J, Standerfer RJ, Starr A. Severe mitral regurgitation in a woman with a double orifice mitral valve. *Br Heart J*. 1986;55:109-111

21. Lee DI, Ha JW, Chung B, Kim Y, Chun KJ, Rim SJ, Chung N. Double-orifice mitral valve. *Clin Cardiol*. 1999;22:425

22. Kim SJ, Shin ES, Lee SG. Congenital double-orifice mitral valve with mitral regurgitation due to flail leaflet in an elderly patient. *The Korean journal of internal medicine*. 2005;20:251-254

23. Karas S, Barbetseas J, Lambrou S, Parissis J, Metzikof D, Toutouzas P. Well-functioning double-orifice mitral valve in a young adult. *Journal of clinical ultrasound : JCU*. 2003;31:170-173

24. Zhu D, Chen A, Zhao Q. Surgical repair for isolated congenital double-orifice mitral valve. *Eur J Cardiothorac Surg*. 2011;39:268-270

25. Marcu CB, Beek AM, Ionescu CN, Van Rossum AC. Double orifice mitral valve visualized on echocardiography and mri. *Netherlands heart journal : monthly journal of the Netherlands Society of Cardiology and the Netherlands Heart Foundation*. 2012;20:380-381

26. Hill AJ, Laske TG, Coles JA, Jr., Sigg DC, Skadsberg ND, Vincent SA, Soule CL, Gallagher WJ, Iaizzo PA. In vitro studies of human hearts. *Ann Thorac Surg*. 2005;79:168-177

27. Chinchoy E, Soule CL, Houlton AJ, Gallagher WJ, Hjelle MA, Laske TG, Morissette J, Iaizzo PA. Isolated four-chamber working swine heart model. *Ann Thorac Surg*. 2000;70:1607-1614

28. Anderson SE, Quill JL, Iaizzo PA. Venous valves within left ventricular coronary veins. *Journal of interventional cardiac electrophysiology : an international journal of arrhythmias and pacing*. 2008;23:95-99

29. Thomas AC, Davies MJ. The demonstration of cardiac pathology using perfusion-fixation. *Histopathology*. 1985;9:5-19

30. Kilner PJ, Ho SY, Anderson RH. Cardiovascular cavities cast in silicone rubber as an adjunct to post-mortem examination of the heart. *Int J Cardiol*. 1989;22:99-107

31. The atlas of human cardiac anatomy.2012

32. Eggen M, Bateman M, Iaizzo PA. Methods to prepare perfusion fixed cardiac specimens for multimodal imaging: The use of formalin and agar gels. *Journal of Medical Devices*. 2011;5:027539-027539

33. Howard SA, Bateman MG, Hill AJ, Anderson RH, Iaizzo PA. In vitro images of a double orifice mitral valve in a reanimated human heart. *Ann Thorac Surg*. 2013;95:1456

34. Alfieri O, Maisano F, De Bonis M, Stefano PL, Torracca L, Oppizzi M, La Canna G. The double-orifice technique in mitral valve repair: A simple solution for complex problems. *J Thorac Cardiovasc Surg*. 2001;122:674-681

35. Quill JL, Bateman MG, St Louis JL, Iaizzo PA. Edge-to-edge repairs of p2 prolapsed mitral valves in isolated swine hearts. *J Heart Valve Dis*. 2011;20:5-12

Appendix A.1

Post-reanimation pathology assessment

Cardiac walls:

Upon inspection of the ventricles there were no septal defects or abnormalities on the endocardial surfaces or within the chamber walls. The left and right ventricle had volumes of approximately 35cm^3 and 140cm^3 respectively with wall thicknesses measured at the papillary levels of 19.7mm and 8.4mm, respectively. This excessive thickness is due to fluid absorption during the reanimation process. The appendages of both atria were unremarkable and no visual abnormalities of the atrial walls were recorded. The atrial septum showed a distinct valve of foramen that was fully closed/sealed. No other congenital wall defects were observed upon examination.

Cardiac vasculature:

The cardiac vasculature showed no evidence of any occlusions or abnormal branching in either the venous or arterial systems. Very slight calcific deposition was noted in the right coronary artery approximately 40 mm from the ostium and in the left coronary artery at the bifurcation of the left anterior descending and the circumflex.

Cardiac valves:

The pulmonary valve exhibited three distinct leaflets and presented with an average annular diameter of 27.0 mm, with no signs of stiffening or fibrosis. The aortic valve annulus presented with a major diameter of 29.5 mm and a minor diameter of 19.5mm and also showed no calcification on either the leaflets or the annulus. The valve presented a typical tri-leaflet anatomy with little to no fibrosis of the left and right coronary leaflets. The non-coronary leaflet shows a fibrotic ridge running from the annulus to the leaflet node; although this may be the initiation of leaflet calcification it was not deemed severe enough to affect leaflet motion. The sinus and ascending aorta showed no signs of calcification (Figure A1).

The tricuspid valve was found to be normal, showing only minor fibrosis of the anterosuperior and septal leaflets. All three leaflets were distinct and showed no signs of commissural fusion. The tricuspid annulus measured 41.9 mm by 41.2 mm. The subvalvular apparatus of the valve

was considered unremarkable: the chordal attachments of the antero-superior and inferior leaflets were shared by the anterior and posterior papillary complexes. Numerous fibrous conduction bands were observed between the two complexes and the surrounding endocardial surface. The smaller septal complex supported the lesser regions of the septal and antero-superior leaflets at the commissure.

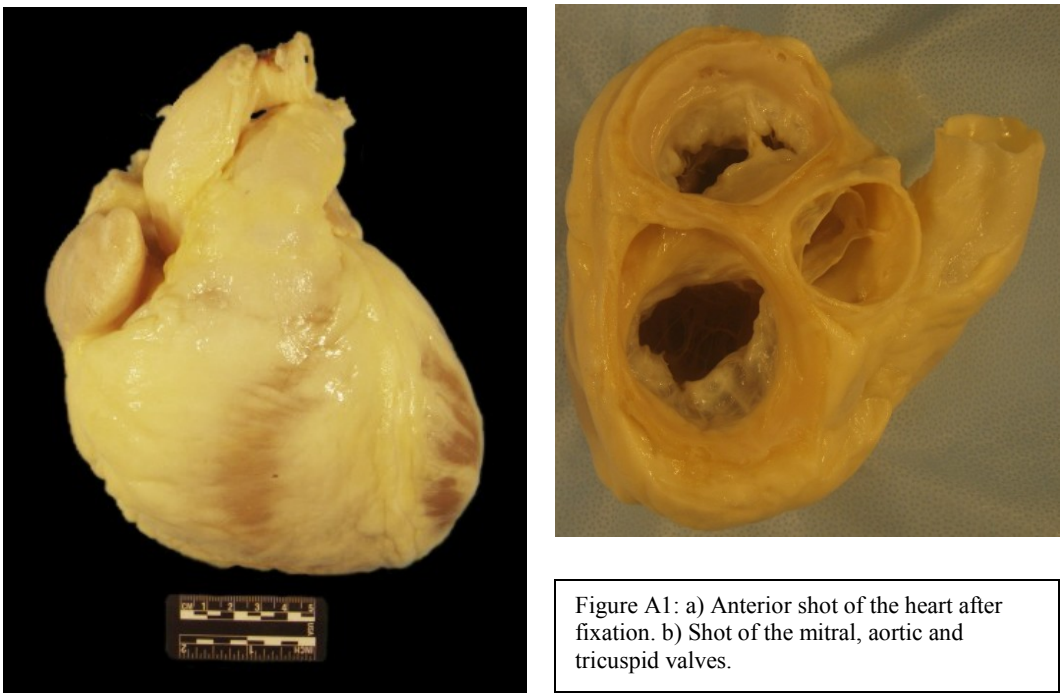

Figure A1: a) Anterior shot of the heart after fixation. b) Shot of the mitral, aortic and tricuspid valves.

The Double Orifice Mitral Valve:

See Figure (A2)

The mitral valve was found to exhibit slight calcifications on the ventricular side of the aortic leaflet and negligible calcifications on the ventricular side of the mural leaflet. The aortic leaflet displayed no visible clefts whereas the mural leaflet possessed two large clefts near the fibrous connection: one toward the superior commissure and one larger cleft toward the inferior commissure, thus presenting three distinct scallops. The mitral annulus measured 40.3mm by 26.7mm. The sub-valvular apparatus was observed to be made up of two distinct papillary complexes. The superoposterior papillary (antero-lateral) complex was formed of one muscle with three distinct heads and six chordal attachments to both leaflets at the superior commissure. This superoposterior complex supported the entire fibrous connection with two large chordal tendons. The rest of the valve appeared to be supported by the larger inferoanterior muscle

complex (posteromedial) formed again of one muscle with three distinct heads. The chordal attachments of this complex were more numerous with twelve counted, all exhibiting more densely fenestrated structures.

The fibrous connection of the mitral valve observed here could best be defined as an incomplete bridge situated toward the superior commissure of the valve. This formation resulted in a smaller superior (anterolateral) orifice, of approximately 25 mm^2, and a larger inferior (posteromedial) orifice, approximately of 148 mm^2.

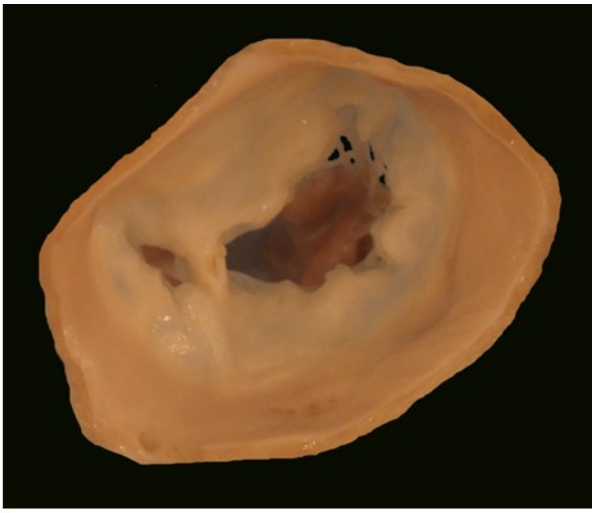

Figure A2: Images of the dissected mitral valve showing: a) the subvalvular apparatus of the valve and b) the valve from the left atrium highlighting the fibrous connection between the valve leaflets.